COMPUTATION OF LATERAL HYDRODYNAMIC FORCES DURING SHIP INTERACTIONS IN SHALLOW WATER

by

Graeme William King

B.Sc.(Hons.)(Ma.Sc.), University of Adelaide

Thesis submitted for the degree of Doctor of Philosophy

in The University of Adelaide

Department of Applied Mathematics
November, 1978.

CONTENTS

SUMMARY

This thesis considers hydrodynamic ship interactions in shallow water. It is assumed that the ships are slender, the fluid is inviscid and incompressible and,that free surface effects can be neglected.

Four separate interaction problems are considered. The first is the interaction of a ship with some depth contour. Only steady interactions are considered, so the ship is moving at a uniform velocity parallel to any depth contours. Two particular contours, namely, a vertical wall and a beach of uniform slope, are considered and results presented.

The model is generalized to include the interaction of two or more slender ships in shallow water, moving in such a manner that the problem is steady. The cases of a flat bottom of uniform depth and a flat bottom with a vertical wall are considered. The results obtained for a wall are of particular interest when applying experimental results to actual ship interactions.

An unsteady model for two dimensional airfoil interactions is formulated next. This provides insight into the significance of unsteady effects in ship manoeuvres, when the bottom clearance is negligible. This work is then extended to provide a model for the unsteady interactions between two or more ships in unbounded shallow water, with underkeel clearance effects included.

Each of the above problems leads to an integral equation, or a system of integral equations, which has to be solved. A suitable algorithm is described in each case and used to compute results. Comparison with experiments shows that the algorithm is useful for computation of the sway force and yaw moment in practical problems. Where possible, qualitative discussions of these results are presented.

SIGNED STATEMENT

I hereby declare that this thesis contains no material which has been submitted to any university for the purpose of obtaining any other degree or diploma and, to the best of my knowledge, it contains no material previously published by another person, except where due reference is made in the text of the thesis.

Graeme King

ACKNOWLEDGEMENTS

I wish to express my thanks to my Supervisor, Professor E.O. Tuck, for suggesting the topic and for his encouragement and valuable discussions. I am also indebted to Mrs. Angela McKay for the typing of the manuscript and to Mrs. Judy Laing for the diagrams she drew. I also wish to acknowledge the support of a Commonwealth Postgraduate Research Award from January 1974 to February 1976.

CHAPTER 1

INTRODUCTION

In recent years interest in hydrodynamic ship interactions has resulted from the number of ship collisions occurring each year. The collisions studied fall into two main classes, those between two or more ships and those between a ship and another object such as a wharf, bank, bridge, or sandbar. Considerable effort has been put into deriving theoretical models, so that additional information about hazardous situations may be obtained.

From a theoretical point of view, ship interactions can be readily divided into those in deep water and,those in water which is shallow when compared to the draft of the vessels. Tuck and Newman [25] have considered the deepwater interaction of two slender ships in both steady and unsteady motion. In practice, this kind of theory is mainly limited to refuelling manoeuvres, as ships are rarely close together in deep water.

A ship is usually in close proximity to another ship or some obstacle when it is moving in restricted waterways such as harbours or canals. Not only is there a lateral restriction on the water, but more importantly, the depth is usually of the same order as the draft. It is convenient to divide shallow water interactions into two cases, steady and unsteady. The steady case is the simpler to analyse of the two, as a vortex wake must be included in the formulation of unsteady problems. Tuck and Newman [25] formulated the shallow-water ship-ship interaction problem for steady interactions in water of constant depth.

In this dissertation, only interactions in shallow water are considered and, except in Chapter 4, the formulation of the modelled

interactions allows for some depth changes. This is done by applying the results of Tuck [24] for slender ships moving in shallow water.

The models formulated all assume that the lateral separation between the ships is comparable with the length of the ships, and large compared to their beam. A nearfield theory for close interactions is described in Yeung and Hwang [27]. As the forces and moments of greatest importance are those acting laterally, they are the only components investigated here.

The approach taken here is to take the simplest problem and to build upon it in successive stages. The first problem considered is the steady interaction of a ship with some depth contours. This is expanded to include the steady interactions of two or more ships in shallow water. Temporarily abandoning this approach the simplest unsteady problem is considered, that is, the two dimensional unsteady interactions of two or more airfoils moving along parallel paths. This is formulated directly from the usual aerodynamic boundary conditions. The most complex problem discussed is the unsteady hydrodynamic interactions between two ships in shallow water. Here it is treated by combining the results of the problems preceding it. In fact all the other problems can be considered to be special cases of this last problem.

The advantage of starting with the simpler problem is that interesting ship interactions of less complexity can be studied more easily without the numerical complications of the hardest case. In fact, the last problem depends on so many parameters that useful cases, which are treated as separate problems here, could easily have been overlooked.

The first type of interactions considered are those between a single ship and some depth contours. So that a steady model can be used, the ship is considered to be moving parallel to any depth contours. Two particular cases are examined in detail, and numerical results presented.

The cases investigated are those of a vertical wall (bank) and a beach of uniform slope. One of the aims of this investigation is to determine whether results for "bank-suction" problems can be generalized to other boundaries. This work has already been presented in King and Tuck [16] and Chapter 2 follows that paper closely.

In Chapter 3 the steady interaction between two ships is considered. The formulation allows for depth contours, and results for a flat bottom of constant depth, and a flat bottom with a vertical wall parallel to the paths of motion of the ships, are presented. The results for a vertical wall are important as they show the quite large effect the presence of a wall has on the sway force and yaw moment of the ships. In fact, the results show that great care needs to be taken when applying the results of model experiments to real situations. This is because experiments are quite often carried out in narrow tanks where the measured forces and moments could easily include the effect of the walls of the channels, even when this is not desired.

A two dimensional model for unsteady ship interactions is formulated in Chapter 4. The model is that for two airfoils moving along parallel paths at different velocities. The theory is appropriate for flow past a vessel in very shallow water, as Tuck [22] has shown that in this case the flow is nearly two dimensional. King [14] describes a formulation which can be used when there are no boundaries in the fluid. A more general derivation is given in Chapter 4, together with some results for interactions in an unrestricted two dimensional fluid.

Underkeel clearance effects are included in the model for unsteady ship interactions in shallow water which is described in Chapter 5. This is the most useful of the theories presented, but because of the large number of variables in such a problem (waterplane, clearance, relative velocities etc.), only results for comparison with experiments are given.

They show that the model can be usefully employed in the study of ship interactions.

Each of the four problems considered is modelled by distributing sources and vortices over the centre-line of the water-plane of the ships. The sources model thickness effects and the vortices camber and interaction effects. When solving the problems the source distribution on each ship is obtained analytically and only depends on the thickness of the ship being considered. A system of singular integral equations is obtained for the vortex distributions. These equations have non-unique solutions, and a Kutta condition on each ship is used to determine the solution appropriate to a given situation.

In each chapter there is a description of a numerical procedure suitable for solving the particular kind of integral equation derived. The procedure is, however, almost identical in each case and involves replacing integration by summation to obtain a matrix equation for the vorticity. In the unsteady problems this is further complicated by the need to include time dependent effects within the matrix equation.

An algorithm for the computation of sway force and yaw moment is described. Where possible, the results from this algorithm are compared with published experimental results. These comparisons show that the algorithm works satisfactorily. The results of some of the calculations done, are discussed in detail. The results are interpretated qualitatively to give insight into what is actually occurring to the ships during some ship manoeuvres.

CHAPTER 2

STEADY INTERACTIONS BETWEEN A SHIP AND THE BOUNDARY OF THE WATER

2.1 INTRODUCTION

Bank suction is a significant problem in ship manoeuvring, and a number of studies have recently appeared of this hydrodynamic problem, e.g. as reviewed by Tuck [24]. In most such studies it is assumed that the water is of constant depth, and that the bank is a vertical wall. Although this assumption allows study of qualitative effects of greatest interest, some doubt remains as to whether the phenomenon is affected by bottom geometry.

A complete theoretical or computational study of ship manoeuvring in variable bottom topography would seem to be out of the question. Unless the bottom contours are straight and parallel to the ship's track, the flow is unsteady, and a new boundary value problem must be solved for Laplace's equation at each instant of time. By restricting consideration to the steady-flow case, the problem is reduced to that of solving only one boundary-value problem.

For general depths, this boundary-value problem is three-dimensional, and involves the complete hull and bottom geometry; again, a somewhat daunting task, at least for routine computations. It will be assumed that the water is shallow, i.e. that the depth is small compared to other important length scales. In the present case, this means small compared to the ship's length. At the same time, it is convenient to assume that the ship is slender, with beam and draft comparable to the water depth.

The effect of this further approximation is to reduce the task to that of solving two sets of two-dimensional boundary-value problems.

The inner problem is to solve the two-dimensional Laplace's equation at each vertical ship cross-section, with uniform (local) depth, no banks, walls or beaches, and a "rigid-wall" free surface. This is a solved problem; work such as that of Taylor [21] and Yeung [26] provides the output quantities of interest, namely parameters which characterize the geometry of the ship as seen by an outer observer far from the ship.

The outer problem is to solve the linearized shallow-water equation, allowing variable depth, banks, wall or beaches. This is a two-dimensional problem in the horizontal plane, in which the ship is modelled as an equivalent infinitesimally-thin porous airfoil. The parameters of this equivalent airfoil (thickness, camber, porosity) are determined from the solution of the inner flow problem at each section.

This outer problem is still a little too difficult for routine solution with arbitrary Froude number and bottom topography. New solutions are provided here only in the case of a uniformly-sloping beach, and assume in this case that the Froude number is zero, i.e. that the free surface is replaced by a rigid wall in the outer as well as the inner region. Known results in the case of a vertical bank, in water of constant depth, are also reproduced.

The zero-Froude-number assumption is not unreasonable, since in the real manoeuvring situation the ship is forced for safety reasons to travel slowly, if there is significant bank suction. However, from the theoretical point of view, there are some difficulties with this assumption near any point where the depth tends to zero, such as at the shoreline of a beach.

An interesting feature of the uniform slope equation, is that it is formally identical to that for axisymmetric flow, the distance from shore playing the role of the radius co-ordinate. Thus the outer problem is the same as for flow through and around an equivalent

"annular airfoil" or collar. Thus it is possible to make use of previously determined solutions to this class of problem. In particular, the fundamental building block for the numerical solution is the velocity potential for a ring vortex, which can be expressed in terms of elliptic functions.

The computed results give the side forces and moments on the ship. Collections of such results for various ship geometries, both for banks and beaches are presented. The results are much as might be expected on intuitive grounds. For example, the force near a beach is greater than that at the same distance from a bank, since the "effective" distance is smaller. An equivalent statement is the volume of water between the ship and the beach is smaller than the volume between the ship and the bank.

This work is contained in the paper King and Tuck [16] and the following discussion will follow that paper closely.

2.2 MATHEMATICAL FORMULATION

Consider a ship moving at uniform speed U in the $-x$ direction along $y = 0$, in water of depth $h = h(y)$. Viewed in a frame of reference fixed in the ship, the flow is steady and the disturbance velocity potential ϕ satisfies the linearized shallow-water equation

$$\left(1 - \frac{U^2}{gh(y)}\right) \phi_{xx} + \phi_{yy} + \frac{h'(y)}{h(y)} \phi_y = 0. \qquad (2.2.1)$$

This equation is valid except very near the ship, as an approximation as $h/\ell \to 0$, where 2ℓ is the ship length. Note that ϕ is, to leading order in shallowness, independent of the vertical co-ordinate z.

Here the limiting case of low Froude number, $U^2/gh \to 0$, is considered, in which case (2.2.1) reduces to

$$\phi_{xx} + \phi_{yy} + \frac{h'(y)}{h(y)} \phi_y = 0. \qquad (2.2.2)$$

In particular, for constant depth h=constant, (2.2.2) reduces to the two-dimensional Laplace equation

$$\phi_{xx} + \phi_{yy} = 0, \qquad (2.2.3)$$

in the (x,y) horizontal plane. The only other specific case treated here is of a uniform slope β, i.e.

$$h(y) = h_0 + \beta y, \qquad (2.2.4)$$

in which

$$\phi_{xx} + \phi_{yy} + \frac{\beta}{h_0+\beta y} \phi_y = 0. \qquad (2.2.5)$$

Defining

$$r = y + h_0/\beta \qquad (2.2.6)$$

and substituting in (2.2.5) gives

$$\phi_{xx} + \phi_{rr} + \frac{1}{r} \phi_r = 0 \qquad (2.2.7)$$

which is the equation for axisymmetric irrotational flow, with r as a cylindrical polar co-ordinate.

The task is to solve (2.2.3) or (2.2.7), subject to suitable boundary conditions. The ship, being slender, is represented in the limit as its beam/length ratio tends to zero, by a line segment $y = 0\pm$, $|x| < \ell$, of the x-axis in the (x,y) plane. The analogy is therefore with a thin airfoil. This airfoil is two-dimensional if h=constant, so that (2.2.3) holds. On the other hand, the equivalent airfoil is in the form of an annulus or "collar" $r = h_0/\beta$ in an axisymmetric flow, in the case of a uniform slope, where (2.2.7) holds.

The actual nature of the limiting boundary condition on the hull must be established by an inner expansion in the immediate neighbourhood of the ship, as in Tuck [23]. In the special case where the ship is a vertical strut, i.e.

$$f^-(x) < y < f^+(x), \quad |x| < \ell \tag{2.2.8}$$

the appropriate boundary condition is simply the usual thin-airfoil condition (Ashley and Landahl, [3])

$$\frac{\partial\phi}{\partial y}(x,0\pm) = U\, f^{\pm\prime}(x) \ . \tag{2.2.9}$$

These two conditions on $y = 0\pm$ can alternatively be expressed in terms of a <u>mean</u> normal velocity

$$\bar{\phi}_y = \tfrac{1}{2}\phi_y(x,0_+) + \tfrac{1}{2}\phi_y(x,0_-) = U\,\bar{f}'(x), \tag{2.2.10}$$

and a <u>jump</u> in normal velocity

$$\Delta\phi_y = \phi_y(x,0_+) - \phi_y(x,0_-) = U\Delta f'(x), \tag{2.2.11}$$

where

$$\bar{f}(x) = \tfrac{1}{2}f^+(x) + \tfrac{1}{2}f^-(x) \tag{2.2.12}$$

is the camber of the strut and

$$\Delta f(x) = f^+(x) - f^-(x) \tag{2.2.13}$$

is its thickness. For a strut with lateral symmetry, yawed at an angle of attack α, the camber is simply

$$\bar{f}(x) = -\alpha x \ . \tag{2.2.14}$$

The most general case of a ship of arbitrary cross section, with non-zero bottom clearance, is discussed by Tuck [23]. The equivalent airfoil is now clearly porous, since the bottom clearance allows some water to pass through the limiting line segment $y = 0\pm$, $|x| < \ell$. So instead of (2.2.10),

$$\bar{\phi}_y - U\bar{f}'(x) = \frac{1}{2h_0 C}\,\Delta\phi \tag{2.2.15}$$

where

$$\Delta\phi(x) = \phi(x,0_+) - \phi(x,0_-) \tag{2.2.16}$$

is the jump in velocity potential across the airfoil, and $C(x)$ is the non-dimensional blockage coefficient (Taylor, [21]) of the ship section at state x in water of depth h_0. If there is no clearance, $C(x) \to \infty$, and (2.2.15) reduces to (2.2.10). Since the jump in pressure across the foil is proportional to $\Delta\phi'(x)$, (2.2.15) indicates a net flow through the equivalent porous airfoil.

In a quite general case with a laterally unsymmetric ship, the appropriate choice of the camber function $\bar{f}(x)$ is not at all obvious, and in general it is necessary to solve an inner-flow problem at each section to determine $\bar{f}(x)$ (Tuck [23]). However, if each ship section possesses lateral symmetry about the mean line $y = \bar{f}(x)$, then $\bar{f}(x)$ may be taken as the appropriate camber function. In particular, in the case of symmetric ships at an angle α of yaw, (2.2.14) still applies.

The normal-velocity jump condition (2.2.11) is also modified in the general case, but in a simpler manner. In fact (2.2.11) still applies, with the strut thickness $\Delta f(x)$ replaced by the mean thickness of the

actual hull, averaged over the local water depth. That is

$$\Delta f(x) = \frac{S(x)}{h_0} , \tag{2.2.17}$$

where $S(x)$ is the immersed cross-sectional area of the hull at station x.

The only remaining boundary conditions are at infinity, where

$$\phi \to 0 \quad \text{as} \quad y \to \infty \tag{2.2.18}$$

and at the location of any bank or shoreline; if such a boundary lies at $y = -Y$, say, then

$$\phi_y(x,-Y) = 0. \tag{2.2.19}$$

2.3 SOLUTION PROCEDURE FOR GENERAL DEPTH CONTOURS

The boundary-value problem formulated in 2.2 can be solved formally by a distribution of sources and vortices over the segment representing the ship. Thus

$$\phi(x,y) = \int_{-\ell}^{\ell} \left\{ q(\xi) G(x,y;\xi,0) + \gamma(\xi) H(x,y;\xi,0) \right\} d\xi , \tag{2.3.1}$$

where $G(x,y;\xi,\eta)$ satisfies (2.2.2) except at $(x,y) = (\xi,\eta)$ where it behaves like a unit source, and $H(x,y;\xi,\eta)$ is the potential for a unit vortex, which is also a singular solution of (3.2.2) and is related to G by

$$H_\xi = - G_\eta + \frac{h'(\eta)}{h(\eta)} G. \tag{2.3.2}$$

In fact G and H depend on x and ξ only via their difference $x - \xi$.

On substitution into the thickness boundary condition (2.2.11), the source strength $q(x)$ is immediately found to be

$$q(x) = \Delta\phi_y$$
$$= U\,\Delta f'(x)$$
$$= U\,S'(x)/h_0 \quad . \tag{2.3.3}$$

Similarly, substitution into the camber boundary condition (2.2.15) gives an integral equation to determine the vortex strength

$$\gamma(x) = -\frac{d}{dx}\,\Delta\phi(x), \tag{2.3.4}$$

namely

$$\int_{-\ell}^{\ell} \gamma(\xi)H_y(x,0;\xi,0)d\xi + \frac{1}{2h_0 C(x)}\int_{-\ell}^{x} \gamma(\xi)d\xi$$
$$= U\,\bar{f}'(x) - \int_{-\ell}^{\ell} q(\xi)\left[\tfrac{1}{2}G_y(x,0_+;\xi,0) + \tfrac{1}{2}G_y(x,0_-;\xi,0)\right]d\xi \quad . \tag{2.3.5}$$

The integral equation (2.3.5) is simplified by introducing a new kernel function K_x, defined by

$$K_x(x,\xi) = H_y(x,0;\xi,0) + \frac{u(x-\xi)}{2h_0 C(x)} \tag{2.3.6}$$

where

$$u(x) = \begin{cases} 0 & x < 0 \\ 1 & x > 0 \end{cases} \quad . \tag{2.3.7}$$

Equation (2.3.5) may be written in the form

$$\int_{-\ell}^{\ell} \gamma(\xi)K_x(x,\xi)d\xi = U\,g'(x), \tag{2.3.8}$$

where $U\,g'(x)$ is written for the function on the right-hand side of (2.3.5), which measures the crossflow due to camber $\bar{f}(x)$ of the ship and in addition an induced crossflow due to the thickness of the ship in a laterally-asymmetric flow. It is convenient to define a kernel $L(x)$ to describe the latter effect, whose derivative satisfies

$$L'(x-\xi) = \tfrac{1}{2}G_y(x,0_+;\xi,0) + \tfrac{1}{2}G_y(x,0_-;\xi,0) \qquad (2.3.9)$$

and set

$$g'(x) = \bar{f}'(x) - \frac{1}{h_0}\int_{-\ell}^{\ell} S'(\xi)L'(x-\xi)d\xi \ . \qquad (2.3.10)$$

Note that if the bottom geometry is symmetric about $y = 0$, then $L = 0$, and the only cross flow is that due to camber of the ship.

2.4 NUMERICAL PROCEDURE FOR SOLVING INTEGRAL EQUATION

A direct numerical procedure is used to solve the integral equation (2.3.8), by replacement of integration with summation using a method of discretization, and inversion of the resulting matrix equation. The method is similar to that used by Tuck and Newman [25].

First take the indefinite integral with respect to x of equation (2.3.8), giving

$$\int_{-\ell}^{\ell} \gamma(\xi)K(x,\xi)d\xi = U\, g(x) + C_0 \qquad (2.4.1)$$

where $K(x,\xi)$ is determined by integration of equation (2.3.6), and $g(x)$ from equation (2.3.10), for the Green's function G appropriate to the particular choice of $H(y)$. The constant C_0 is for the moment an arbitrary constant of integration, ultimately determined by application of the Kutta condition at the trailing edge.

To find a numerical solution, suppose the unknown function $\gamma(x)$ can be represented by a step function on the ship, the value on the j^{th} interval $x_{j-1} < x < x_j$ being taken as the constant $\gamma(x) = \gamma_j$. Since square root singularities are expected at the ends of the ship, the distribution of the points x_j must be chosen so as to counter these singularities. A distribution of the points with the correct properties is

$$x_j = -\ell \cos(j\pi/N), \tag{2.4.2}$$

for a mesh of $N + 1$ points on the ship.

Replacing $\gamma(x)$ in equation (2.4.1) by such a step function gives

$$\sum_{j=1}^{N} \gamma_j \int_{x_{j-1}}^{x_j} K(x,\xi)d\xi = U\, g(x) + C_0 \ . \tag{2.4.3}$$

The integral is evaluated at points $x = \bar{x}_i$ which are near the centre of the i^{th} interval, specifically

$$\bar{x}_i = -\ell \cos((i-\tfrac{1}{2})\pi/N). \tag{2.4.4}$$

The equation may then be written as

$$\sum_{j=1}^{N} \gamma_j \int_{x_{j-1}}^{x_j} K(\bar{x}_i,\xi)d\xi = U\, g(\bar{x}_i) + C_0, \quad i = 1,2,\ldots,N, \tag{2.4.5}$$

or, equivalently, the matrix equation

$$A\underset{\sim}{\gamma} = U\, \underset{\sim}{g} + C_0 \underset{\sim}{e} \tag{2.4.6}$$

where

$$A = [A_{ij}], \ \underset{\sim}{\gamma} = [\gamma_j], \ \underset{\sim}{g} = [g(\bar{x}_i)] \text{ and } \underset{\sim}{e} = [1], \tag{2.4.7}$$

with

$$A_{ij} = \int_{x_{j-1}}^{x_j} K(\bar{x}_i,\xi)d\xi \ . \tag{2.4.8}$$

In practice the matrix element A_{ij} are evaluated by separating out the logarithmic singularity at $\xi = x$, and writing

$$K(x,\xi) = \frac{1}{2\pi} \log|x-\xi| + K_{(1)}(x,\xi) \tag{2.4.9}$$

where $K_{(1)}$ is non-singular and without loss of generality can be assumed to vanish at $\xi = x$. Now integrating the logarithm exactly and the non-singular function $K_{(1)}$ by the mid-point rule, yields

$$A_{ij} = \frac{1}{2\pi}\{(x_j - \bar{x}_i)\log|x_j - \bar{x}_i| - (x_{j-1} - \bar{x}_i)\log|x_{j-1} - \bar{x}_i| - (x_j - x_{j-1})\}$$

$$+ (x_j - x_{j-1})K_{(1)}(\bar{x}_i, \bar{x}_j). \qquad (2.4.10)$$

Note that $K_{(1)}$ does not contribute to the diagonal elements A_{ii}.

The solution $\underset{\sim}{\gamma}$ is obtained by direct matrix inversion, with the two right-hand sides $\underset{\sim}{g}$ and $\underset{\sim}{e}$, and may be written as

$$\underset{\sim}{\gamma} = U\,\underset{\sim}{\gamma}^{g} + C_0\underset{\sim}{\gamma}^{e} \qquad (2.4.11)$$

where

$$\underset{\sim}{\gamma}^{g} = A^{-1}\,\underset{\sim}{g},$$

and

$$\underset{\sim}{\gamma}^{e} = A^{-1}\,\underset{\sim}{e}.$$

This is a numerical approximation to a corresponding representation of the actual vortex strength $\gamma(x)$, namely

$$\gamma(x) = U\gamma^{g}(x) + C_0\gamma^{e}(x). \qquad (2.4.12)$$

Thus a numerical approximation to the general solution of the singular integral equation (2.4.1) can be obtained, with C_0 a constant to be determined by the Kutta condition.

The Kutta condition for this class of problem is that the vorticity must vanish on the trailing edge, i.e.

$$\gamma(\ell) = 0. \qquad (2.4.13)$$

There are two ways in which this can be applied. A crude but effective procedure is to require the vorticity on the trailing element to be zero, so that

$$(\underset{\sim}{\gamma})_N = 0,$$

or

$$C_0 = - U(\underset{\sim}{\gamma}^g)_N/(\underset{\sim}{\gamma}^e)_N \ , \qquad (2.4.14)$$

from equation (2.4.11).

A more satisfactory method is to use some of the expected properties of the solution to the singular integral equation as $x \to \ell$. For example, any solution of (2.3.8) must have the property that as $x \to \ell$

$$\gamma(x) \to \frac{D}{\sqrt{\ell-x}} + E\sqrt{\ell-x} \ , \qquad (2.4.15)$$

for some constants D,E. By fitting this function to the last two elements $(\underset{\sim}{\gamma}^{g,e})_{N-1}$ and $(\underset{\sim}{\gamma}^{g,e})_N$, the four constants $D = D^{g,e}$ and $E = E^{g,e}$ may be determined. In order that the Kutta condition (2.4.13) holds, the sum of the inverse-square-root terms involving D must be zero, i.e.

$$UD^g + C_0 D^e = 0,$$

so that

$$C_0 = - UD^g/D^e \ . \qquad (2.4.16)$$

In all results presented the second application of the Kutta condition is used.

2.5 EVERYWHERE-UNIFORM DEPTH

If h=constant everywhere, then

$$G(x,y;\xi,\eta) = \frac{1}{2\pi} \log\sqrt{(x-\xi)^2+(y-\eta)^2} \qquad (2.5.1)$$

and

$$H(x,y;\xi,\eta) = \frac{1}{2\pi} \arctan \frac{y-\eta}{x-\xi} \quad . \tag{2.5.2}$$

Thus the kernel functions K_x and L' defined by (2.3.6), (2.3.9) become

$$K_x = \frac{1}{2\pi(x-\xi)} + \frac{u(x-\xi)}{2h_0 C(x)} \tag{2.5.3}$$

and

$$L' = 0 \quad . \tag{2.5.4}$$

Equation (2.5.4) is expected from the symmetry of the bottom geometry about the ship location $y = 0$.

After integrating (2.5.3) the kernel K is of the form (2.4.9), with $K_{(1)} = K_{(0)}$, where

$$K_{(0)}(x,\xi) = \frac{u(x-\xi)}{2h_0} \int_{-\ell}^{x} \frac{dt}{C(t)} \quad . \tag{2.5.5}$$

The kernel $K_{(0)}$ measures the effect of bottom clearance, and vanishes for zero clearance $(C \to \infty)$. If $K_{(0)} \equiv 0$, the integral equation (2.3.8) is the classical thin-airfoil equation

$$\frac{1}{2\pi} \int_{-\ell}^{\ell} \frac{\gamma(\xi)d\xi}{x-\xi} = U\bar{f}'(x) \tag{2.5.6}$$

whose solution subject to the Kutta condition (2.4.13) is

$$\gamma(x) = -\frac{2U}{\pi} \sqrt{\frac{\ell-x}{\ell+x}} \int_{-\ell}^{\ell} \sqrt{\frac{\ell+\xi}{\ell-\xi}} \frac{\bar{f}'(\xi)}{x-\xi} \, d\xi \quad . \tag{2.5.7}$$

If the clearance is not zero, the problem is that of a porous airfoil, and (2.3.8) becomes

$$\frac{1}{2\pi} \int_{-\ell}^{\ell} \frac{\gamma(\xi)d\xi}{x-\xi} + \frac{1}{2h_0 C(x)} \int_{-\ell}^{x} \gamma(\xi)d\xi = U\bar{f}'(x), \tag{2.5.8}$$

which was first obtained by Newman [17]. Although no closed-form solution such as (2.5.7) appears to exist for arbitrary $C(x)$, $\bar{f}(x)$, integral equations of this type may be readily solved numerically by the procedure described in §3.4. An alternative treatment of (2.5.8) is by the Cauchy Inversion technique as described in Yeung [26]. Non-zero sway force and yaw moment only occur when the ship is yawed to its direction of motion or there is another body or obstacle in the flow.

In the more general cases which follow, it is convenient to express the kernel of the integral equation as a correction to the uniform-depth kernel, that is

$$K(x,\xi) = \frac{1}{2\pi} \log|x-\xi| + K_{(0)}(x,\xi) + \bar{K}(x-\xi) \qquad (2.5.9)$$

or $K_{(1)} = K_{(0)} + \bar{K}$, where $\bar{K}(0) = 0$. Note that all effects of clearance between ship and bottom, are incorporated in $K_{(0)}$, and $\bar{K}$ depends only on the bottom topography.

2.6 MOTION PARALLEL TO A VERTICAL WALL IN UNIFORM DEPTH

If there is a vertical wall at $y = -Y$, this wall may be modelled by images, obtaining the potential for a unit source at (ξ,η) as

$$G(x,y;\xi,\eta) = \frac{1}{2\pi} \log\sqrt{(x-\xi)^2 + (y-\eta)^2} + \frac{1}{2\pi} \log \sqrt{(x-\xi)^2 + (y+\eta+2Y)^2} \qquad (2.6.1)$$

and the potential for a unit vortex at (ξ,η) as

$$H(x,y;\xi,\eta) = \frac{1}{2\pi} \arctan \frac{y-\eta}{x-\xi} - \frac{1}{2\pi} \arctan \frac{y+\eta+2Y}{x-\xi} . \qquad (2.6.2)$$

Thus the necessary kernel function for (2.5.9) is

$$\bar{K}(x) = -\frac{1}{4\pi} \log\left[1 + \frac{x^2}{4Y^2}\right] \qquad (2.6.3)$$

where $\bar{K}(0) = 0$ as required and the induced-camber kernel is

$$L(x) = \frac{1}{4\pi} \arctan \frac{x}{2Y} \quad . \tag{2.6.4}$$

This is the bank-suction problem. Recently Hess [10] has investigated this with particular emphasis on the yaw angle (which is usually small) and rudder angle required to give a zero sway force and yaw moment.

2.7 MOTION PARALLEL TO A UNIFORM BEACH

Consider a uniformly-sloping beach with a shoreline at $y = -Y$, i.e. with slope $\beta = h_0/Y$. The appropriate Green's function is that for a ring source of radius $r = Y$, where $r = y + Y$, as in (2.2.6). The potential of such a source can be written as an integral of Bessel functions, i.e.

$$G(x,y;0,0) = -\tfrac{1}{2}Y \int_0^\infty e^{-p|x|} J_0(pr)J_0(pY)dp \tag{2.7.1}$$

and the corresponding ring vortex is given by

$$\operatorname{sgn} x.H(x,y;0,0) = -\tfrac{1}{2}Y \int_0^\infty e^{-p|x|} J_0(pr)J_1(pY)dp. \tag{2.7.2}$$

These integrals can also be written in terms of complete elliptic integrals, e.g.

$$G(x,y;0,0) = -\frac{Y}{\pi R} \underset{\sim}{K}(m) \tag{2.7.3}$$

where

$$\begin{aligned} R^2 &= x^2 + (r+Y)^2 \\ &= x^2 + (y+2Y)^2, \end{aligned} \tag{2.7.4}$$

$$m = \frac{4rY}{R^2} \quad , \tag{2.7.5}$$

and

$$\underset{\sim}{K}(m) = \int_0^{\pi/2} \frac{d\theta}{\sqrt{1-m\sin^2\theta}} \tag{2.7.6}$$

is a complete elliptic integral (Abramowitz and Stegun [1]). Upon carrying out the required differentiations and integrations, it is found that the necessary kernel functions are

$$\bar{K}(x) = -\frac{1}{\pi m^{1/2}}\left[(1-\tfrac{1}{2}m)\underset{\sim}{K}(m)-\underset{\sim}{E}(m)\right] - \frac{1}{2\pi}\log|x| - \frac{1}{\pi} + \frac{1}{2\pi}\log 8Y \tag{2.7.7}$$

and

$$L(x) = \frac{x}{2\pi R}\underset{\sim}{K}(m) \tag{2.7.8}$$

where now $y = 0$ or $r = Y$ in the definitions of R and m, i.e.

$$R = \sqrt{x^2 + 4Y^2} \tag{2.7.9}$$

and

$$m = \frac{4Y^2}{x^2 + 4Y^2}\,. \tag{2.7.10}$$

$\underset{\sim}{E}(m)$ is the corresponding elliptic integral of the first kind. Note that as $x \to 0$, $m \to 1$ and the elliptic integral $\underset{\sim}{K}$ possesses a logarithmic singularity of the correct strength so that the function $\bar{K}$ is well behaved. The constants " $-\frac{1}{\pi} + \frac{1}{2\pi}\log 8Y$" are included so that $\bar{K}(0) = 0$, as required.

2.8 SWAY FORCE AND YAW MOMENT

The quantities of main interest are the sway force Y and the yaw moment N' acting on the ship. The linearized Bernoulli equation yields the pressure

$$p = - \rho U \phi_x \tag{2.8.1}$$

where ρ is the density of water. The sway force can then be calculated by finding the total y-directed pressure. That is,

$$Y = - \iint_{\substack{\text{hull of} \\ \text{ship}}} p\,dx\,dz$$

$$= - \rho U \int_{-\ell}^{\ell} dx \int_{C(x)} \phi_x \, dz \tag{2.8.2}$$

where $C(x)$ is the cross section curve of the ship at station x. It is convenient to introduce a function Γ such that

$$\Gamma = \int_{C(x)} \phi_x \, dz = \int_{C(x)} \phi_x \frac{\partial y}{\partial n} \, d\ell \tag{2.8.3}$$

where $\underset{\sim}{n}$ is the normal into the fluid.

Consider the closed path of integration shown in Figure 2.1. Since this is an inner problem, the local water depth may be assumed constant. By Green's theorem for this path

$$\oint \phi_x \frac{\partial y}{\partial n} \, d\ell = \oint y \frac{\partial \phi_x}{\partial n} \, d\ell \, , \tag{2.8.4}$$

which, together with the boundary conditions that $\frac{\partial \phi}{\partial z} = 0$ on the free surface, and $\frac{\partial \phi}{\partial n} = 0$ on C and $z = h(z)$, gives

$$\Gamma = \oint y \frac{\partial \phi_x}{\partial n} \, d\ell - \oint_{S_{\pm\infty}} \phi_x \frac{\partial y}{\partial n} \, d\ell \, . \tag{2.8.5}$$

But,

$$\oint y \frac{\partial \phi_x}{\partial n} \, d\ell = 0, \tag{2.8.6}$$

so

$$\Gamma = - \int_{S_{\pm\infty}} \phi_x \frac{\partial y}{\partial n} \, d\ell$$

$$= h \, \gamma(x) \tag{2.8.7}$$

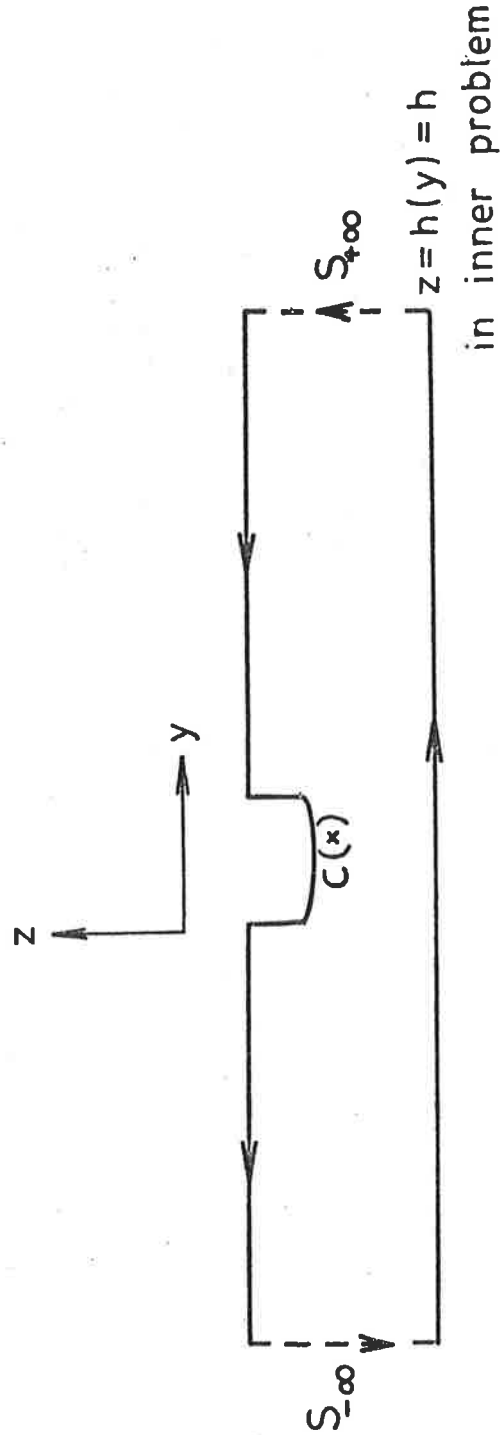

2.1 Path of Integration used in determining the sway force and yaw moment.

by equation (2.3.4) when considering this as an inner problem. Thus the expression for the sway force is

$$Y = \rho U h \int_{-\ell}^{\ell} dx\ \gamma(x). \qquad (2.8.8)$$

Similarly the yaw moment is given by

$$N = \rho U h \int_{-\ell}^{\ell} dx\ x\ \gamma(x). \qquad (2.8.9)$$

2.9 RESULTS

The preceding sections provided a formulation and a numerical solution technique for an arbitrary slender body moving parallel to a beach or a bank in shallow water. Here the application is to ships, so consider slender bodies which are laterally symmetric, and nearly (but not necessarily exactly) fore-and-aft symmetric. The formulation itself made no symmetry assumptions, so the effects of yaw on the motion of a ship can now be studied.

In order that the blockage coefficient C can be evaluated easily when needed, only ships with rectangular cross-sections and constant draught are considered. Then, if the clearance-to-draft ratio is small, Taylor's [21] formula for the blockage coefficient may be used. This restricts the investigation to situations with small clearance-to-draught ratios, but, as the results show that the magnitude of the forces and moments on the ship decrease rapidly as the clearance increases, this is the most interesting region.

The quantities of main interest are the sway force Y and the yaw moment N acting on a ship near a wall or beach. So that subsequent results can be presented as dimensionless coefficients, the dimensionless sway force coefficient C_Y and dimensionless yaw moment coefficients C_N about amidships are

$$C_Y = \frac{Y}{\frac{1}{2}\rho U^2 L^2} \tag{2.9.1}$$

and

$$C_N = \frac{N}{\frac{1}{2}\rho U^2 L^3} \tag{2.9.2}$$

respectively where $L = 2\ell$ is the length of the ship and the sway force Y and the yaw moment N are given by (2.8.8) and (2.8.9).

The programs used to produce the following results were written in FORTRAN and run on the University of Adelaide's Control Data Cyber 173. The execution time for a typical computation was 458 seconds. In that time the sway force and yaw moment on a ship in the presence of a wall and,separately,a beach,were calculated for twenty different depths of water. At each of these depths the porosity contributions to the matrix equations had to be recalculated. Also, the computation is considerably slower in the beach case, as the elliptic integrals required are much slower to calculate than the corresponding terms for a vertical wall.

To check the validity of the results, the calculations required to produce Figures 2 and 3 of Hess [10] were carried out using the above technique. It was found that, to graphing accuracy, when using a mesh of 40 points on the ship, the results computed by the above theory were indistinguishable to those of Hess for a ship moving parallel to a wall.

In the first place, it is desirable to investigate the effect of changing the shape of a ship, so that the extent to which results for mathematically-defined bodies may be generalized to real ships can be estimated. For ships which have a beam/length ratio of 1/8 and draught/length ratio of 1/16, the effect of varying the water depth on various ship shapes was studied, with the ships a distance η of 0.2ℓ from a vertical wall or the shoreline of a uniformly-sloping beach.

Figure 2.2 shows the five different water-plane shapes which were investigated. In Figures 2.3 and 2.4, the sway force is plotted against the local water depth at the ship, for a vertical wall and a beach respectively. It can be seen that results for ships A, B and D and ships C, E are essentially identical. The graphs all show the same decreasing behaviour as the depth increases, and hence the bottom clearance increases. Even though ship C is ship B running backwards, there is a significant difference in the sway force. Ships A,B and D, which have the same water-plane for $x > 0$ have the same sway force. Similarly for ships C and E. So, for the five ship shapes considered, it appears that the sway force is determined more by the aft shape of the ship than the fore of the ship. These figures show that although it is hard to predict what effect changing the shape will have on the sway force, it appears that some general quantitative conclusions can be made about the sway force, regardless of the shape of the ship.

When the corresponding results for the yaw moment are examined (Figures 2.5 and 2.6) it can be seen that now the values of the moment are quite scattered. In the zero-clearance case (depth/draught = 1)it can be seen that there is a non-zero moment for the ships which are not fore-aft symmetric. Also, at zero clearance, the direction of the non-zero moment is such that the blunter end moves towards the boundary and the yaw moment acting on ship B is equal and opposite to that on ship C. It is not surprising that ships A and D give such similar results, as their shapes are quite similar. In contrast to the force case, it is necessary to be cautious when generalizing the results for the yaw moment to real hull geometries, since the moment depends to a much greater extent on the shape of the ship. All subsequent results are for a ship of parabolic water-plane shape (i.e. type E).

Before comparing the results for a constant-slope beach with those for a vertical wall, it is convenient to examine the effect of changing the beach angle. The numerical values for four different beach angles β (see Figure 2.7) are given in Figures 2.7 to 2.11. The horizontal scale on all the figures is the depth/draught ratio at the ship's position. For a given depth/draught ratio, the four lines on each graph are therefore at four different distances from the shore. Figure 2.7 is a graph of the sway force, for the ship moving parallel to the shoreline at zero angle of attack, whereas Figure 2.8 shows the sway force for a ship yawed to an angle of attack of $\arctan 0.1 \simeq 5.7$ degrees to the shoreline. In the case of zero angle of attack, the sway force is toward the shore, and for a given depth it is greater for beaches of greater slope, since the ship is nearer to the shore in such cases. If the sway force had been plotted instead against distance from the shore, it would have appeared that in general the sway force is greatest for the beach of <u>least</u> slope. In Figure 2.8, it can be seen that, even for this small angle of attack, the sway force has already become repulsive (i.e. force away from the beach). In fact, for an angle of attack of only 0.5 degrees away from the beach, the sway force is repulsive for $\beta = 0.05$.

The yaw moments corresponding to the situations of Figures 2.7 and 2.8 respectively are given in Figures 2.9 and 2.10. Here it can be seen that, at zero angle of attack, the moment turns the bow away from the wall, and that yawing the bow increases this moment. It is interesting to find the angle α at which the ship must be yawed to make the sway force or yaw moment zero. The tangent of this angle is shown in Figures 2.11 and 2.12, for the force and moment respectively. Two features are immediately apparent from these figures. Firstly, the angle required is very small, for both force and moment, and secondly the sign of the angle is different in each case. This means that a

symmetric ship without a rudder cannot yaw itself so as to experience simultaneously zero sway force and yaw moment, when moving parallel to a boundary. In a slowly-varying dynamic situation, the above results show that the ship would begin to turn away from the shore and, as this would decrease the attractive force and increase the bow-away moment, the ship would subsequently turn further away. Eventually even the sway force itself would be away from the shore, accelerating this tendency.

It is of interest to compare the forces and moments due to a vertical wall with those from a uniformly-sloping beach. To do this, consider a ship at a distance η from the shoreline or wall, and in water of depth h. This will then determine the appropriate beach angle. To graph the results η was fixed at various values and h varied, which means that the beach angle β is different for each value of h.

In Figures 2.13 to 2.16 the numerical results for a wall and a beach are compared, for three different values of η. The results for the wall are given by solid lines and for the beach by dashed lines. The sway force for a ship which is not yawed is given in Figure 2.13. Immediately, it can be seen that the force due to a wall is smaller than that due to the beach, which could have been anticipated, since there is a greater volume of water between the ship and the wall than between the ship and the beach. The yaw moment corresponding to this sway force is shown in Figure 2.14. Again, the values for the beach are greater than those for the corresponding wall. All moments are zero for zero bottom clearance, and rise rapidly to a maximum as a function of water depth before decreasing. The moments are zero for zero bottom clearance as ship E is fore-aft symmetric, whereas if a ship without this symmetry is used, a non-zero yaw moment would be expected. It is apparent that, unlike the sway force, whose maximum

occurs for zero clearance, the yaw moment reaches its maximum at a small but non-zero clearance.

When the ship is yawed at an angle whose tangent is 0.1, the sway force and yaw moment are shown in Figures 2.15 and 2.16. In contrast to before, the force is greater in the case of the wall than the beach. In general, the yaw moment due to the beach is greater than that for the wall for the corresponding distance from the boundary.

This chapter provides a technique which can be used to find the effect of different bottom topographies on the motion of a ship. It shows that the results obtained from a bank suction investigation cannot always be readily used to predict the effect of some other bottom topography. Thus care must be taken when trying to formulate general conclusions from such an investigation.

$$
\left.\begin{array}{ll}
\text{SHIP A} & b(x) = b\sqrt{1-x^2} \\
\text{SHIP B} & b(x) = \begin{cases} b(1-x^2) & x \leqslant 0 \\ b\sqrt{1-x^2} & x > 0 \end{cases} \\
\text{SHIP C} & b(x) = \begin{cases} b\sqrt{1-x^2} & x \leqslant 0 \\ b(1-x^2) & x > 0 \end{cases} \\
\text{SHIP D} & b(x) = \begin{cases} b(1-x^4) & x \leqslant 0 \\ b\sqrt{1-x^2} & x > 0 \end{cases} \\
\text{SHIP E} & b(x) = b(1-x^2)
\end{array}\right\} \quad |x| \leqslant 1
$$

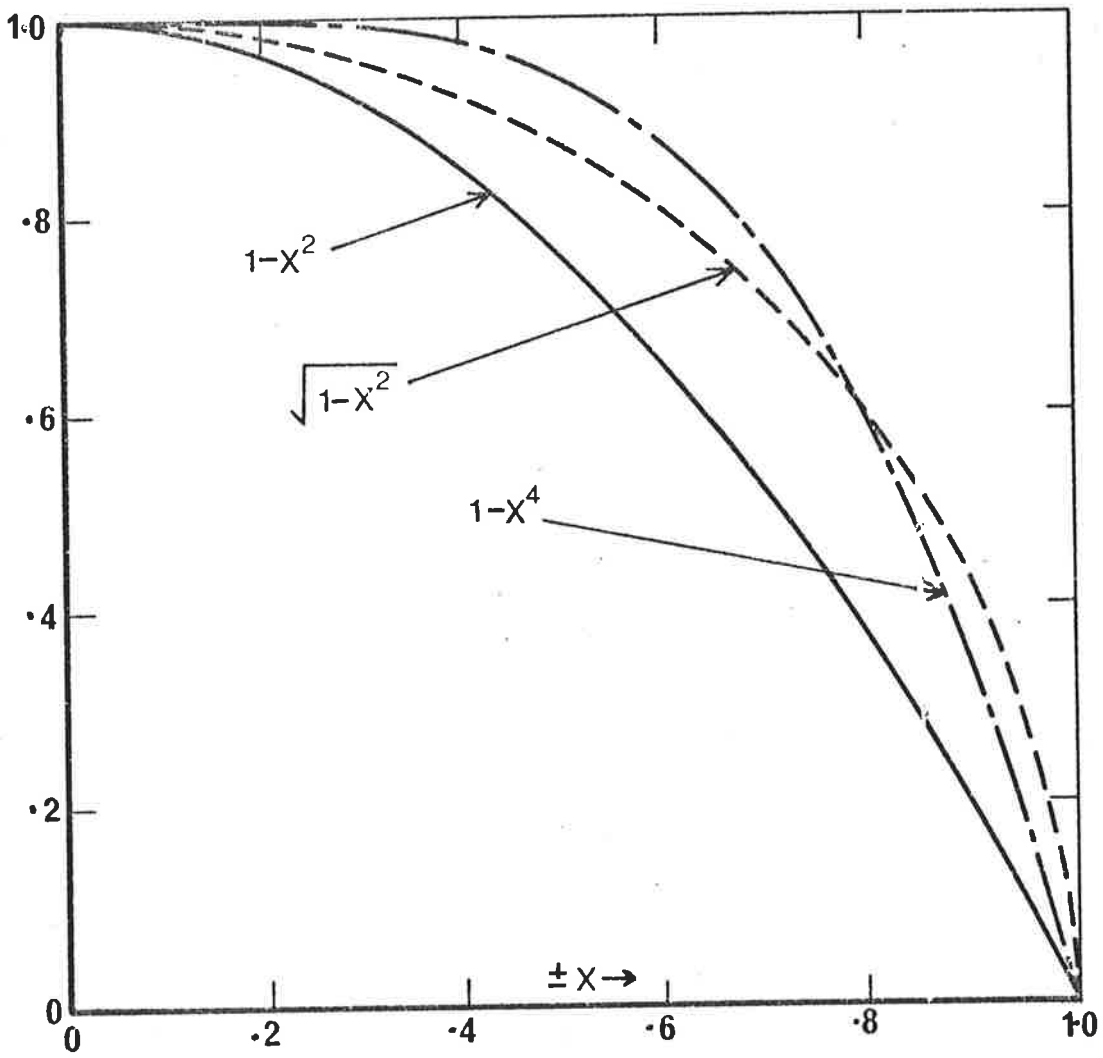

2.2 Functions describing the breadth of a ship $b(x)$ for a maximum beam b and a ship length 2.

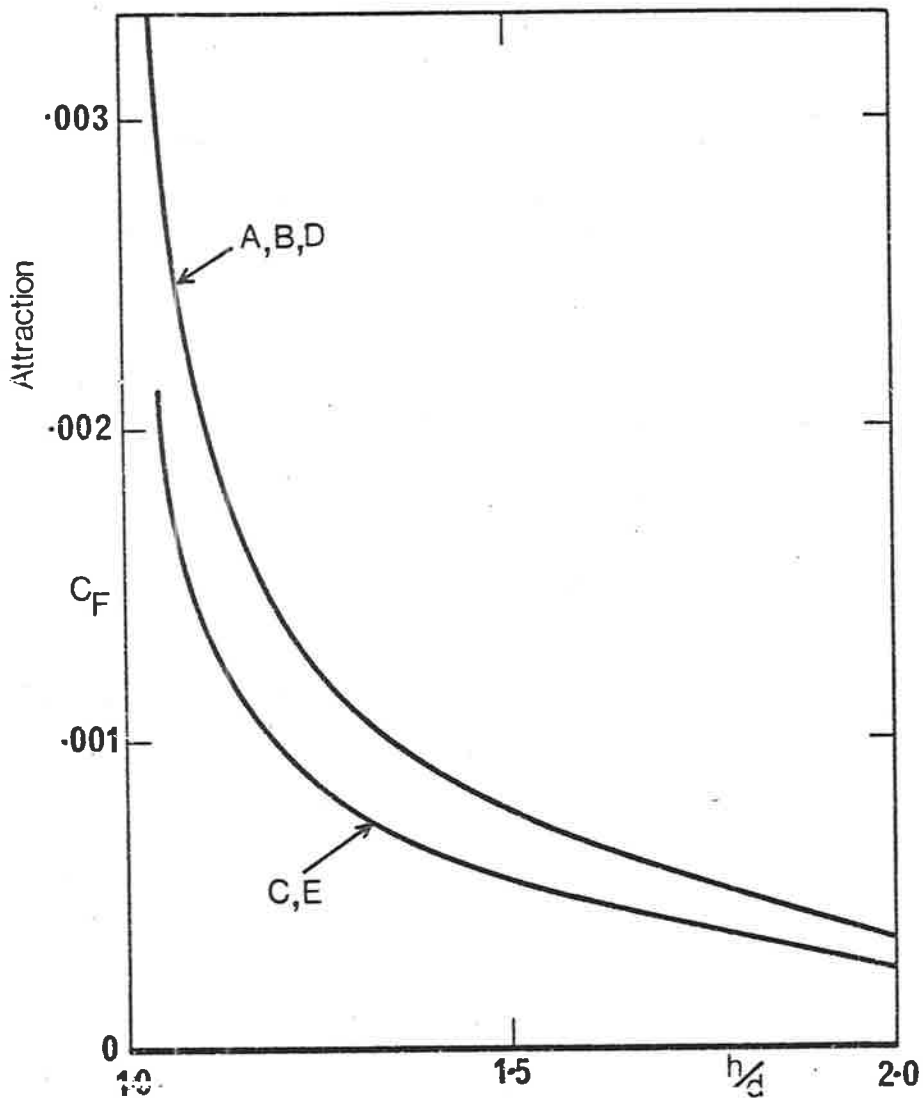

2.3 Variation of coefficient of sway force C_F as the depth to draught ratio h/d increases for the ships moving parallel to a vertical wall.

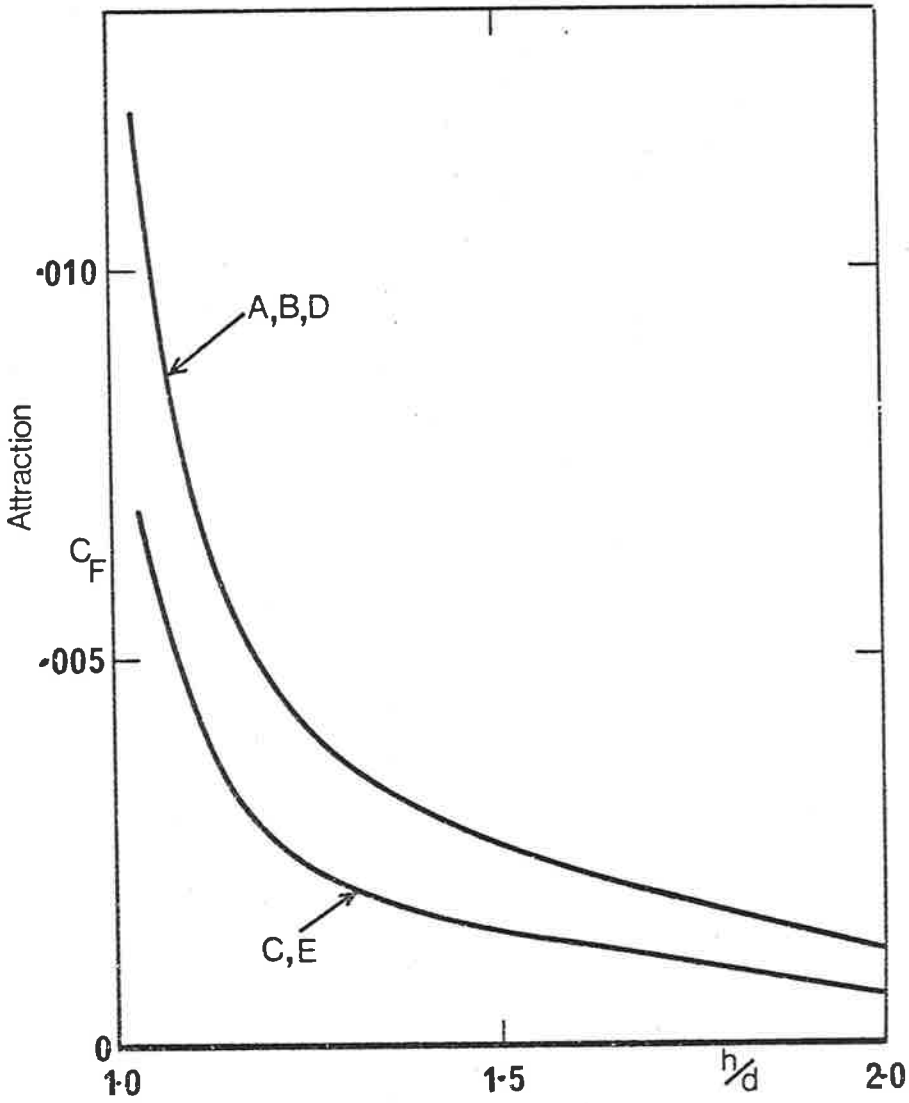

2.4 Variation of coefficient of sway force C_F as the depth to draught ratio h/d increases for the ships moving parallel to a beach.

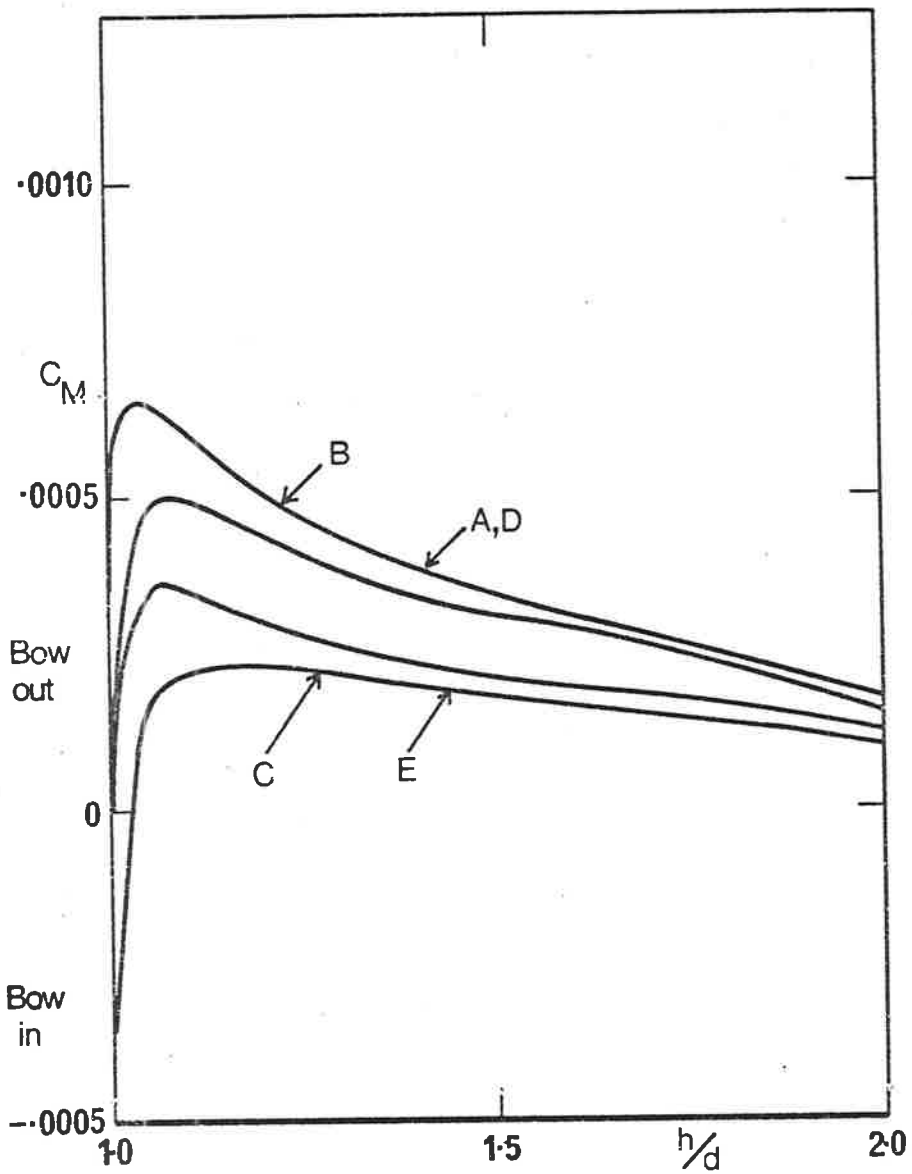

2.5 Variation of coefficient of yaw moment C_M as the depth to draught ratio h/d increases for the ships moving parallel to a vertical

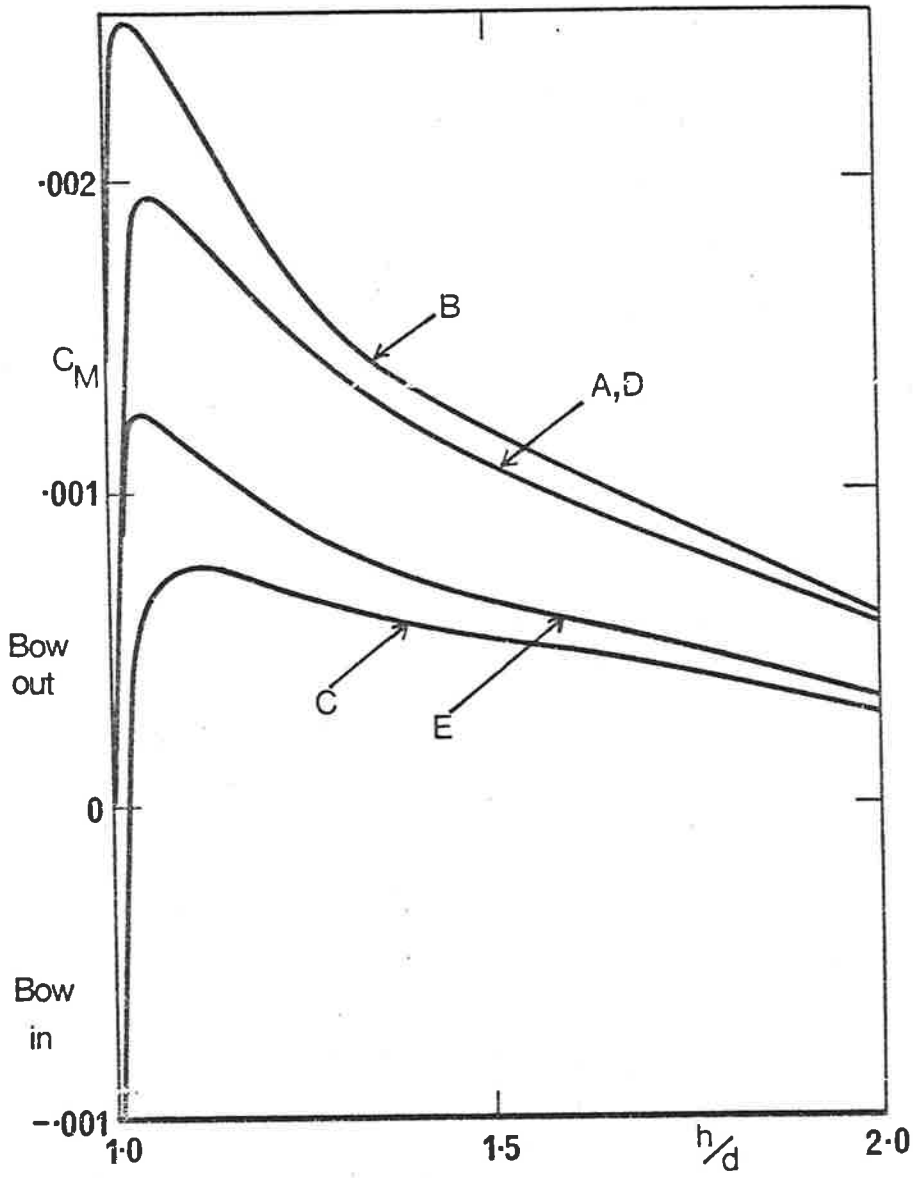

2.6 Variation of coefficient of yaw moment C_M as the depth to draught ratio h/d increases for ships moving parallel to a beach.

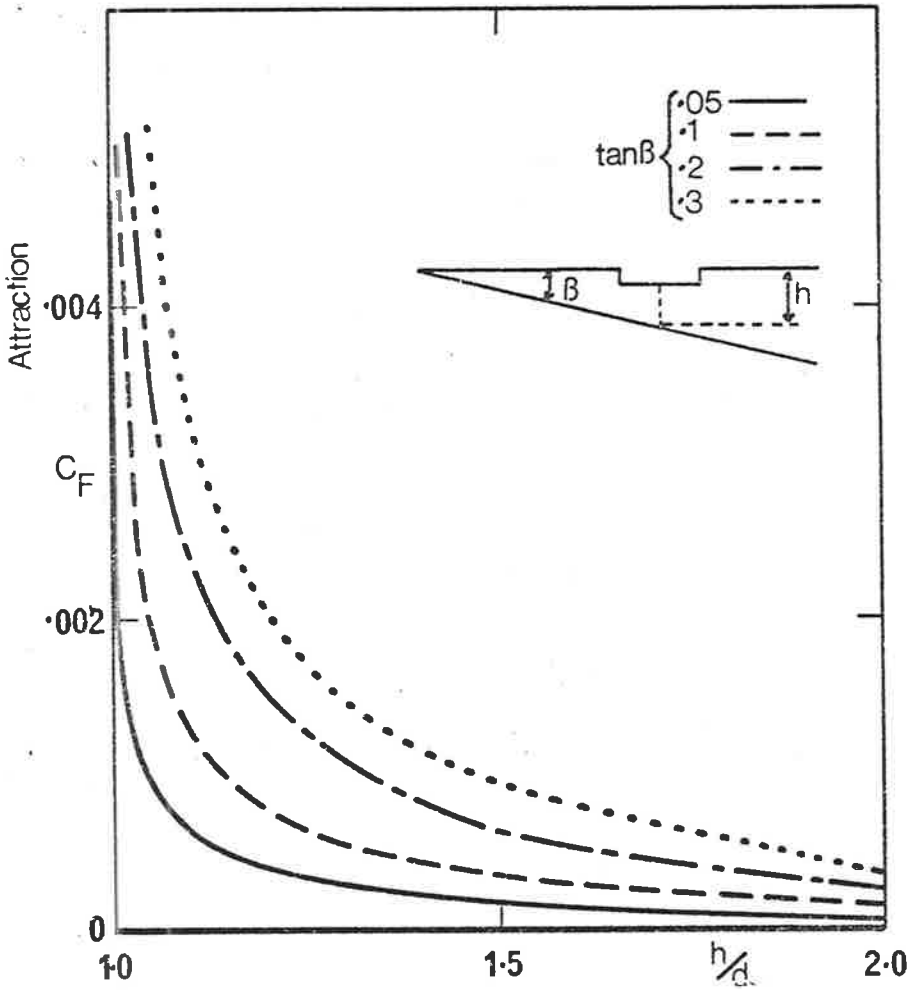

2.7 Beach induced coefficient of sway force C_F as a function of the depth to draught ratio h/d for various beach angles β for ship E moving parallel to the beach.

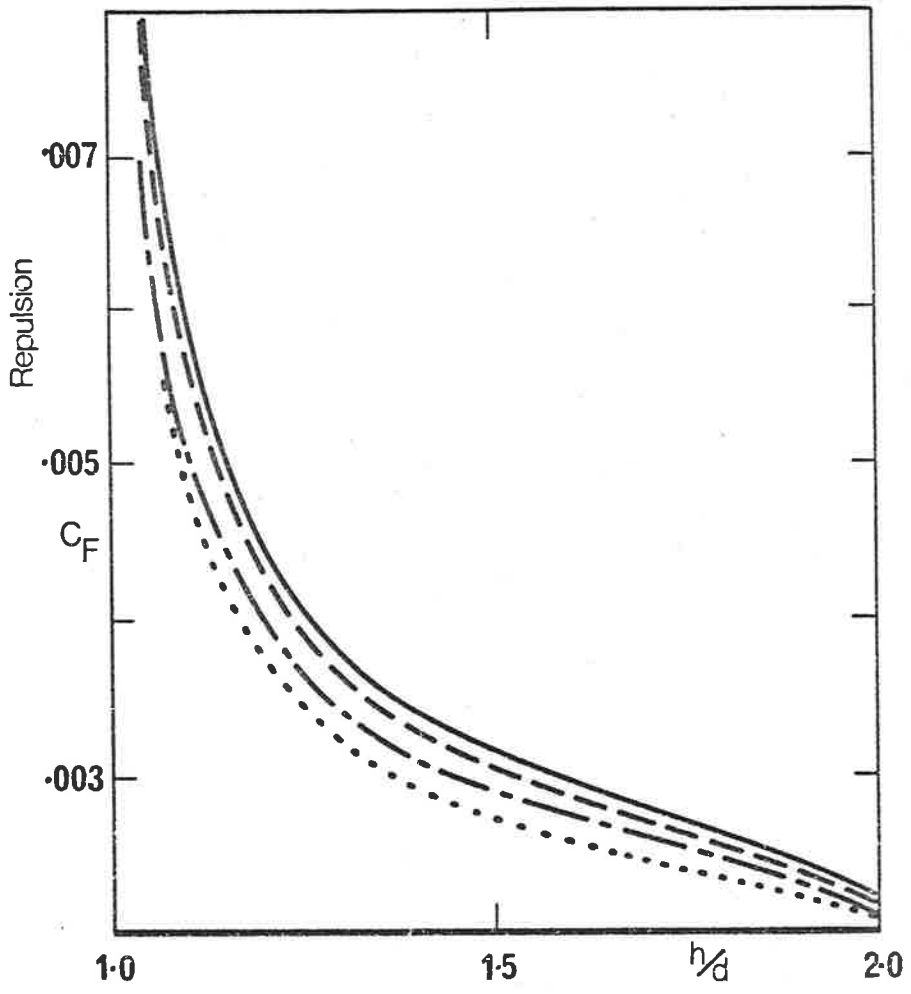

2.8 Beach induced coefficient of sway force C_F as a function of the depth to draught ratio h/d for various beach angles β for ship E moving at an angle of arctan 0.1 away from the beach.

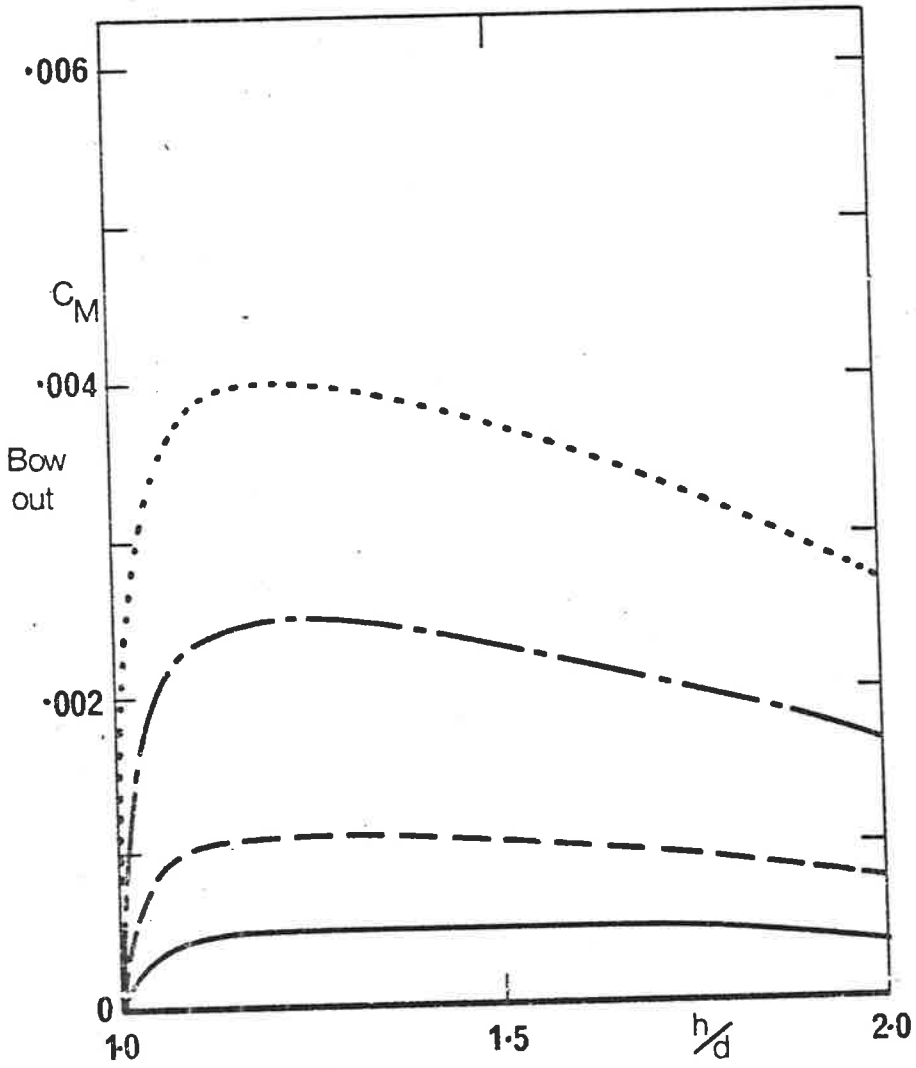

2.9 Beach induced coefficient of yaw moment C_M as a function of the depth to draught ratio h/d for various beach angles β for ship E moving parallel to the beach.

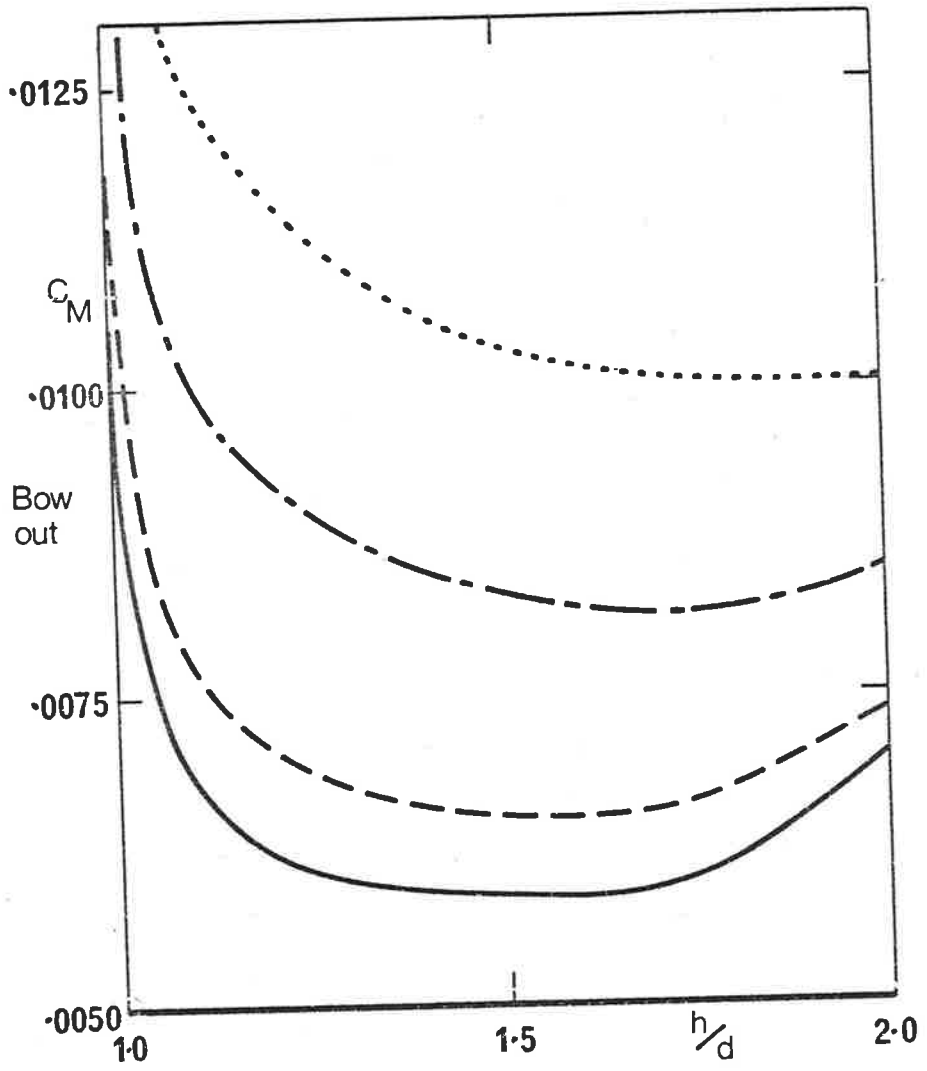

2.10 Beach induced coefficient of yaw moment C_M as a function of the depth to draught ratio h/d for various beach angles β for ship E moving at an angle of arctan 0.1 away from the beach.

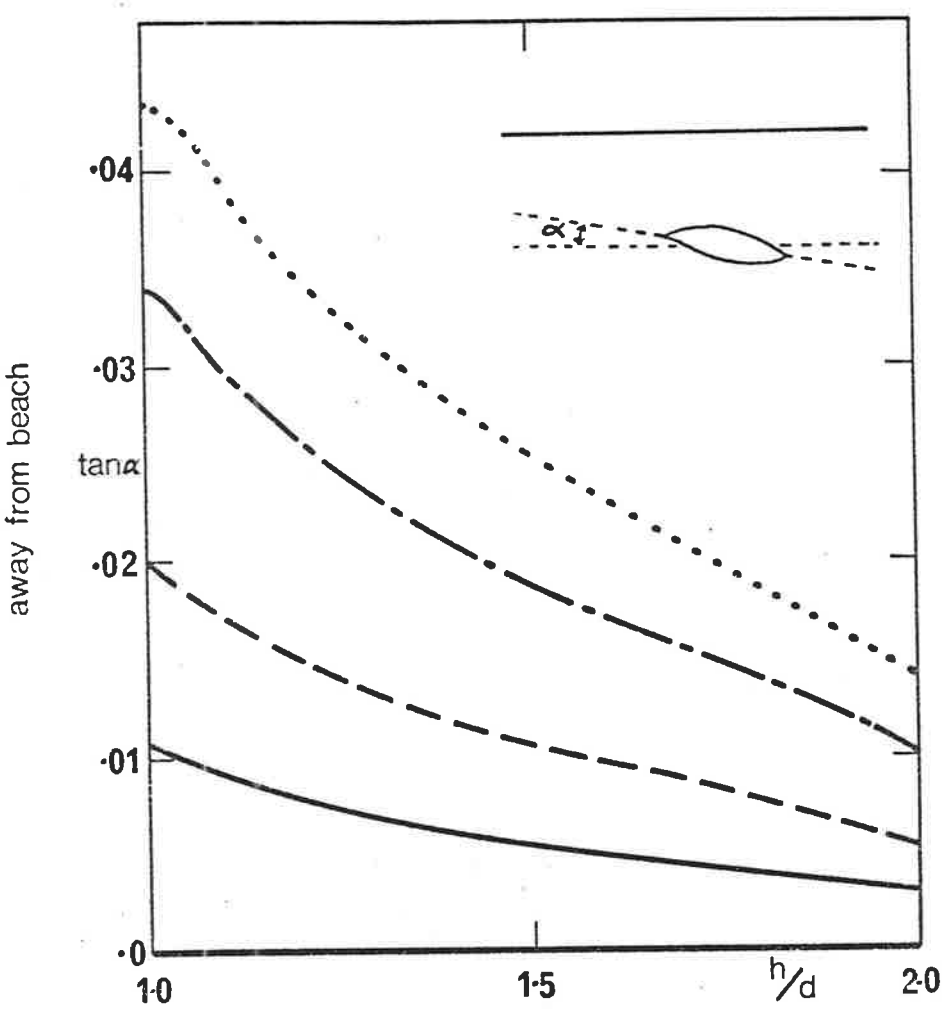

2.11 Tangent of angle α which ship E is yawed to cancel the beach-induced sway force, for various beach angles β, as a function of the depth-to-draught ratio h/d.

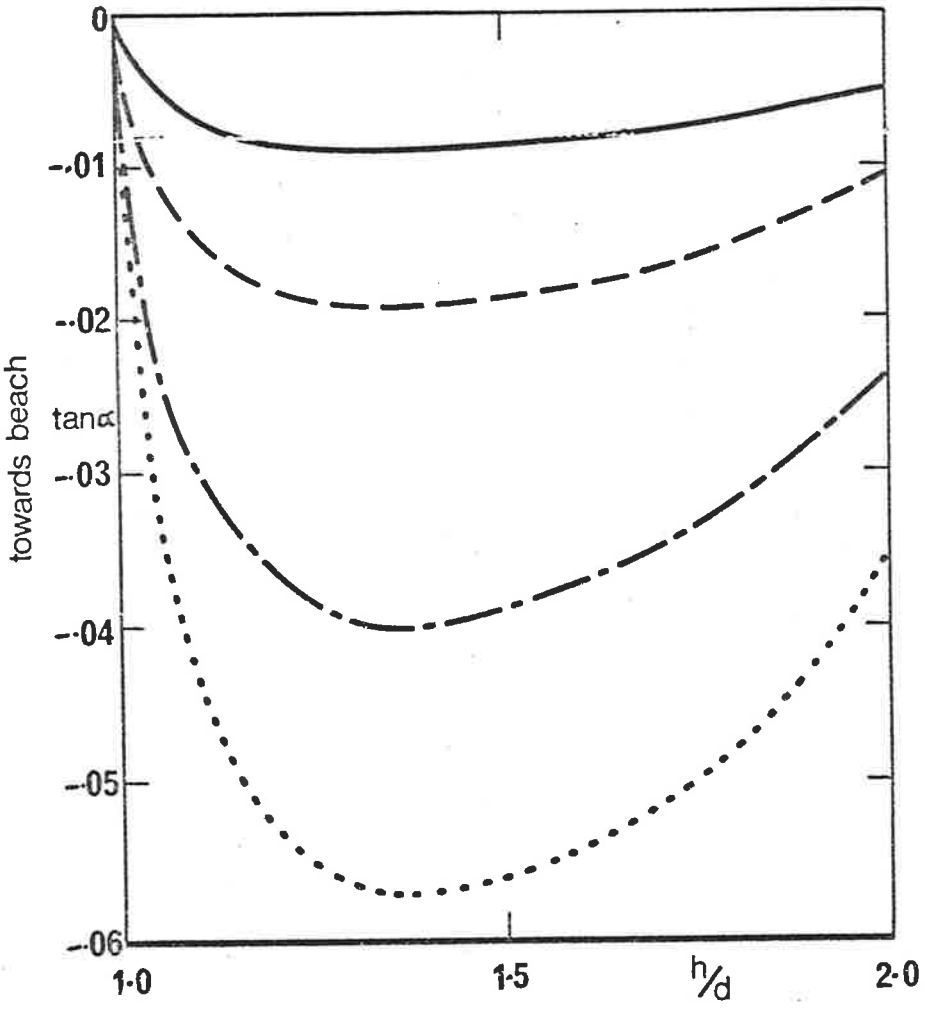

2.12 Tangent of angle α which ship E is yawed to cancel the beach-induced yaw moment, for various beach angles β, as a function of the depth-to-draught ratio h/d.

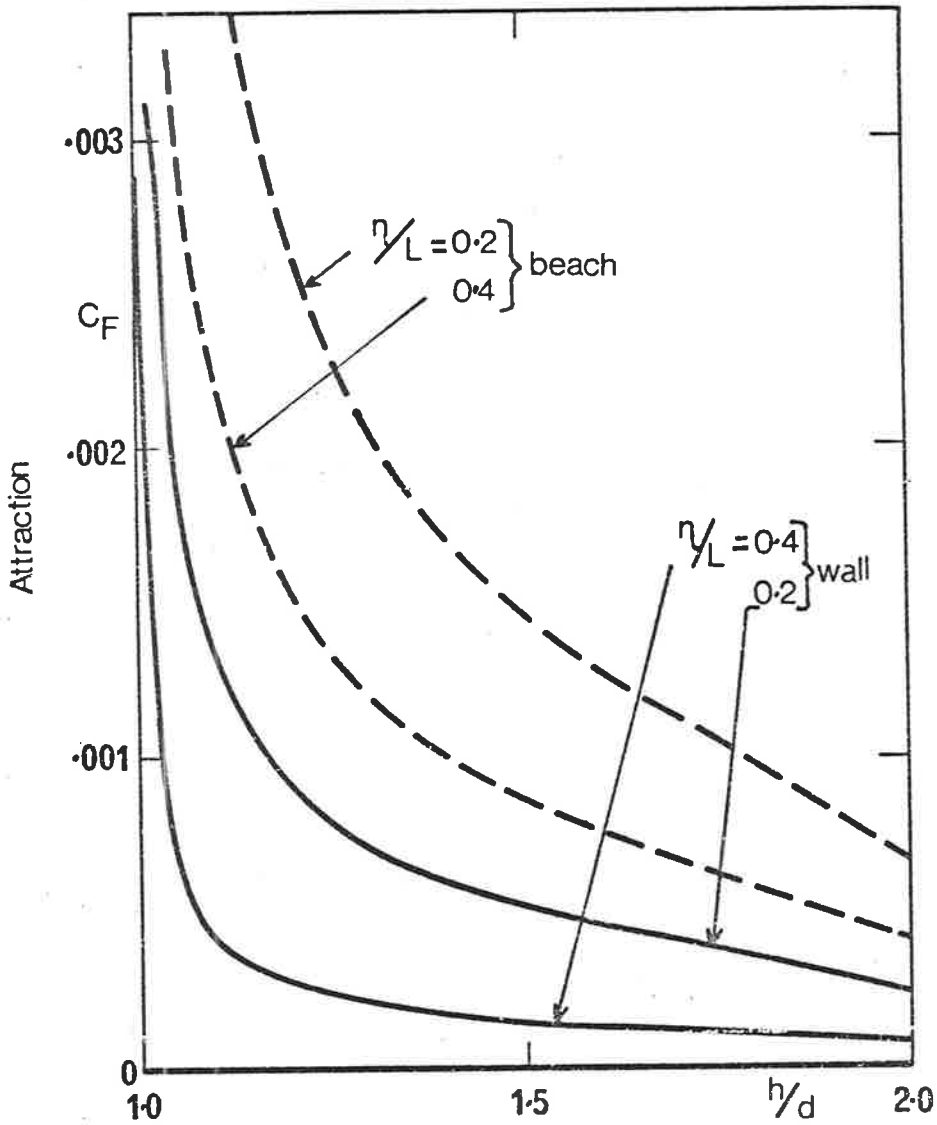

2.13 Comparison of coefficient of sway force for walls and beaches for fixed distance to length ratio η/L as a function of h/d for ship E moving parallel to the beach or wall.

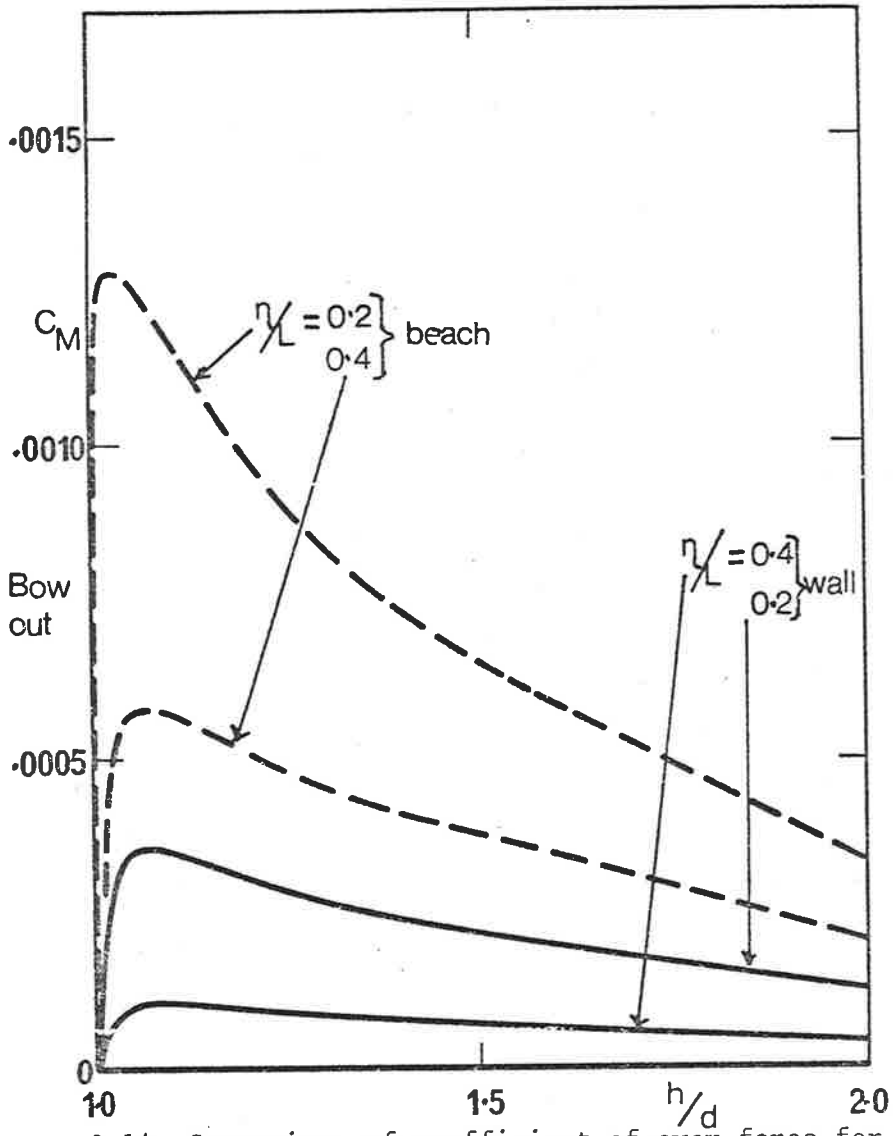

2.14 Comparison of coefficient of sway force for walls and beaches for fixed distance to length ratio η/L as a function of h/d for ship E yawed at an angle of arctan 0.1 away from the beach or wall.

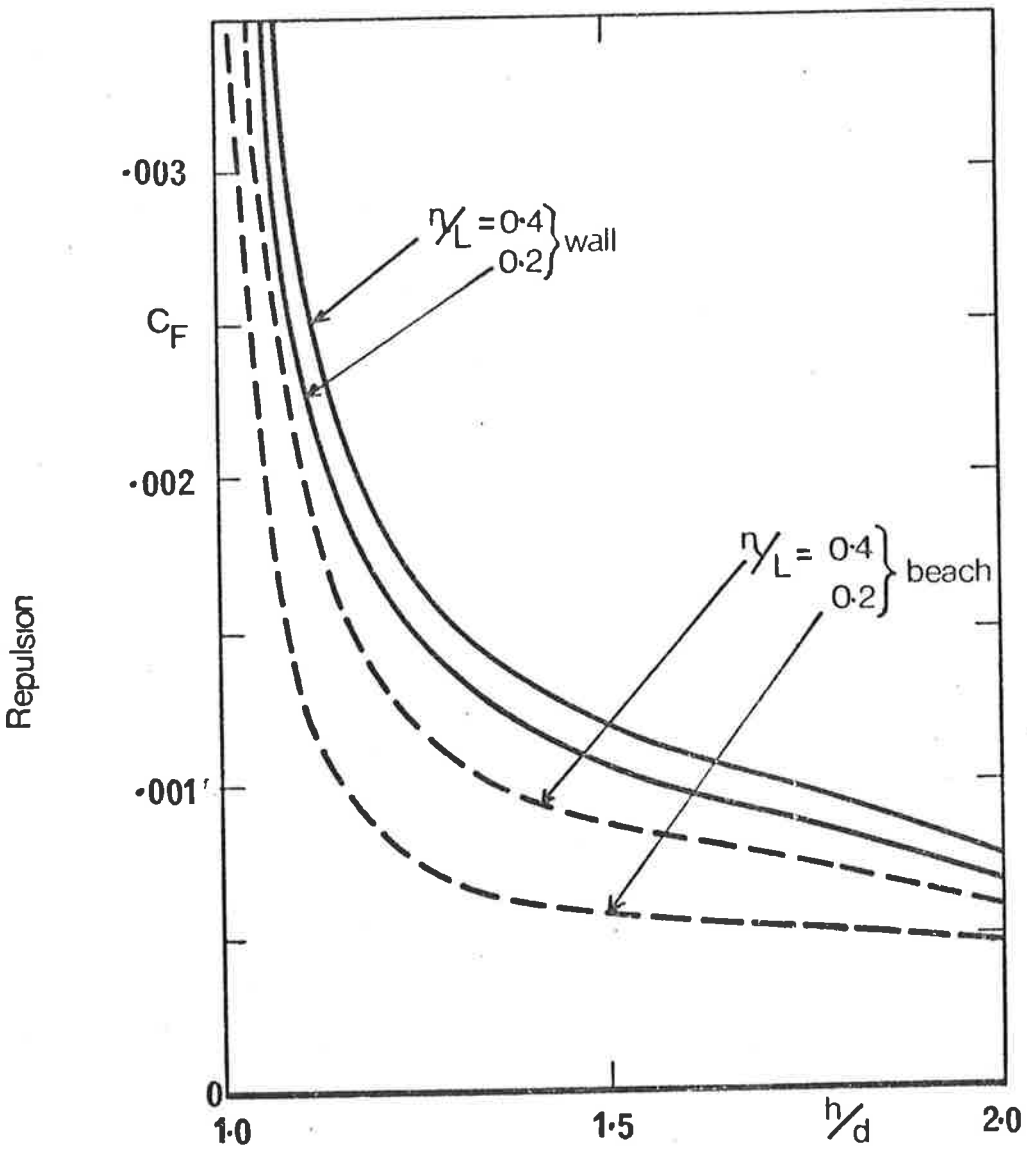

2.15 Comparison of coefficient of yaw moment for walls and beaches for fixed distance to length ratio η/L as a function of h/d for ship E moving parallel to the beach or wall.

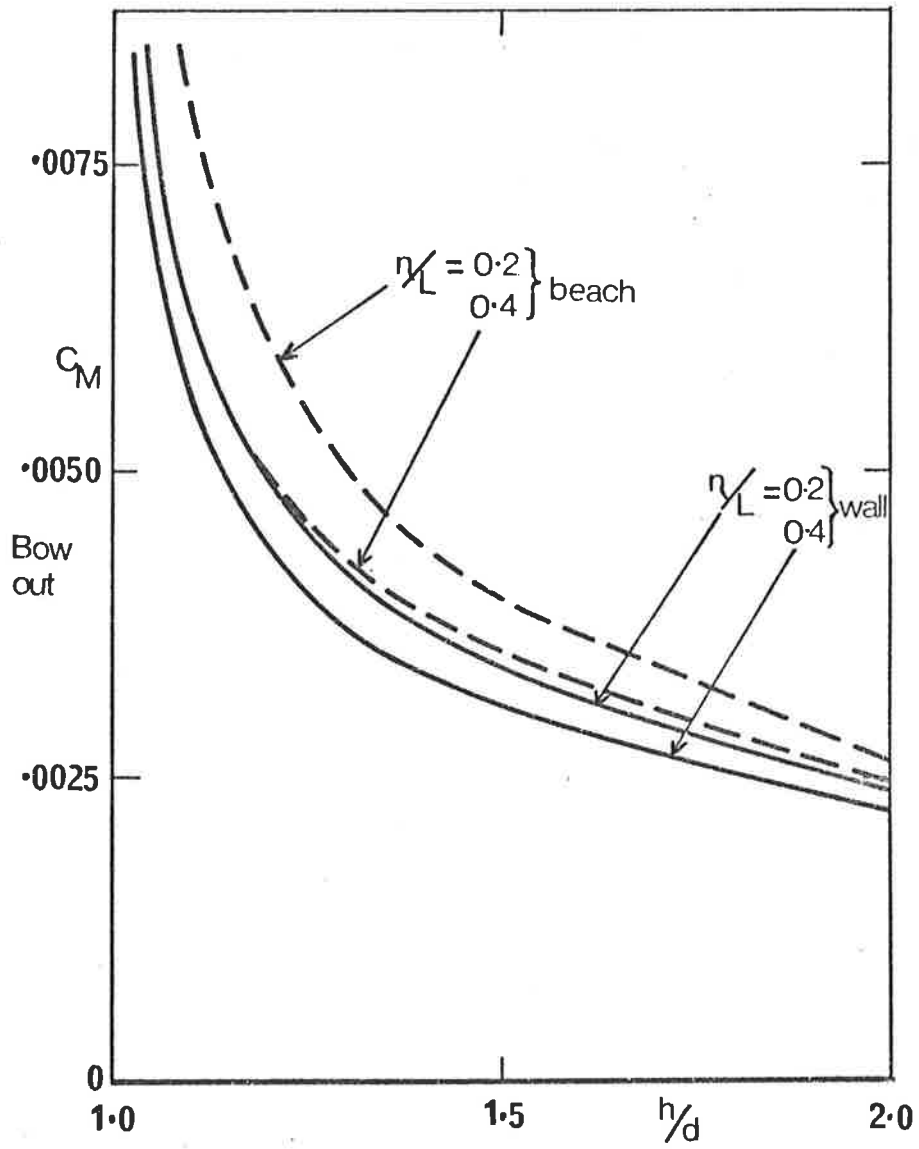

2.16 Comparison of coefficient of yaw moment for walls and beaches for fixed distance to length ratio η/L as a function of h/d for ship E yawed at an angle of arctan 0.1 away from the beach or wall.

CHAPTER 3

STEADY INTERACTIONS BETWEEN TWO OR MORE SHIPS MOVING OVER A FLAT BOTTOM OR NEAR TO A BANK

3.1 INTRODUCTION

When two ships pass each other each ship experiences forces and moments induced by the presence of the other ship, in addition to any effect from the boundaries of the fluid. The problem may be considered as steady, if the ships are moving along parallel paths at the same constant velocity, and if any depth contours are parallel to the tracks of the ships. Otherwise the problem should be considered to be unsteady. In this section only the steady problem will be considered, and the unsteady problem left for Chapters 4 and 5.

The same restrictions on the shallowness of the water and the slenderness of the ship will apply as described in section 2.1. The inner problem to be solved is the two-dimensional Laplace's equation at all vertical sections of each ship in turn, with uniform (local) depth, no banks, wall or other ships, and a "rigid-wall" free surface. This problem has already been solved, and Taylor [21] and Yeung [26] provide the blockage coefficient of a ship, which describes how the geometry is seen by an outer observer far from the ships.

The outer problem to be solved is the linearized shallow water equation, allowing for two ships as well as variable depth. As in Chapter 2, this is a two-dimensional problem in the horizontal plane, in which the ships are modelled by equivalent thin porous airfoils. In this outer problem the free surface is replaced by a rigid wall, so the Froude number is again assumed to be zero.

When the interaction between the ships is taking place with zero bottom clearance, a uniform flat bottom and a small stagger, the problem is equivalent to that of the two-dimensional stream-wise section of the wings of a biplane. This problem has been investigated by several classical aerodynamicists, notably Karman and Burgers [12] .

Collatz [6] presented a theory for the interaction of two bluff ellipses, with no underkeel clearance or circulation around the bodies. His results motivated experiments by Oltmann [18]. Tuck and Newman [25] produced a theory for the zero-underkeel clearance case, which is the same as the procedure given here for zero clearance, and compared their results with those of Collatz and the experiments of Oltmann. They found that the results from their theory gave better quantitative agreement with Oltmann's experiments for sway force but were not significantly better for the yaw moment than those resulting from Collatz's theory.

In addition Tuck and Newman provide an intuitive derivation of the theory for two ships interacting over a uniform-depth flat bottom with small bottom clearance. In section 3.2 a more rigorous derivation which allows for some depth variation is given.

A numerical technique suitable for solving the resulting system of singular integral equations is presented, and results are given for three interaction problems, namely two identical ships passing over a flat bottom and near a wall, and two ships of different sizes. The results of these computations show that, in practice, steady ship-interaction problems should be considered individually because there are so many parameters involved, such as shape of waterplane, length, draft and breadth ratio of each ship and between ships, separation of the paths of the ships and the distance to any boundary of the water. This makes difficult the task of obtaining any general conclusions, which could avoid the necessity of calculating the sway force and yaw moment for all new problems.

3.2 DERIVATION OF GOVERNING SYSTEM OF INTEGRAL EQUATIONS

Consider the hydrodynamic interactions between two ships in a steady flow situation. This means that the ships have a fixed position relative to each other, and are moving at constant velocity, parallel to any depth contours. This may be modelled by having two fixed ships with an incident free stream of velocity U, parallel to any depth contours $h(y)$, and possibly at a small angle of attack to both ships.

The geometry of this situation is shown in Figure 3.1. Ship j has half length ℓ_j and occupies a section of the x-axis β_j at a position $y = y_j$. Ship j also has cross-sectional area $S_j(x)$ at station x in the segment β_j. If each section of ship j possesses lateral symmetry about the mean line $y = \bar{f}_j(x)$, then $\bar{f}_j(x)$ may be taken as the appropriate camber function. The depth contours $h(y)$ give the local water depth below ship j as $h_j = h(y_j)$.

The quantities of most interest in this problem are the sway force and yaw moment, especially the manner in which they are effected by the stagger and separation of the two ships and the distance from any boundary or significant depth contour. The stagger S is the distance between the centres of the two ships, measured from ship 2. The separation η is the length of the gap between the paths of the two ships, that is

$$\eta = |y_1 - y_2| \quad . \tag{3.2.1}$$

The differential equation for the perturbation velocity potential ϕ, caused by the presence of the ships in the free stream, is still, (3.2.2), the linearized shallow water equation for low Froude number. But, now there is the added complication that body boundary conditions must be satisfied on <u>both</u> bodies separately. In this case, the

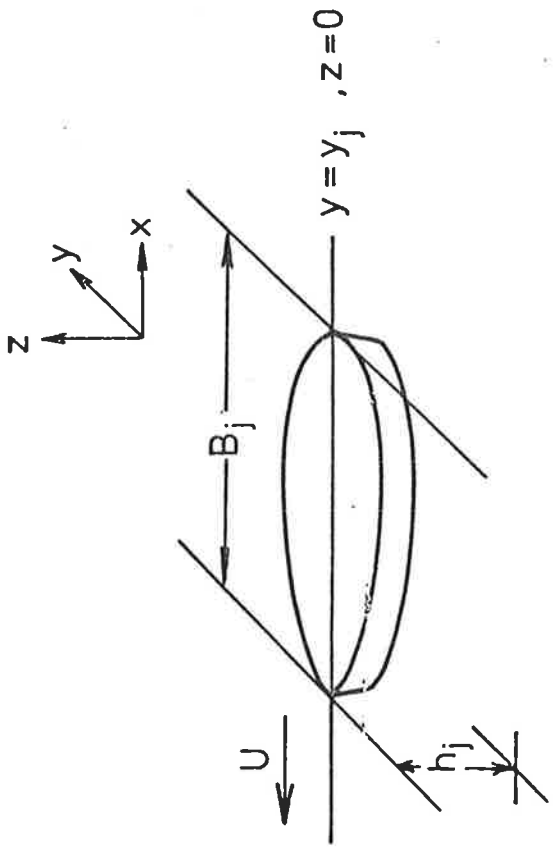

3.1 Geometry of Ship j

thickness boundary condition (2.2.11) on ship j may be written as

$$\Delta\phi_y = U\,\Delta f_j'(x) \quad \text{at} \quad y = y_j \ , \tag{3.2.2}$$

and the camber boundary condition (2.2.15) on ship j as

$$\bar{\phi}_y - U\,\bar{f}_j'(x) = \frac{1}{2h_j C_j}\,\Delta\phi \quad \text{at} \quad y = y_j \tag{3.2.3}$$

where at $y = y_j$

$$\Delta\phi_y = \phi_y(x, y_j + 0) - \phi_y(x, y_j - 0), \tag{3.2.4}$$

$$\Delta\phi = \phi(x, y_j + 0) - \phi(x, y_j - 0), \tag{3.2.5}$$

and $\Delta f_j(x)$ is the mean thickness of the hull of ship j. Ship j has blockage coefficient C_j, so this time the model being developed is that for the interaction of two porous airfoils in steady motion along parallel paths.

This boundary-value problem can be solved by distributing sources and vortices over the segments representing the ships. Thus the velocity potential may be written as

$$\phi(x,y) = \sum_{j=1}^{2} \int_{\beta_j} \{q_j(\xi)G(x,y;\xi,y_j) + \gamma_j(\xi)H(x,y;\xi,y_j)\}d\xi \tag{3.2.6}$$

where G and H are given as in section 2.3 and q_j and γ_j are the source and vortex strengths respectively on ship j.

On substitution into the thickness boundary condition (3.2.2) the source strength on ship i is found to be

$$\begin{aligned} q_i(x) &= \Delta\phi_y \qquad \text{at} \quad y = y_i \\ &= U\,S_i'(x)/h_i \ . \end{aligned} \tag{3.2.7}$$

Similarly substitution into the camber boundary condition gives a system of integral equations to determine the vortex strength on ship i

$$\gamma_i(x) = -\frac{d}{dx}\Delta\phi(x) \quad \text{at } y = y_i \ , \tag{3.2.8}$$

namely

$$\sum_{j=1}^{2} \int_{\beta_j} \gamma_j(\xi) H_y(x,y_i;\xi,y_j) + \frac{1}{2h_i C_i(x)} \int_{\beta_i} \gamma_i(x) u(x-\xi)\,d\xi$$

$$= U\,\bar{f}_i'(x) - \sum_{j=1}^{2} \int_{\beta_j} q_j(\xi)\,[\tfrac{1}{2}G_y(x,y_i+0;\xi,y_j)$$

$$+ \tfrac{1}{2}G_y(x,y_i-0;\xi,y_j)]\,d\xi \qquad i = 1,2 \tag{3.2.9}$$

where

$$u(x) = \begin{cases} 0 & x < 0 \\ 1 & x > 0 \end{cases} .$$

This may be solved for $\gamma(x)$, as the right hand side is known. The system of integral equations may be simplified by introducing the new kernel function

$$K_x^{ij}(x,\xi) = H_y(x,y_i;\xi,y_j) + \frac{\delta_{ij}}{2h_i C_i(x)}\, u(x-\xi) \tag{3.2.10}$$

where

$$\delta_{ij} = \begin{cases} 0 & i \neq j \\ 1 & i = j \end{cases} .$$

Then the system of integral equations may be written as

$$\sum_{j=1}^{2} \int_{\beta_j} \gamma_j(\xi) K_x^{ij}(x,\xi)\,d\xi = U\,g_i'(x) \qquad \text{for } i = 1,2 \tag{3.2.11}$$

where

$$g_i'(x) = \bar{f}_i'(x) - \sum_{j=1}^{2} \frac{1}{h_j} \int_{\beta_j} S_j'(\xi)\,[\tfrac{1}{2}G_y(x,y_j+0;\xi,y_j)$$

$$+ \tfrac{1}{2}G_y(x,y_i-0;\xi,y_j)] \quad \text{for } i = 1,2. \tag{3.2.12}$$

The function $g_i'(x)$ measures

(i) the cross flow due to the camber of ship i,

(ii) the induced cross flow due to thickness of ship i in a laterally asymmetric flow due to bottom geometry, and

(iii) the cross flow induced by the thickness of the other ship in the flow.

To simplify the notation it is convenient to introduce a kernel $L^{ij}(x)$ so that

$$L^{ij\,\prime}(x-\xi) = \tfrac{1}{2}G_y(x,y_i+0;\xi,y_j) + \tfrac{1}{2}G_y(x,y_i-0;\xi,y_j) \qquad (3.2.13)$$

and then

$$g_i'(x) = \bar{f}_i'(x) - \sum_{j=1}^{2} \frac{1}{h_j} \int_{\beta_j} S_j'(\xi) L^{ij\,\prime}(x-\xi)\,d\xi \,. \qquad (3.2.14)$$

If the bottom geometry is symmetric $L^{ii}(x) = 0$ and the cross flow on ship i is due only to its own camber and the presence of the other ship. If the bottom is flat, i.e. $h(y) = h$, then the system of integral equations (3.2.11) can be shown to be the same as those derived by Tuck and Newman [25] .

3.3 NUMERICAL PROCEDURE FOR SOLVING THE SYSTEM OF INTEGRAL EQUATIONS

In section 2.4 a direct numerical procedure for solving an integral equation was described. Here that method is expanded so that a system of integral equations of the form of (3.2.11) can be solved numerically. The technique is a generalization of Tuck and Newman [25].

Taking the indefinite integral with respect to x of equation (3.2.10) gives

$$\sum_{j=1}^{2} \int_{\beta_j} \gamma_j(\xi) K^{ij}(x,\xi)\,d\xi = U\, g_i(x) + C_i \quad \text{for } i = 1,2 \qquad (3.3.1)$$

where $K^{ij}(x,\xi)$ is determined by integration of (3.2.9) and $g_i(x)$ from (3.2.13). The constants C_i are arbitrary constants of integration which take values so that the Kutta condition holds at the trailing edges of both ships.

As in section 2.4, the unknown functions $\gamma_1(x)$ and $\gamma_2(x)$ are represented by step functions on their respective ships, with the value on the j^{th} interval of ship i $x_{ij-1} < x < x_{ij}$ being taken as the constant $\gamma_i(x) = \gamma_{ij}$. To simplify the procedure, the same number of mesh points are taken on each ship. However, the method described can readily be altered to include different numbers of mesh points on each ship. Since square-root singularities may be anticipated at the end of each ship, the distribution of points x_{ij} on ship i is chosen so that

$$x_{ij} = -\ell_i \cos\left(j\frac{\pi}{N}\right) + a_i$$

$$j = 0,1,2,\ldots,N,\ i = 1,2 \qquad (3.3.2)$$

which provides the right increase in density of points near the ends of each ship. The variable a_i in (3.3.2) is the x-coordinate of the centre of ship i.

Replacing $\gamma_j(x)$ in (3.3.1) by such step functions gives

$$\sum_{j=1}^{2}\sum_{k=1}^{N}\gamma_{jk}\int_{x_{jk-1}}^{x_{jk}} K^{ij}(x,\xi)\,d\xi = U\,g_i(x) + C_i \quad \text{for } i = 1,2. \qquad (3.3.3)$$

To solve this system of equations the integrals are evaluated at points $x = \bar{x}_{ik}$ which are near the centre of the k^{th} interval on ship i. A useful way of choosing these "mid-points" is to use

$$\bar{x}_{ik} = -\ell_i \cos((k-\tfrac{1}{2})\pi/N) + a_i \quad i = 1,2. \qquad (3.3.4)$$

The system may then be written as

$$\sum_{j=1}^{2}\sum_{k=1}^{N}\gamma_{jk}\int_{x_{j\,k-1}}^{x_{jk}} K^{ij}(\bar{x}_{i\ell},\xi)d\xi = U\,g_i(\bar{x}_{ik}) + C_i$$

$$\text{for}\quad i = 1,2\quad\text{and}\quad \ell = 1,\ldots,N. \qquad (3.3.5)$$

This is a system of $2N$ simultaneous equations in $2N$ unknowns γ_{jk} and may be written as the matrix equation

$$A\underset{\sim}{\gamma} = U\underset{\sim}{g} + C_1\underset{\sim}{e}^{(1)} + C_2\underset{\sim}{e}^{(2)} \qquad (3.3.6)$$

where

$$A = [A_{ij}],\quad \underset{\sim}{\gamma} = \begin{bmatrix}\gamma_{11}\\ \gamma_{12}\\ \vdots\\ \gamma_{1N}\\ \gamma_{21}\\ \vdots\\ \gamma_{2N}\end{bmatrix},\quad \underset{\sim}{g} = \begin{bmatrix}g_1(\bar{x}_{11})\\ g_1(\bar{x}_{12})\\ \vdots\\ g_1(\bar{x}_{1N})\\ g_2(\bar{x}_{21})\\ \vdots\\ g_2(\bar{x}_{2N})\end{bmatrix},$$

$$\underset{\sim}{e}^{(1)} = \begin{bmatrix}1\\ \vdots\\ 1\\ 0\\ \vdots\\ 0\end{bmatrix}\quad\text{and}\quad \underset{\sim}{e}^{(2)} = \begin{bmatrix}0\\ \vdots\\ 0\\ 1\\ \vdots\\ 1\end{bmatrix}.$$

The matrix elements A_{ij} are such that

$$A_{(i-1)N+\ell,\,(j-1)N+k} = \int_{x_{j\,k-1}}^{x_{jk}} K^{ij}(\bar{x}_{i\ell},\xi)d\xi\ . \qquad (3.3.7)$$

Quite often for simple geometries the integration in (3.3.7) may be performed analytically. For more complex geometries it may be necessary to evaluate the matrix elements A_{ij} by a quadrature procedure.

By using standard matrix-inversion techniques with the three right-hand sides, (3.3.6) may be solved to give the solution vector

$$\underset{\sim}{\gamma} = U \underset{\sim}{\gamma}^{(0)} + C_1 \underset{\sim}{\gamma}^{(1)} + C_2 \underset{\sim}{\gamma}^{(2)} \tag{3.3.8}$$

where

$$\underset{\sim}{\gamma}^{(0)} = A^{-1} \underset{\sim}{g}, \tag{3.3.9}$$

$$\underset{\sim}{\gamma}^{(1)} = A^{-1} \underset{\sim}{e}^{(1)} \tag{3.3.10}$$

and

$$\underset{\sim}{\gamma}^{(2)} = A^{-1} \underset{\sim}{e}^{(2)} . \tag{3.3.11}$$

This is a numerical approximation to the corresponding representation of the actual vortex strength $\gamma_i(x)$, namely

$$\gamma_i(x) = U \gamma_i^{(0)}(x) + C_1 \gamma^{(1)}(x) + C_2 \gamma^{(2)}(x). \tag{3.3.12}$$

It is now necessary to determine the constants C_i from the Kutta condition on the trailing edge of each ship. The condition is the same as that used in chapter 2; that is, the vorticity must vanish at the trailing edge of each ship, so

$$\gamma_i(\ell_i) = 0 \quad i = 1,2. \tag{3.3.13}$$

Again, there are two ways in which this can be applied. A naive but effective procedure is to make the vorticity on the end interval of each ship zero, so that

$$(\underset{\sim}{\gamma})_N = (\underset{\sim}{\gamma})_{2N} = 0$$

or expanding these terms

$$U(\underset{\sim}{\gamma}^{(0)})_N + C_1(\underset{\sim}{\gamma}^{(1)})_N + C_2(\underset{\sim}{\gamma}^{(2)})_N = 0 \qquad (3.3.14)$$

and

$$U(\underset{\sim}{\gamma}^{(0)})_{2N} + C_1(\underset{\sim}{\gamma}^{(1)})_{2N} + C_2(\underset{\sim}{\gamma}^{(2)})_{2N} = 0, \qquad (3.3.15)$$

which can be solved to give C_1 and C_2 .

A more satisfactory method is to use the expected property of a square-root singularity in $\gamma_i(x)$ at the trailing edge, that is as $x \to \ell_i$ on $y = y_i$

$$\gamma_i(x) \to \frac{D_i}{\sqrt{\ell_i - x}} + E_i\sqrt{\ell_i - x} \qquad (3.3.16)$$

for constants D_i and E_i . By fitting this function to the last two elements of each ship i for $(\underset{\sim}{\gamma}^{(\ell)})_{i\,N-1}$ and $(\underset{\sim}{\gamma}^{(\ell)})_{i\,N}$ for $\ell = 0,1,2$ and $i = 1,2$ the 12 constants $D_i = D_i^{(\ell)}$ and $E_i = E_i^{(\ell)}$ may be determined. So that the Kutta condition (3.3.13) holds, the sum of the inverse square-root terms involving D must be zero for each ship, i.e.

$$\begin{aligned} UD_1^{(0)} + C_1D_1^{(1)} + C_2D_1^{(2)} &= 0 \\ UD_2^{(0)} + C_1D_2^{(1)} + C_2D_2^{(2)} &= 0 \end{aligned} \qquad (3.3.17)$$

From this C_1 and C_2 may be determined, so that by using (3.3.8) the numerical approximation to the vortex strength may be obtained. As in the preceding chapter the second application of the Kutta condition is used for all results presented.

3.4 EVERYWHERE-UNIFORM DEPTH

Following section 2.5 if h=constant everywhere then G and H are given by (2.5.1) and (2.5.2) respectively. Thus from (3.2.10) the

kernel K_x^{ij} is given by

$$K_x^{ij}(x,\xi) = \frac{1}{2\pi}\frac{x-\xi}{(y_i+y_j)^2+(x-\xi)^2} + \delta_{ij}\frac{u(x-\xi)}{2h_i C_i(x)} \qquad (3.4.1)$$

and from (3.2.13) the kernel

$$L^{ij\,\prime}(x) = \frac{1}{2\pi}\frac{y_i-y_j}{x^2+(y_i-y_j)^2} \qquad (3.4.2)$$

This gives $L^{ii}(x) = 0$ which is expected as there is no bottom asymmetry but $L^{ij}(x) \neq 0$ for $i \neq j$ and shows the effect of the thickness of ship j on ship i.

Substitution of K_x^{ij} and $L^{ij\,\prime}$ into (3.2.11) yields equations (96) and (97) of Tuck and Newman [25] (except for a missing factor of π in their equations).

After integrating (3.4.1) the kernel K^{ij} is obtained as

$$K^{ij}(x,\xi) = \frac{1}{2\pi}\log\sqrt{(y_i-y_j)^2+(x-\xi)^2} + \delta_{ij}\frac{u(x-\xi)}{2h_i}\int_{a_i-\ell_i}^{x}\frac{dt}{C_i(t)} \qquad (3.4.3)$$

and integrating (3.4.2) gives

$$L^{ij}(x) = \frac{1}{2\pi}\arctan\left(\frac{y_i-y_j}{x}\right) \qquad (3.4.4)$$

These kernels may then be substituted into (3.3.1) and by the numerical procedure in that section the system of integral equations may be solved for $\gamma_i(x)$, $i = 1,2$.

3.5 MOTION PARALLEL TO A VERTICAL WALL IN UNIFORM DEPTH

If there is a vertical wall at $y = -Y$, this wall may be modelled by images obtaining the kernels G and H given in (2.6.1) and (2.6.2) respectively. The wall should not lie between the two ships, as this would reduce to the situation of one ship and a vertical wall, as described

in section 2.6. Thus, from (3.2.10) and (3.2.13), the necessary kernel functions are

$$K_x^{ij}(x,\xi) = \frac{1}{2\pi}\frac{x-\xi}{(x-\xi)^2+(y_i-y_j)^2} + \frac{1}{2\pi}\frac{x-\xi}{(x-\xi)^2+(y_i-y_j+2Y)^2}$$

$$+ \frac{\delta_{ij}}{2h_i C_i(x)}\, u(x-\xi) \qquad (3.5.1)$$

and

$$L^{ij\,\prime}(x) = \frac{1}{2\pi}\frac{y_i-y_j}{x^2+(y_i-y_j)^2} + \frac{1}{2\pi}\frac{y_i-y_j+2Y}{x^2+(y_i-y_j+2Y)^2}\,. \qquad (3.5.2)$$

Integrating (3.5.1) and (3.5.2) gives

$$K^{ij}(x,\xi) = \frac{1}{2\pi}\log\sqrt{(y_i-y_j)^2+(x-\xi)^2} + \frac{1}{2\pi}\log\sqrt{(x-\xi)^2+(y_i-y_j+2Y)^2}$$

$$+ \delta_{ij}\,\frac{u(x-\xi)}{2h_i}\int_{a_i-\ell_i}^{x}\frac{dt}{C_i(t)} \qquad (3.5.3)$$

and

$$L^{ij}(x) = \frac{1}{2\pi}\arctan\frac{y_i-y_j}{x} + \frac{1}{2\pi}\arctan\frac{y_i-y_j+2Y}{x}\,. \qquad (3.5.4)$$

Comparing the two kernels above with those for a uniform depth (3.4.3) and (3.4.4), it can be seen that the effect of the wall is to introduce additional terms. These new terms have a similar form to the other terms, and represent the effect of the vertical wall via the image ships.

Although the effect of a uniform sloping beach may readily be investigated by following the above steps with the kernels G and H from 2.7, this is not done here. The effect of this and other bottom geometries may all be readily handled by the techniques described above. One case of particular interest is that of ships in a canal, and the necessary kernels can be found in Beck [4].

3.6 RESULTS

Using the numerical technique described in the preceding pages the effect of changing the clearance between the keel and the bottom is investigated. This is done mainly for a flat bottom of uniform depth, but the effect of a vertical wall parallel to the paths of the ships is also considered. As in 2.9 the non-dimensional coefficients of sway force and yaw moment given by (2.9.1) and (2.9.2) are used with the actual force and moment being calculated from (2.8.8) and (2.8.9) which are still valid.

Consider two identical ships with a parabolic water-plane, a breadth to length ratio of 1:10, and draft to depth ratio of 1:20, moving along paths separated by a distance of $0.625.\frac{1}{2}L$ where L is the length of the ships. To see the effect of the underkeel clearance, curves for the coefficients of sway force and yaw moment for several draft to depth ratios are plotted against the stagger S of the two ships. The stagger is the length along the x-axis from the projection on the x-axis of the centre of ship 2 to the projection of the centre of ship 1.

When the draft to depth ratio is unity, this is the case of two thin wings undergoing steady interactions in a two-dimensional stream; that is, no variation in the fluid flow occurs with depth. This is the interaction between thin bodies in steady two-dimensional flow investigated by Tuck and Newman [25]. As they did not give results for the more general situation with depth effects, the effect of varying the underkeel clearance is investigated here.

Figures 3.2 and 3.3 show the numerical results obtained for the coefficients of sway force and yaw moment. The graphs shown are for ship 1 but the results for ship 2 are only a lateral inversion of

those given. It can readily be seen that this must be true for identical ships, by considering the symmetry of the problem, and this was confirmed by the numerical results.

It can be seen in Figure 3.2 that even for small clearances the peak sway force rapidly decreases as the draft to depth ratio decreases, so that for a draft to depth ratio of 0.83 the peak sway force is about one twentieth of that for zero underkeel clearance (i.e. d/h = 1.0). Also, the magnitude of the peak attractive force and peak repulsive force tend to become comparable in magnitude whereas the peak attractive force was about 25% larger than the peak repulsive force for zero clearance. The results show that although values for zero clearance are easier and faster to calculate than those for non-zero clearance, they could at best only be considered as a rough guide, even for quite small non-zero clearances. Figure 3.2 shows that the peaks of the sway force occur at almost the same values of the stagger, as the clearance changes. Also the (negative) stagger value at which the force changes sign is almost independent of the draft to depth ratio. So the zero clearance results can be used to give a qualitative idea of at what stagger the peaks in the sway force occur, and the relative positions of the ships when the sway force is zero.

In contrast to the sway force the peak yaw moment (Figure 3.3) only decreases slowly with decreasing draft to depth ratio, and the peaks for the moment occur at widely different staggers for different clearances. Also, the yaw moment at zero stagger is only zero when the draft to depth ratio is unity, and for other ratios it is bow inwards.

Having considered the main features of the results, it is interesting to view the results for sway force and yaw moment together, as if on ship 1. While ship 1 leads ship 2 (negative stagger) the sway force is such that the two ships are forced apart for staggers less than $-\frac{1}{2}L$,

whereas the yaw moment is bow in. It is here that the main danger lies in ship manoeuvres, because if the ships are allowed to swing around because of these yaw moments, their own engines will then drive them together. The force on ship 1 rapidly changes to an attractive force at zero stagger, with a small (or zero if d/h = 1) bow-inwards moment. The yaw moment then rapidly becomes bow outwards, even though the sway force is attractive. This is less hazardous, as the ship's propellors will tend to drive ship 1 away from ship 2.

While this is happening to ship 1, the same events are occurring in the opposite order to ship 2. So, even for two identical ships, the interactions are quite complex and in a real situation are further complicated by any steering or propulsion action taken by the ship's master.

It is of interest to see how the relative sizes of the two vessels influence the sway force and yaw moment. The numerical results for the force and moment on two ships of greatly different sizes are shown in Figures 3.4 to 3.7. Both ships have a parabolic water-plane, but the small ship has its length, breadth and draft only half those of the large ship. This means that, when the large ship is touching the bottom, the small ship has a draft to depth ratio of 0.5. For comparison of the coefficients of sway force and yaw moment on both ships, the non-dimensionalization is done by using the dimension of the large ship.

The coefficient of sway force on the large ship is given in Figure 3.3, which shows the same qualities as the sway force for identical ships given in Figure 3.2. The main difference is that the force is two orders of magnitude smaller. The sway force on the small ship as shown in Figure 3.5 is much less sensitive than the large ship to changes in clearance. The peak sway force is about one third that of the large ship, and as the small ship has one eighth the volume of the large ship,

and hence the smaller mass, it would experience the larger acceleration as a result of the sway force. Also, the added mass for sideways motion of the small ship is much less than that of the large ship, so this would again give the small ship a greater acceleration than the bigger ship.

The coefficient of yaw moment for the large and small ships is given in Figures 3.6 and 3.7 respectively. They show much the same properties as in the case of identical ships, and again the small ship is less sensitive to clearance changes. This is a result of the large clearance already beneath the small ship, even when the large ship is already touching the bottom. At a draft to depth ratio of unity, the large ship experiences twice the yaw moment of the small ship, but when the draft to depth ratio is decreased to 0.83 the two ships experience almost the same moment. So, by similar arguments to those used for the sway force, the torque induced by the sway force is larger on the small ship.

In section 3.5 the kernels for the system of integral equations for flow over a uniform flat bottom with a vertical wall at $y = -Y$ are given. To see the effect of this wall on ship interactions a numerical study was undertaken of the effect a wall would have on the interaction of the two identical ships discussed above. As zero clearance was shown to give a reasonable qualitative result, the interaction was considered for a draft to depth ratio of 1:1. The numerical results obtained are presented in Figures 3.8 to 3.11.

An examination of Figures 3.8 and 3.9 shows that as the wall is moved away from the two ships the sway force rapidly converges to the results obtained with no wall. The presence of the wall increases the sway force on the ships by up to a factor of 3 for the cases considered, showing that the hazard when the two ships pass is significantly increased by the wall.

The coefficient of yaw moment for the two ships is given in Figures 3.10 and 3.11. For ship 1, which is further away from the wall than ship 2, the presence of the wall has a smaller effect than it does on ship 2. The change in the yaw moment on ship 2 for $Y = \frac{1}{2}L$ indicates a particularly hazardous situation, because the yaw moment is nearly always bow inwards, that is towards the other ship. Hence the wall makes it more likely for ship 2 to turn towards the path of ship 1. The yaw moment on ship 2 converges more slowly to the no-wall result than that on ship 1, but by the time $Y = L$ it is almost identical to the no-wall case.

The results presented above for two ships near a wall are quite important for experimenters. They show that when an experiment is conducted, and the effects of the walls are not wanted, both ships must always be at least one ship length away from the nearest boundary. This may be difficult to achieve, as model experiments of this type are often carried out in narrow channels with one of the models near to a bank.

The above results show some interesting properties of the interaction of two ships, but they also highlight the need to study each interaction situation as a separate case. Some additional results which have been computed show that the sway force and yaw moment can also be quite sensitive to the shape of each ship, and to the separation between the paths of the ships.

The programs used to calculate the results presented in this section had an execution time of 114 seconds each on a CYBER 173 computer. In that time the sway force and yaw moment on both ships could be calculated at different staggers so that one curve for the corresponding quantity could be plotted in each of the Figures 3.4 to 3.7.

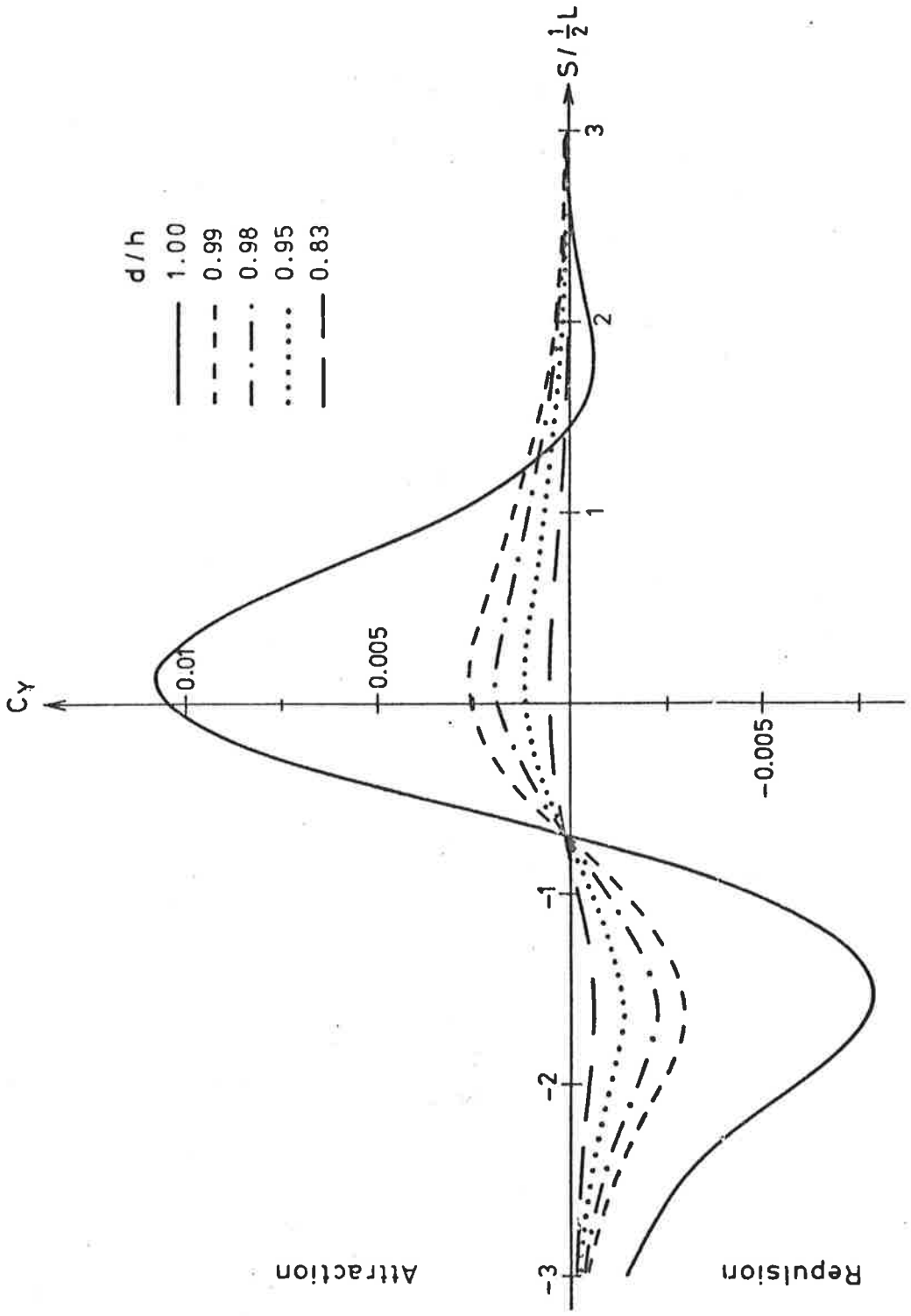

3.2 Coefficient of sway force for identical ships in various depths.

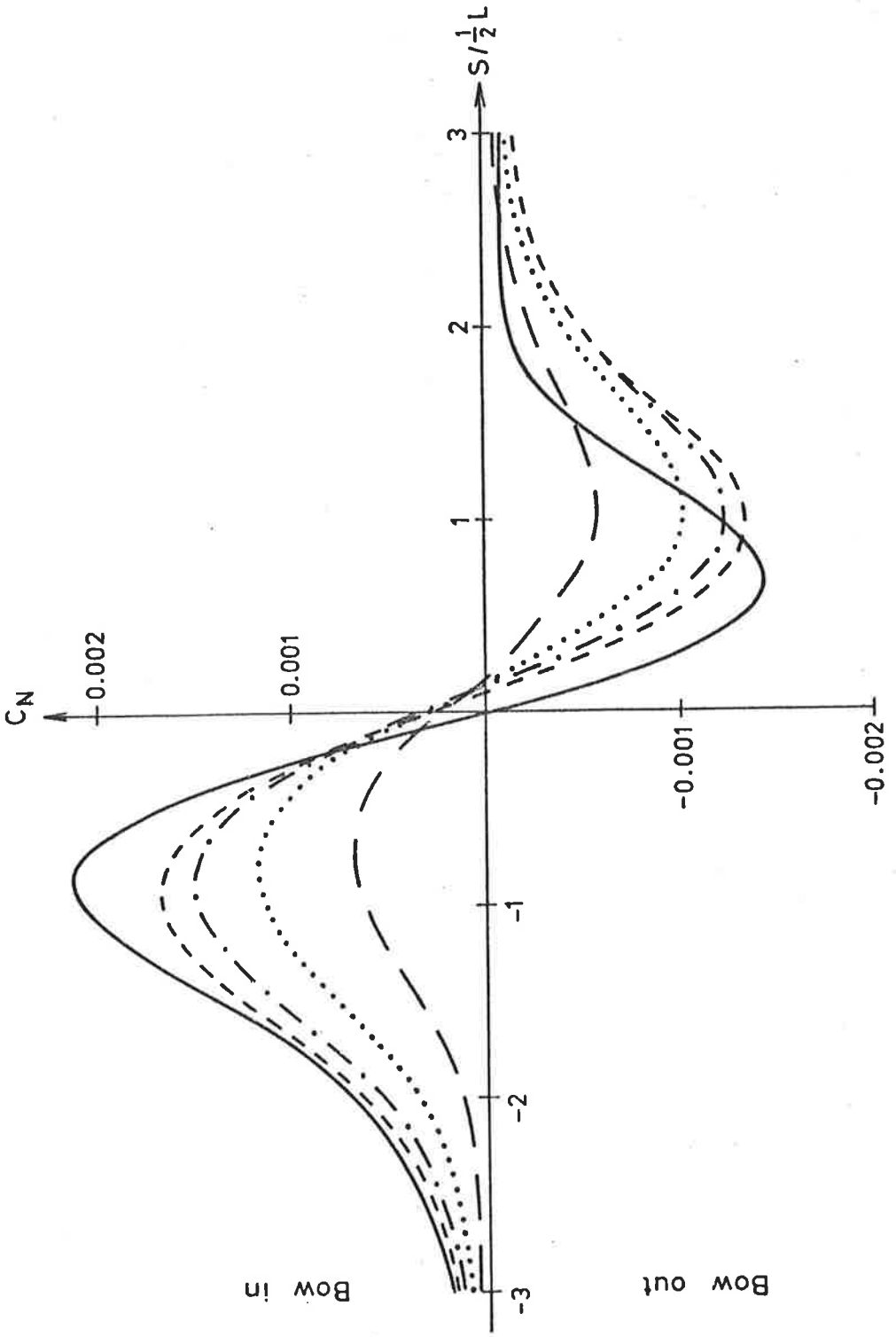

3.3 Coefficient of yaw moment for identical ships in various depths.

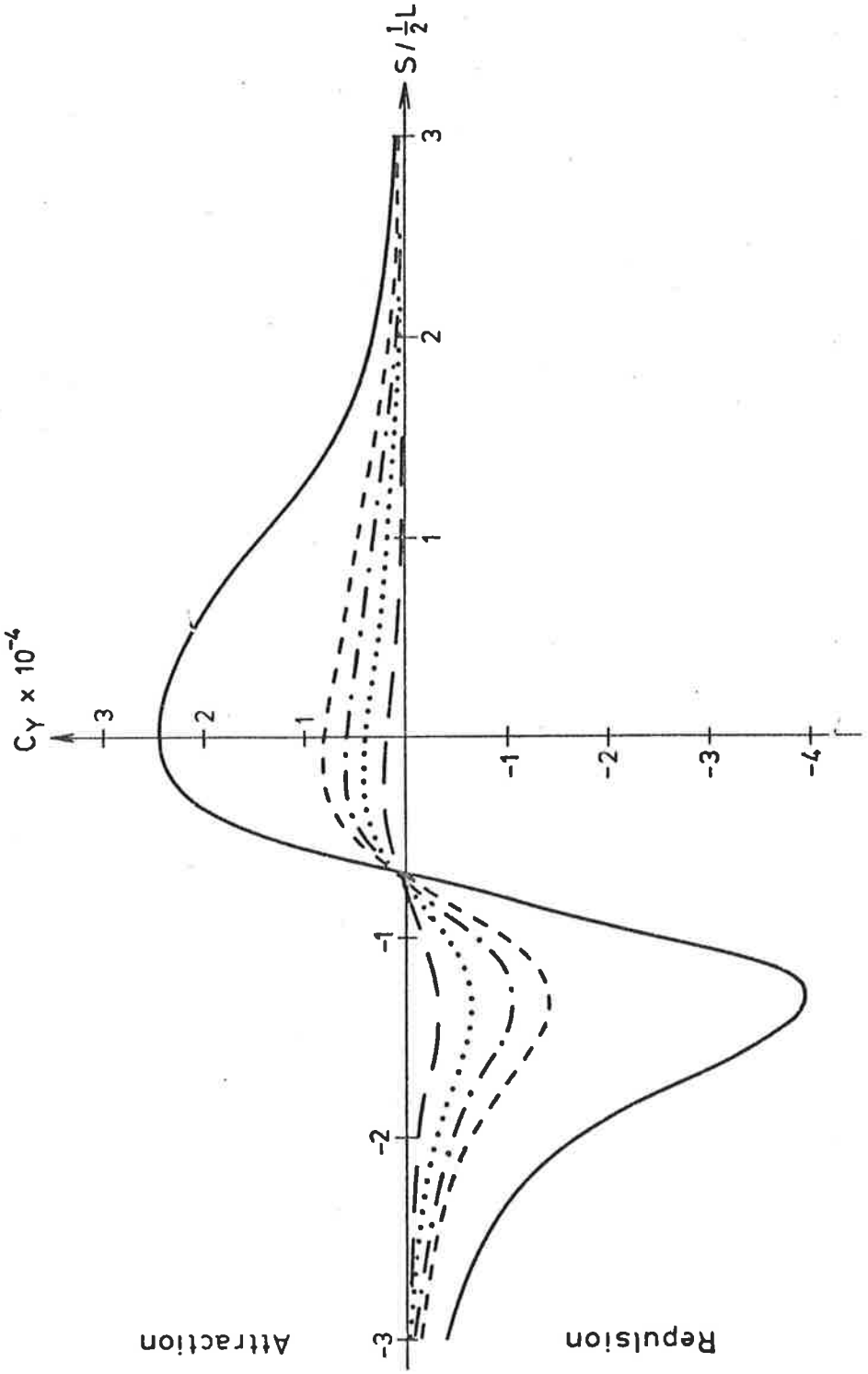

3.4 Coefficient of sway force for larger of two different size ships.

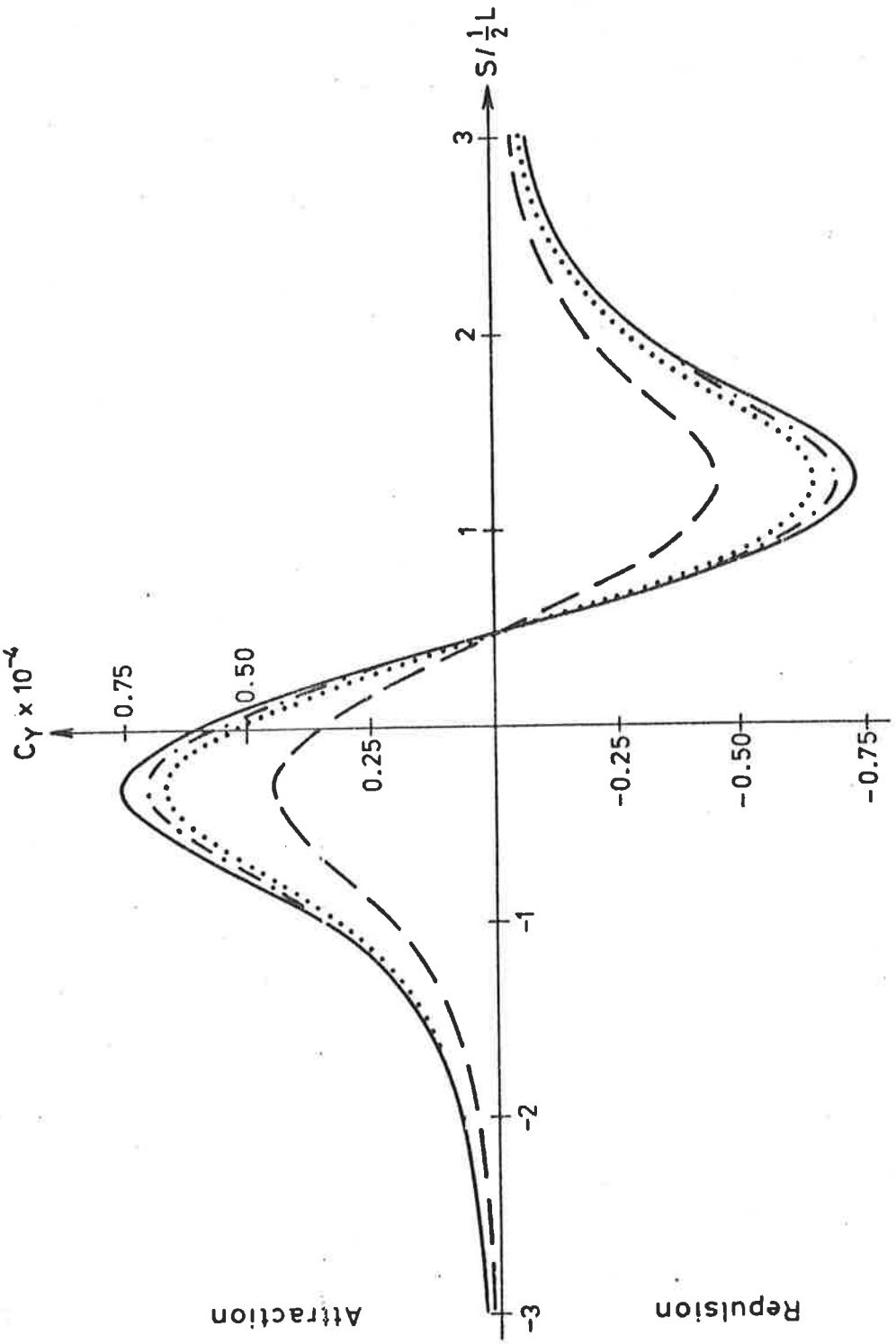

3.5 Coefficient of sway force for smaller of two different size ships.

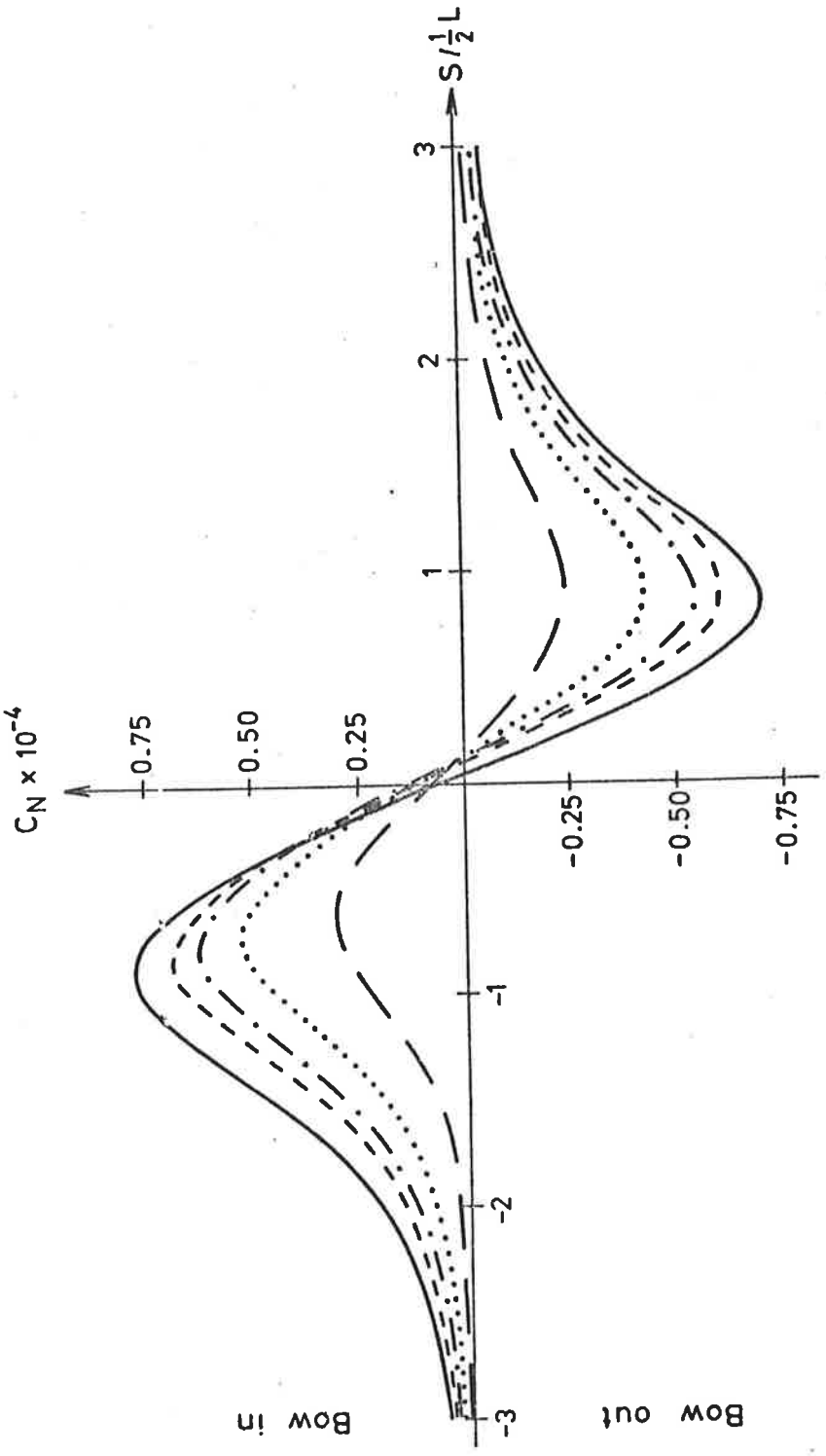

3.6 Coefficient of yaw moment for larger of two different size ships.

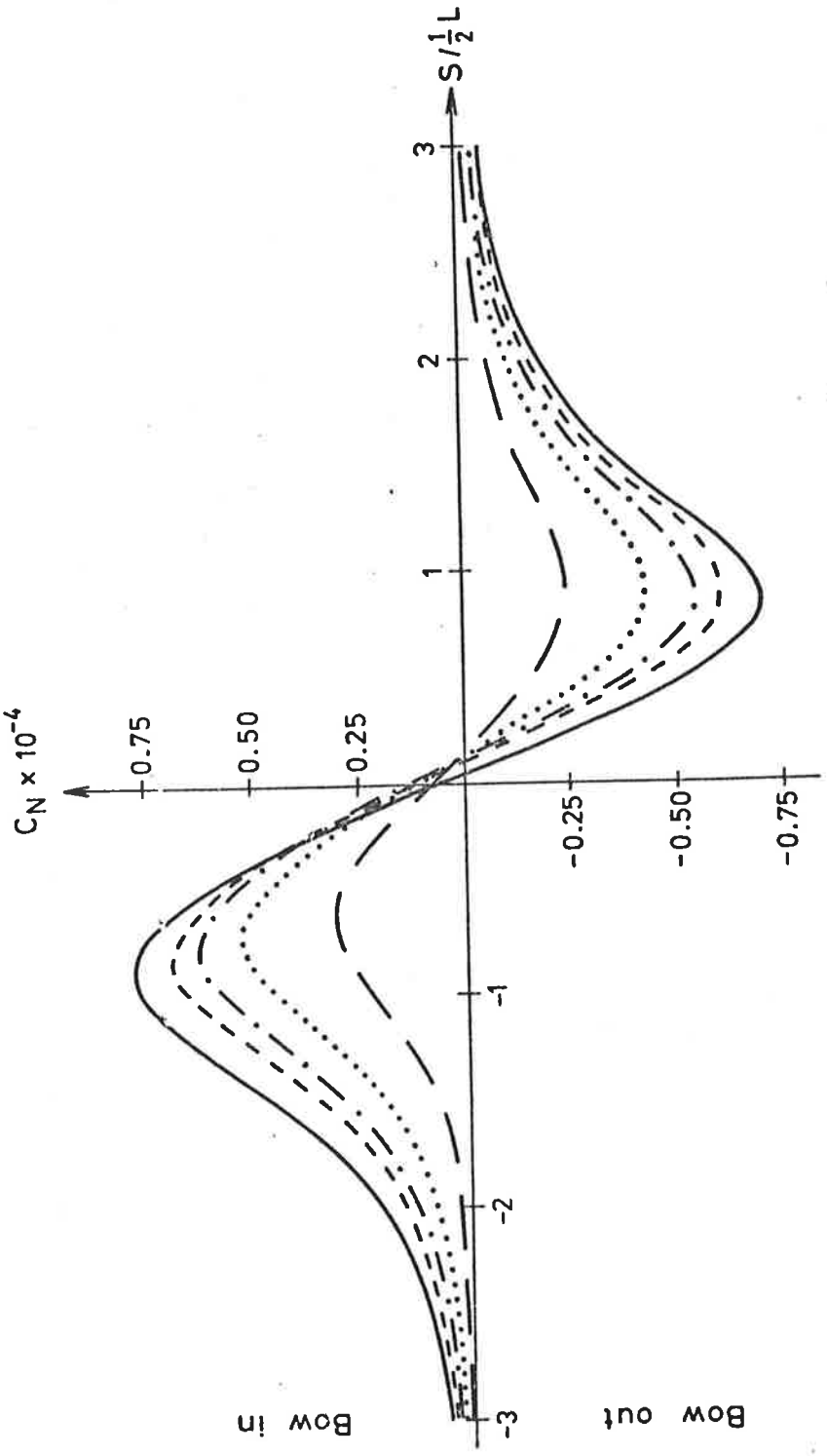

3.6 Coefficient of yaw moment for larger of two different size ships.

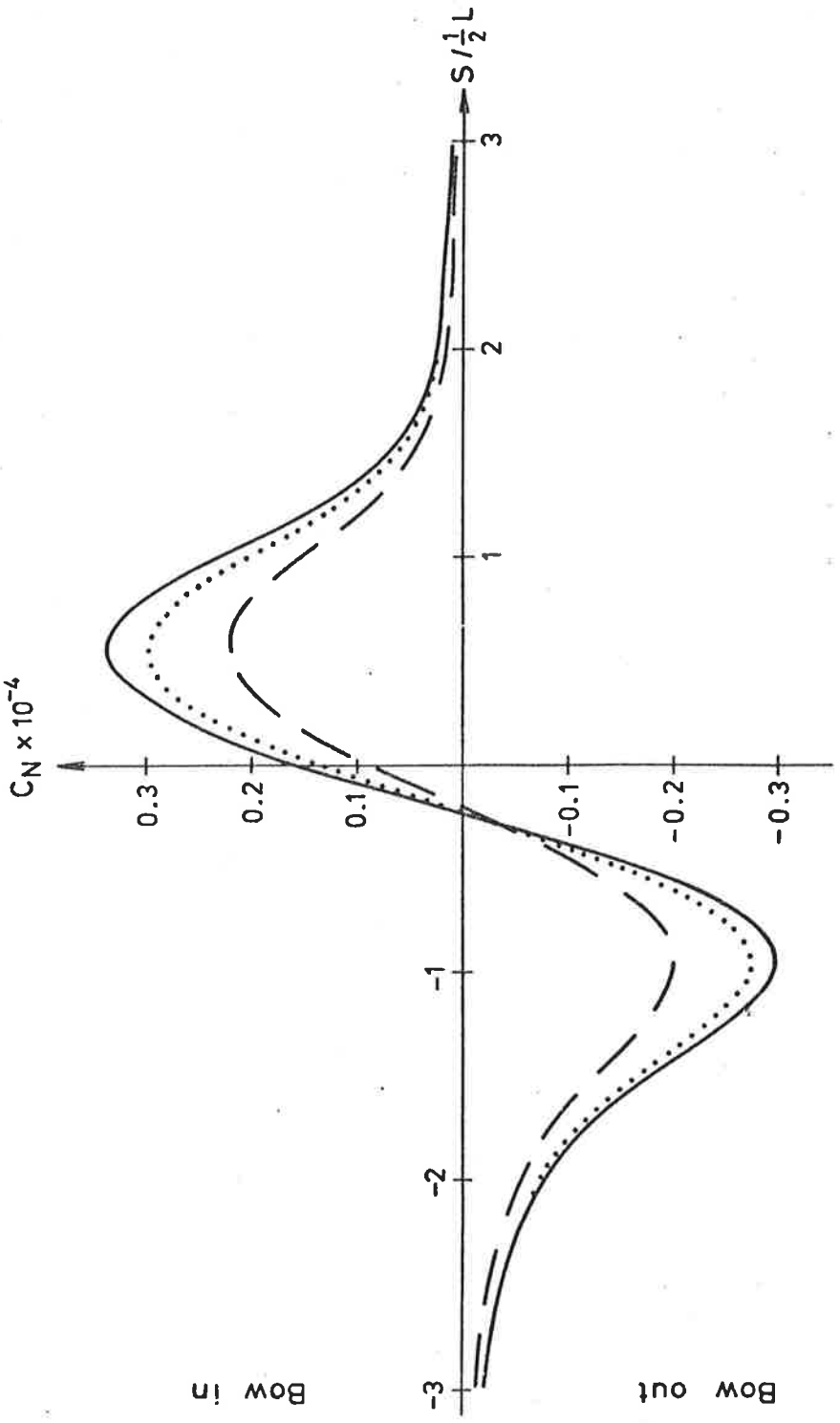

3.7 Coefficient of yaw moment for smaller of two different size ships.

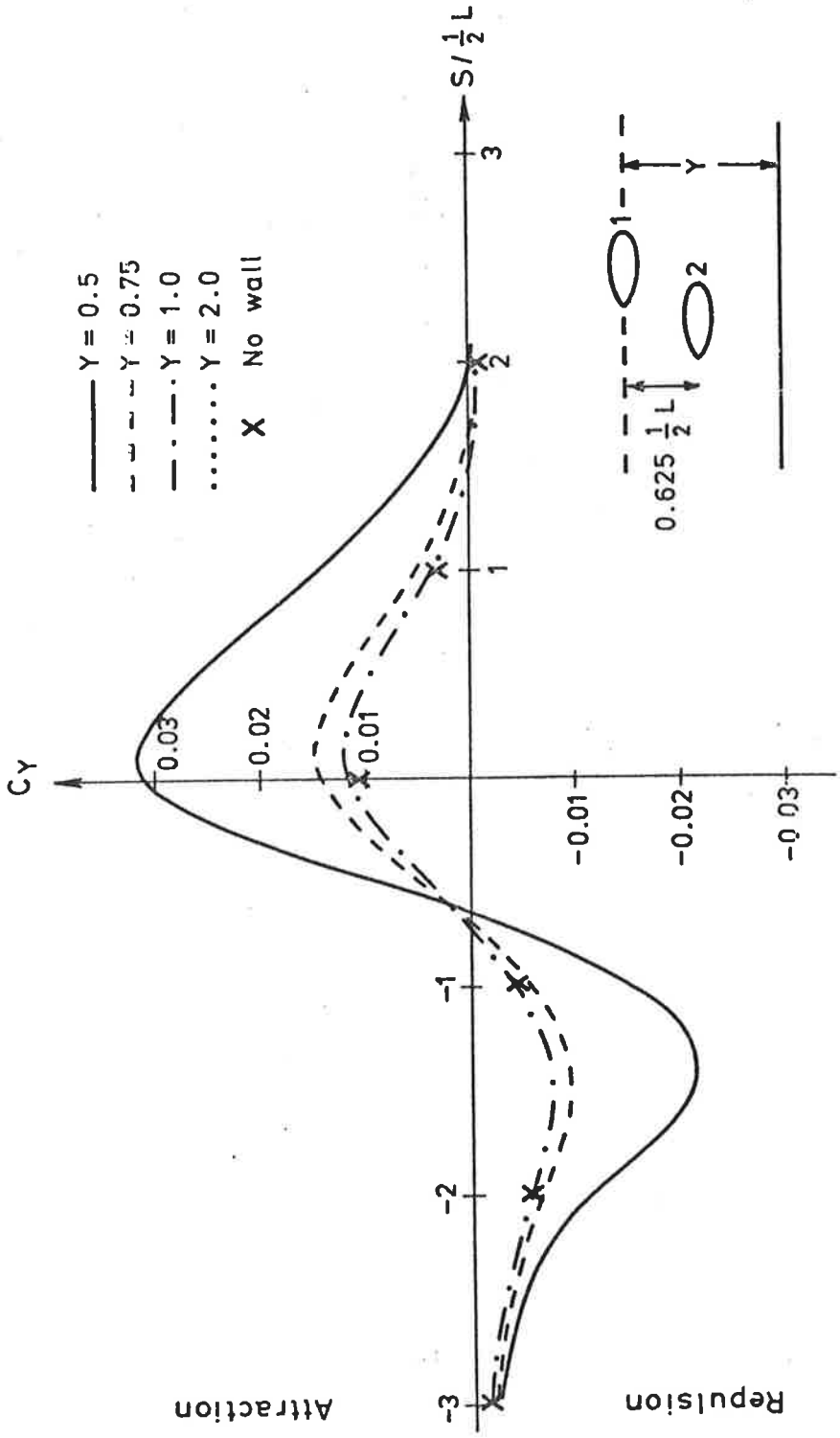

3.8 Coefficient of sway force for ship 1.

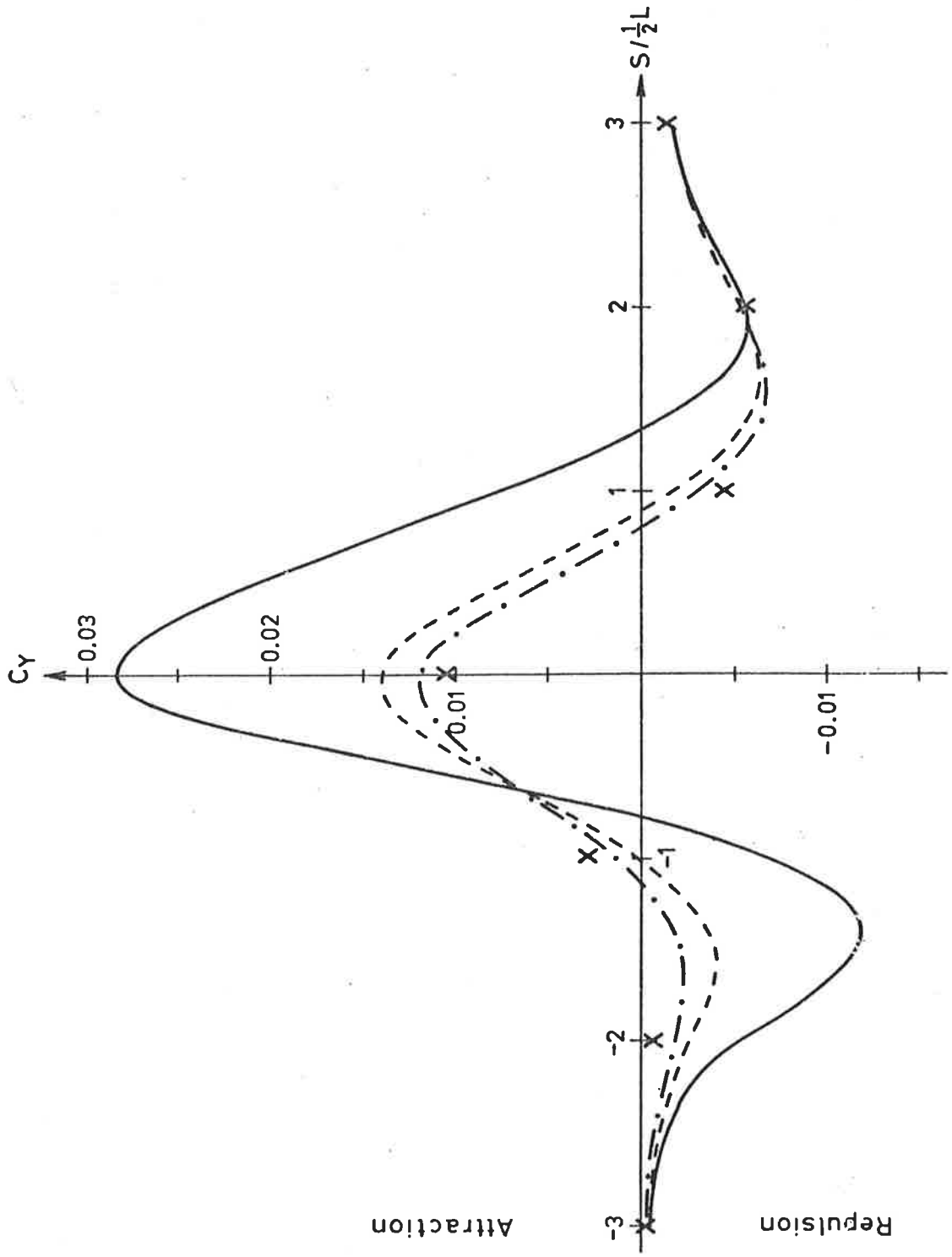

3.9 Coefficient of sway force for ship 2.

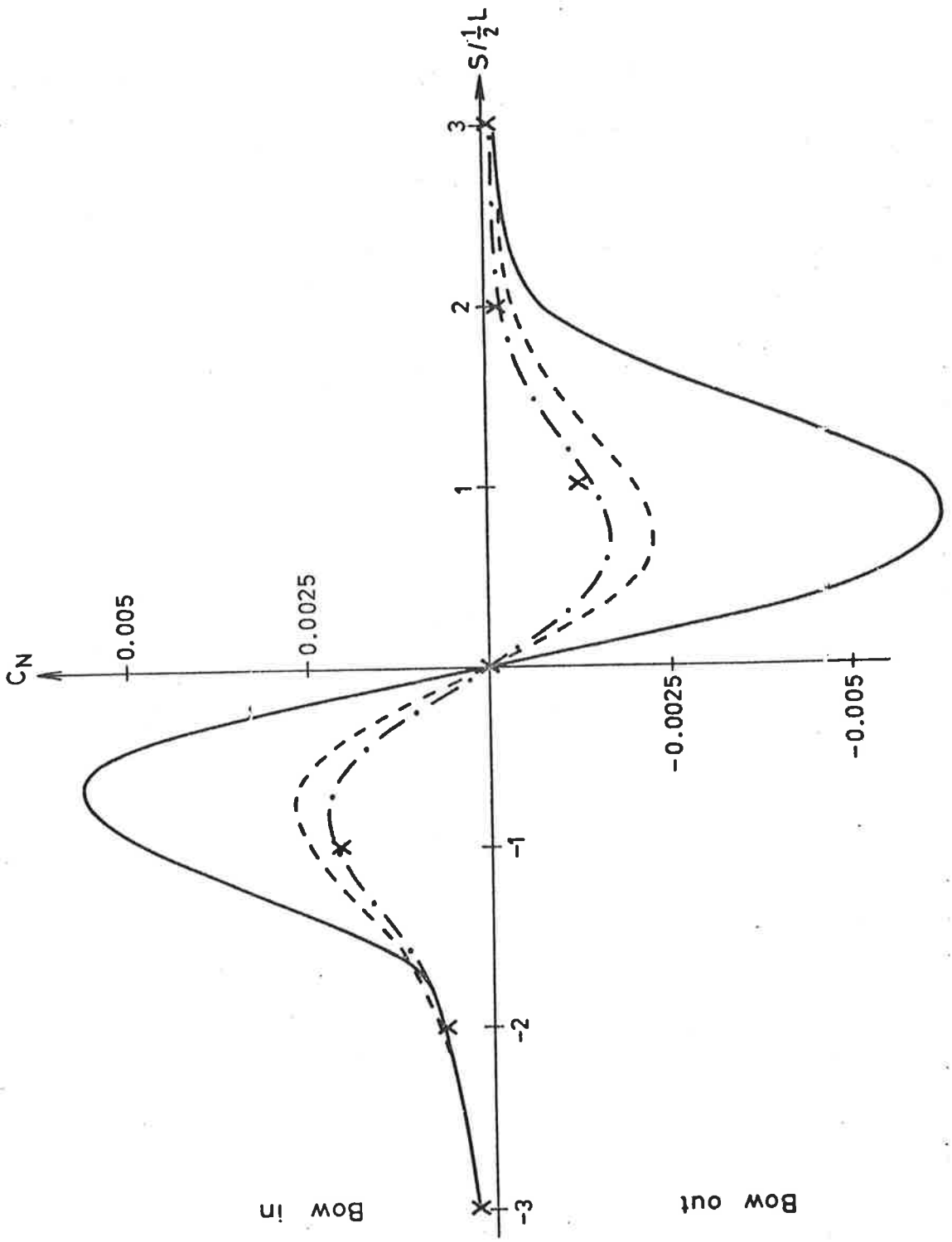

3.10 Coefficient of yaw moment for ship 1.

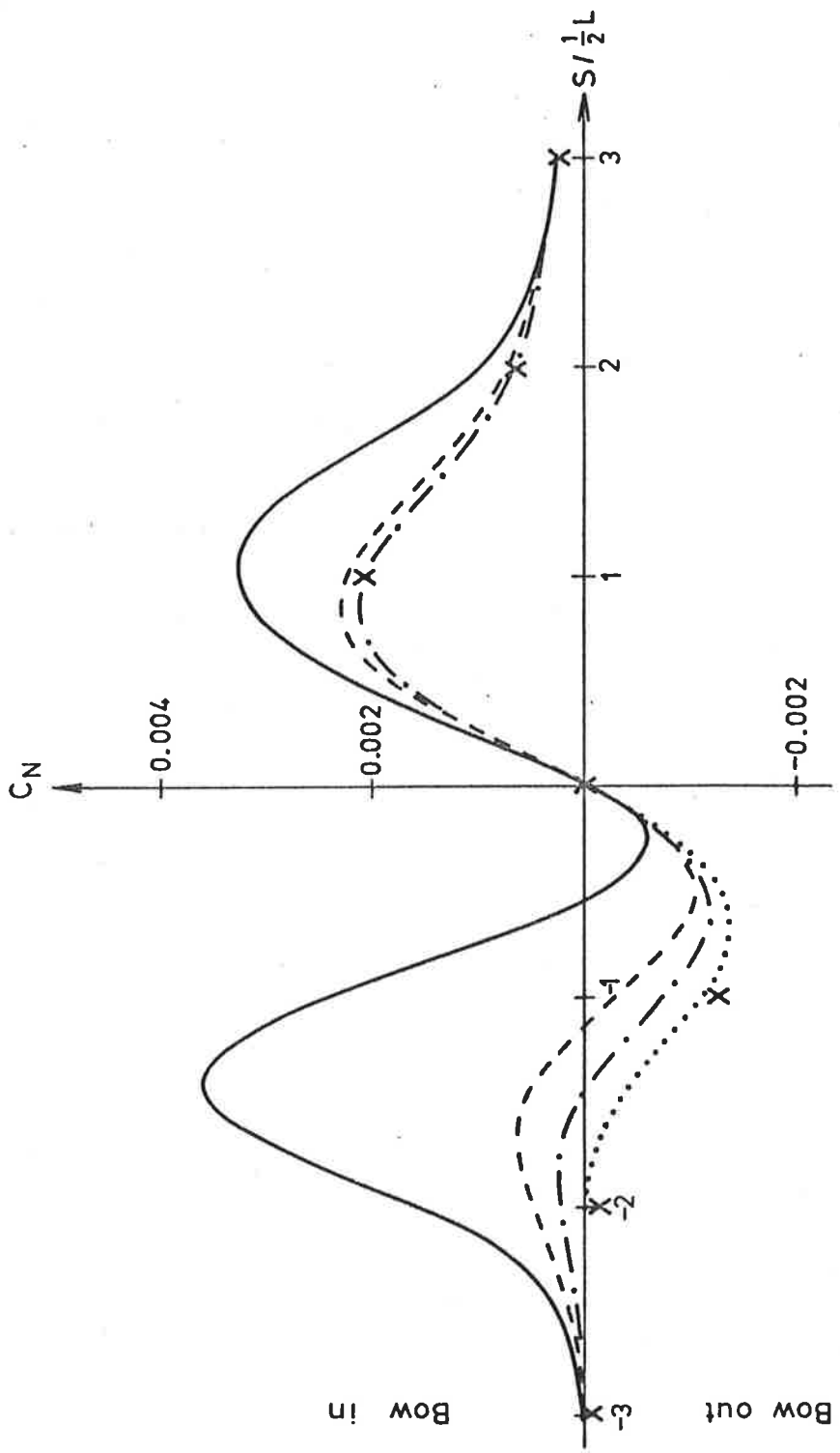

3.11 Coefficient of sway force for ship 2.

CHAPTER 4

A TWO-DIMENSIONAL MODEL FOR UNSTEADY INTERACTIONS

4.1 INTRODUCTION

A problem of interest in a number of different areas is the calculation of interaction forces and moments acting on two or more bodies moving in an unsteady manner. There are applications in both hydrodynamics and aerodynamics, although here the theory is developed with ship-ship interactions in mind.

In Chapter 3 the steady interactions of two ships were considered. In the present chapter, the unsteady situation of two or more ships moving at different velocities along parallel paths in very shallow water is discussed. A mathematical model for two-dimensional unsteady interactions is set up and numerically solved. A two-dimensional theory is appropriate for very shallow water as Tuck [22] has shown that flow past a vessel, in shallow water, with a small underkeel clearance is nearly two-dimensional.

A non-linear numerical technique for interactions between bodies in arbitrary motion has been devised by Giesing [9]. His theory is for two-dimensional potential flow and is used to examine the shape of vortex wakes as well as the forces on the bodies. The theory developed here is linearized, so no wake displacement occurs.

Another possible application of this type of theory is the aerodynamics of the interactions between passing motor vehicles. This is a ground effect problem to which much experimental effort has been devoted, and a number of papers giving experimental results have been published. Brown's [5] paper is on this topic, and [2] contains several other relevant papers.

The theory described here is essentially that presented in King [14], but a more general derivation, which can be used to allow for boundaries in the fluid (such as a wall), is given. First a mathematical model is set up for the two-dimensional motion of a group of thin bodies and their respective wakes, in a fluid which is assumed to be incompressible and inviscid. The Froude number is assumed to be sufficiently small, so that free surface effects can be neglected by replacing the fluid surface by a rigid wall. It is also assumed that the bodies are thin; that is they have a small beam to length ratio, and that the lateral separation between bodies is comparable with their lengths, and large compared to their beams.

Following Tuck and Newman [25] in an extension of classical thin-wing theory, the model is formulated as a system of coupled singular integral equations which have non-unique solutions. The solution which is feasible for a given problem is obtained by having zero circulation around stationary bodies, and by using a Kutta condition on moving bodies. A suitable condition for determining the rate of vortex shedding into the wake of each body is also required.

A numerical procedure for finding a solution according to this theory is developed, and the results obtained are compared with the experiments of Oltmann [18] and the theory of Collatz [6]. The results show reasonable agreement for the sway force with Oltmann's experiments and in this respect seem to be an improvement on Collatz's theory. The calculated yaw moment is not significantly better than that resulting from Collatz's theory.

A related mathematical model is used by Dand [7,8], with circulation being ignored in his first paper (i.e. essentially Collatz's theory), and only a crude first approximation to the effects of circulation being used in the second paper. Dand's theory gives excessively large values for forces and moments, when compared with experiments.

4.2 DERIVATION OF GOVERNING SYSTEM OF INTEGRAL EQUATIONS

Consider the motion in two dimensions of N thin bodies, all moving with (possibly) time-varying velocity parallel to the x-axis. It is convenient to consider this problem in an absolute frame of reference (that is, fluid at rest at infinity). Thus, for a velocity potential $\phi(x,y,t)$ and velocity $q(x,y,t)$

$$\underset{\sim}{q} = \underset{\sim}{\nabla}\phi, \text{ where } \phi \to 0 \text{ at } \infty . \tag{4.2.1}$$

The geometry of the j^{th} body, when it is moving to the left, is represented as in Figure 4.1. The body surfaces are given by

$$y = y_j + f_j^{\pm}(x,t), \; a_j(t) \leqslant x \leqslant b_j(t) \tag{4.2.2}$$

with a plus sign for the upper surface and a minus sign for the lower surface. The body segment B_j is represented by the interval $a_j(t) \leqslant x \leqslant b_j(t)$ and, for a body moving to the left, the wake segment W_j by interval $b_j(t) < x < \infty$. For body j the exact boundary condition is

$$\frac{\partial\phi}{\partial y} = \frac{\partial f_j^{\pm}}{\partial t} + \frac{\partial\phi}{\partial x}\frac{\partial f_j^{\pm}}{\partial x} , \text{ on } y = y_j \pm f_j^{\pm} \tag{4.2.3}$$

since the fluid cannot penetrate the body surface. For a thin body, this can be linearized to give

$$\phi_y(x, y_j \pm 0, t) = \frac{\partial}{\partial t} f_j^{\pm}(x,t) , \text{ on } B_j . \tag{4.2.4}$$

In order that the wake remains stationary after it has been shed, a condition that there is no pressure jump across the wake is required, namely

$$\Delta p = p(x, y_j + 0, t) - p(x, y_j - 0, t) = 0, \text{ across } W_j , \tag{4.2.5}$$

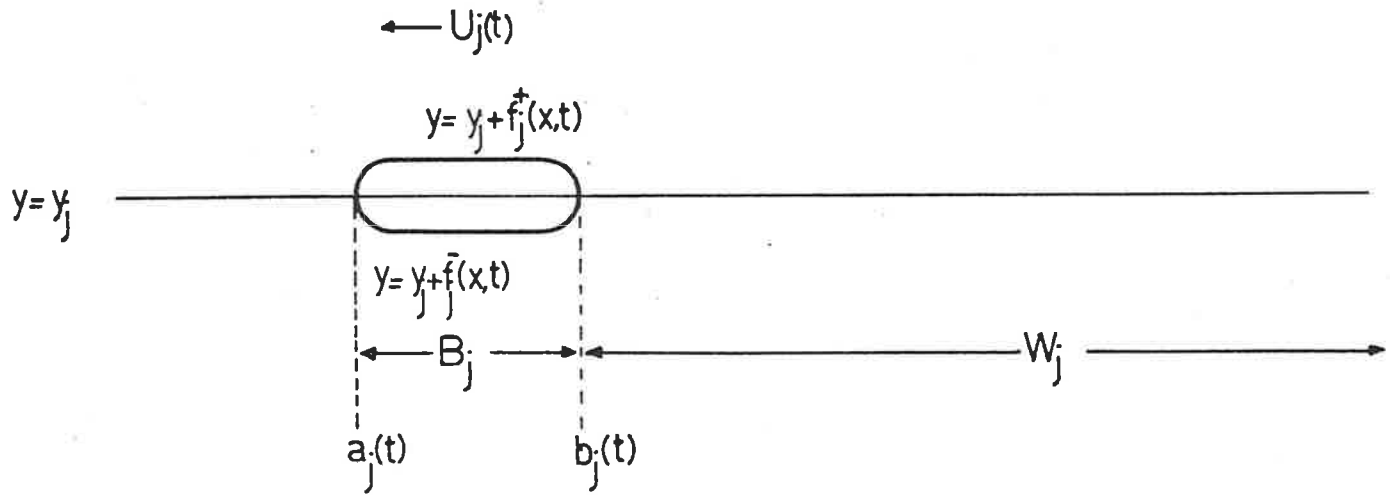

4.1 Geometry of j^{th} body.

where p is the pressure. By linearizing the Bernoulli equation

$$p = - \rho \frac{\partial \phi}{\partial t} \tag{4.2.6}$$

is obtained, where ρ is density, so from (4.2.5)

$$\Delta p = - \rho \Delta \frac{\partial \phi}{\partial t} = 0, \text{ across the wake .} \tag{4.2.7}$$

Therefore

$$\Delta \frac{\partial \phi}{\partial t} = 0, \text{ across the wake.} \tag{4.2.8}$$

Thus the jump in the potential

$$\Delta \phi = \phi(x, y_j + 0, t) - \phi(x, y_j - 0, t) \tag{4.2.9}$$

is a function of position x only across the wake W_j . Hence the strength of the wake does not vary with time.

The velocity potential ϕ satisfies the two-dimensional Laplace Equation

$$\phi_{xx} + \phi_{yy} = 0, \tag{4.2.10}$$

with the possibility of some further conditions due to any restriction of the x-y plane such as the presence of walls. In this formulation it will be assumed that the paths of the bodies are parallel to any boundary. As with conventional thin-wing theory, the lifting effects are modelled by vortices of strength $\gamma_j(x,t)$ on $B_j + W_j$ and the thickness effects are modelled by sources of strength $q_j(x,t)$ on B_j . The vortex strength $\gamma_j(x,t)$ on $y = y_j$ is given by

$$\gamma_j(x,t) = - \frac{\partial}{\partial x} \Delta \phi, \text{ across } y = y_j \tag{4.2.11}$$

$$= \begin{cases} 0, \text{ ahead of } B_j \\ \text{unknown on } B_j \\ \gamma_j^W(x), \text{ on } W_j \end{cases} \tag{4.2.12}$$

Hence the disturbance velocity potential due to N bodies has the representation

$$\phi(x,y,t) = \sum_{j=1}^{N} \left\{ \int_{B_j} q_j(\xi,t) G(x,y;\xi,y_j)\, d\xi \right.$$

$$\left. + \int_{B_j + W_j} \gamma_j(\xi,t) H(x,y;\xi,y_j)\, d\xi \right\} \qquad (4.2.13)$$

where $G(x,y;\xi,\eta)$ is the velocity potential at (x,y) for a unit source located at (ξ,η) and $H(x,y;\xi,\eta)$ is the velocity potential at (x,y) for a unit vortex at (ξ,η). Both these potentials must be chosen so as to satisfy any restrictions on the two-dimensional fluid. If there are any branches in the velocity potential for a unit vortex H, then these branches must be chosen so that any discontinuities in the potential function occur across a wake, so that the velocity potential satisfies

$$\Delta \frac{\partial \phi}{\partial x} = - \gamma_j^w, \text{ across } W_j \ . \qquad (4.2.14)$$

The unit source potential $G(x,y;\xi,\eta)$ is determined by solving

$$G_{xx} + G_{yy} = \delta(x-\xi)\delta(y-\eta) \qquad (4.2.15)$$

together with any boundary conditions on the fluid, and will have the asymptotic behaviour that as $(x,y) \to (\xi,\eta)$

$$G(x,y;\xi,\eta) \to \frac{1}{2\pi} \log\sqrt{(x-\xi)^2+(y-\eta)^2} \ . \qquad (4.2.16)$$

The unit vortex potential $H(x,y;\xi,\eta)$ is obtained by solving

$$\frac{\partial H}{\partial \xi} = - \frac{\partial G}{\partial \eta} \qquad (4.2.17)$$

which has the asymptotic behaviour

$$H(x,y;\xi,\eta) \to \frac{1}{2\pi} \arctan\left[\frac{y-\eta}{x-\xi}\right] \text{ as } (x,y) \to (\xi,\eta). \qquad (4.2.18)$$

The velocity potential ϕ must also satisfy the body boundary condition (4.2.4). So, if $x \in B_i$, equations(4.2.4) and (4.2.13) give

$$\phi_y(x,y_i \pm 0,t) = \tfrac{1}{2}q_i(x,t)$$

$$+ \sum_{\substack{j=1 \\ (j\neq i)}}^{N} \int_{B_j} q_j(\xi,t)G_y(x,y_i \pm 0;\xi,y_j)d\xi$$

$$+ \sum_{j=1}^{N} \int_{B_j+W_j} \gamma_j(\xi,t)H_y(x,y_i \pm 0;\xi,y_j)d\xi$$

$$= \frac{\partial}{\partial t} f_i^{\pm}(x,t) \quad , \qquad i = 1,\ldots,N \ . \tag{4.2.19}$$

Subtracting the plus and minus parts of equation (4.2.19) gives

$$q_i(x,t) = \frac{\partial}{\partial t}\left\{f_i^{+}(x,t) - f_i^{-}(x,t)\right\} \quad i = 1,\ldots,N. \tag{4.2.20}$$

This is equivalent to the usual aerodynamic relation for the source strength in terms of the slope of the thickness function, recalling that such relations are normally expressed in a frame of reference which is moving with the body. Thus the source strength is completely determined.

Adding the plus and minus parts gives the system of integral equations

$$\sum_{j=1}^{N} \int_{B_j} \gamma_j(\xi,t)H_y(x,y_i \pm 0;\xi,y_j)d\xi$$

$$= F_i'(x,t) + G_i'(x,t) + H_i'(x,t),$$

$$i = 1,\ldots,N \tag{4.2.21}$$

where a prime denotes $\frac{\partial}{\partial x}$ and where

$$F_i'(x,t) = \frac{\partial}{\partial t}\left\{f_i^{+}(x,t) + f_i^{-}(x,t)\right\} \tag{4.2.22}$$

$$G_i'(x,t) = -\sum_{\substack{j=1 \\ (j\neq i)}}^{N} \int_{B_j} q_j(\xi,t)G_y(x,y_i \pm 0;\xi,y_j)d\xi \tag{4.2.23}$$

and

$$H_i'(x,t) = -\sum_{j=1}^{N} \int_{W_j} \gamma_j^w(\xi) H_y(x, y_i \pm 0; \xi, y_j) d\xi \ . \qquad (4.2.24)$$

These three functions are all known once $\gamma_j^w(x) = \gamma_j(x,t)$, $x \in W_j$ is known. To determine this last quantity γ_j^w, some means of finding the vorticity shed into the wake is required.

As the system of integral equations (4.2.21) does not possess a unique solution, an additional condition for each body is required. For body j Kelvin's circulation theorem must hold around the body B_j and its wake W_j. So the circulation $\Gamma_j(t)$ around body j must be zero, that is

$$\Gamma_j(t) = \int_{B_j + W_j} \gamma_j(\xi,t) d\xi = 0 \ . \qquad (4.2.25)$$

This is the only condition required on a body stationary relative to the fluid which has no wake, so equation (4.2.25) becomes

$$\int_{B_j} \gamma_j(\xi,t) d\xi = 0 \ . \qquad (4.2.26)$$

For a moving body, Sears [20] has shown that the appropriate Kutta condition on the trailing edge of a body is that the vorticity at the trailing edge be equal to the vorticity in the wake immediately adjacent; that is, for moving body j

$$\gamma_j(b_j(t),t) = \gamma_j^w(b_j(t)) \ . \qquad (4.2.27)$$

This is equivalent to the Kutta-Jowkowski condition, that the pressure above and below the trailing edge must be equal. By using the above conditions as required, the unique solution for a given problem may be obtained.

4.3 FORCES AND MOMENTS

The quantities which are of most interest in this problem are the sway force and yaw moments on the bodies. These are of principal importance during ship manoeuvres, as they may cause some situations to be hazardous.

The net y-directed force (sway) on body j is

$$Y_j(t) = -\int_{B_j} \Delta p \, dx \tag{4.3.1}$$

$$= -\rho \int_{B_j} \frac{\partial \Delta\phi}{\partial t} \, dx \tag{4.3.2}$$

by using equation (4.2.6). From equation (4.2.11)

$$\Delta\phi = -\int_{a_j(t)}^{x} \gamma_j(x,t)dx \text{ across } y = y_j \tag{4.3.3}$$

and substituting into (4.3.2) gives

$$Y_j(t) = -\rho \int_{B_j} \frac{\partial}{\partial t} \int_{a_j(t)}^{x} \gamma_j(\zeta,t)d\zeta \, dx. \tag{4.3.4}$$

The net yaw moment about the centre of body j is

$$N_j(t) = -\rho \int_{B_j} \Delta p(x-(a_j(t)+b_j(t))/2)dx. \tag{4.3.5}$$

So using equations (4.2.6) and (4.3.3) gives

$$N_j(t) = \tfrac{1}{2}\rho \int_{B_j} (a_j(t)+b_j(t)-2x) \frac{\partial}{\partial t} \int_{a_j(t)}^{x} \gamma_j(\zeta,t)d\zeta \, dx \, . \tag{4.3.6}$$

The sway force is defined to be positive to the starboard and the yaw moment positive for the bow turning to starboard.

4.4 NUMERICAL TECHNIQUES FOR SOLVING SYSTEM OF INTEGRAL EQUATIONS IN UNSTEADY PROBLEM

A numerical technique which is an extension of that described in Chapter 3 is developed. Here there is the additional difficulty of having a trailing wake, and the necessity of including some kind of time-stepping process.

The general form of the system of singular integral equations which was derived for the unsteady problem in section 4.2 is

$$\sum_{j=1}^{N} \int_{B_j} \gamma_j(\xi,t) K_x(x,\xi;y_i-y_j)\,d\xi = R_i'(x,t) + H_i'(x,t) \qquad i = 1,\ldots,N \tag{4.4.1}$$

where $K_x(x,\xi;\eta)$ is a kernel which has a logarithmic singularity at $x = \xi$ and $R_i'(x,t)$ is the right-hand-side of the integral equation except for the wake term $H_i'(x,t)$. Both of the right-hand-side terms are known at a given time t.

An indefinite integration with respect to x of equation (4.4.1) yields

$$\sum_{j=1}^{N} \int_{B_j} \gamma_j(\xi,t) K(x,\xi;y_i-y_j)\,d\xi = R_i(x,t) + H_i(x,t) + C_i(t) \qquad i = 1,\ldots,N \tag{4.4.2}$$

where $C_i(t)$ is an arbitrary "constant" of integration. Integral equations of the form of equation (4.4.1) with the singular behaviour of K_x have non-unique solutions and this is asserted here by the "constants" $C_i(t)$, which are determined by the vortex shedding condition.

A numerical solution to equation (4.4.2) at time T can be found if $R_i(x,T)$ and $H_i(x,T)$ are known. This suggests an iteration scheme with a forward time-stepping process. To simplify the evaluation of any terms involving the wake vorticity, it is useful to assume that constant

vorticity is shed into the wake during each time step. If the sequence of time-steps used is $t_0 = 0, t_1, t_2, \ldots$ and the position of the trailing edge of body j at these time-steps is $p_{j0}, p_{j1}, p_{j2}, \ldots$ then, if vorticity γ^w_{ik} is shed into the wake by body j at time point t_k, the vorticity of the wake in the interval (p_{jk+1}, p_{jk}) is γ^w_{jk}

To find a numerical solution it is necessary to divide the body segments B_j into intervals in which the vorticity may be represented by step functions. At the ends of each body a square-root singularity may be anticipated so B_j is divided into M intervals $x_{ji-1}(t) < x < x_{ji}(t)$ with vorticity $\gamma_{ji}(t)$, where

$$x_{ji}(t) = -\tfrac{1}{2}|a_j(t)-b_j(t)| \cos\frac{i\pi}{M} + \frac{a_j(t)+b_j(t)}{2}, \qquad i = 0,1,\ldots,M \tag{4.4.3}$$

which provides the correct increase in density of points near the ends necessary to counter the singularities.

The system of integral equations can now be written as

$$\sum_{j=1}^{N}\sum_{k=1}^{M} \gamma_{jk}(t) \int_{x_{jk-1}(t)}^{x_{jk}(t)} K(x,\xi;y_i-y_j)\,d\xi = R_i(x,t) + H_i(x,t) + C_i(t), \quad i = 1,\ldots,N. \tag{4.4.4}$$

The integral in equation (4.4.4) can usually be evaluated analytically at any value of x. In particular at $x = \bar{x}_{j\ell}(t)$ where $\bar{x}_{j\ell}(t)$ is a point near the centre of the ℓ^{th} interval of body j at time t, specifically

$$\bar{x}_{j\ell}(t) = -\tfrac{1}{2}|a_j(t)-b_j(t)| \cos[(\ell-\tfrac{1}{2})\pi/M] + \frac{a_j(t)+b_j(t)}{2}, \qquad \ell = 1,2,\ldots,M. \tag{4.4.5}$$

It is now convenient to introduce the kernel function

$$\chi(x,\xi;\eta) = \int K(x,\xi;\eta)d\xi \qquad (4.4.6)$$

in terms of which equation (4.4.4) can be written as

$$\sum_{j=1}^{N}\sum_{k=1}^{M} \gamma_{jk}(t)[\chi(\bar{x}_{i\ell}(t),x_{jk}(t);y_i-y_j) - \chi(\bar{x}_{i\ell}(t),x_{jk-1}(t);y_i-y_j)]$$

$$= R_i(\bar{x}_{i\ell}(t),t) + H_i(\bar{x}_{i\ell}(t),t) + C_i(t),\ i = 1,\ldots,N. \qquad (4.4.7)$$

If T time steps have elapsed, from equations (4.2.24) and (4.4.6)

$$H_i(\bar{x}_{i\ell},t_T)$$

$$= -\sum_{j=1}^{N}\sum_{k=0}^{T-1} \gamma^{w}_{jk}[\chi(\bar{x}_{i\ell}(t_T),p_{jk};y_i-y_j) - \chi(\bar{x}_{i\ell}(t_T),p_{jk+1};y_i-y_j)]\ . \qquad (4.4.8)$$

By letting

$$A(t)_{(i-1)m+\ell,(j-1)m+k} = \chi(\bar{x}_{i\ell}(t),x_{jk}(t);y_i-y_j)$$

$$- \chi(\bar{x}_{i\ell}(t),x_{jk-1}(t);y_i-y_j) \qquad (4.4.9)$$

equation (4.4.7) can be written as

$$\sum_{j=1}^{N}\sum_{k=1}^{M} A(t)_{(i-1)m+\ell,(j-1)m+k}\gamma_{jk}(t)$$

$$= R_i(\bar{x}_{i\ell}(t),t) + H_i(\bar{x}_{i\ell}(t),t) + C_i(t)$$

$$i = 1,\ldots,N,\ \ell = 1,\ldots,M \qquad (4.4.10)$$

which is a system of NM simultaneous equations for $\gamma_{jk}(t)$, to be solved at each time step. This can be expressed as the matrix equation

$$A(t)\underset{\sim}{\gamma}(t) = \underset{\sim}{g}(t) + \sum_{j=1}^{N} \underset{\sim}{e}^{(j)} C_j(t) \qquad (4.4.11)$$

where $A(t)$ is a $NM \times NM$ matrix such that

$$A(t) = [A_{ij}(t)] \tag{4.4.12}$$

and the NM vectors

$$\underset{\sim}{\gamma}(t) = \begin{bmatrix} \gamma_{11}(t) \\ \vdots \\ \gamma_{1M}(t) \\ \gamma_{21}(t) \\ \vdots \\ \gamma_{N1}(t) \\ \vdots \\ \gamma_{NM}(t) \end{bmatrix}, \quad \underset{\sim}{g}(t) = \begin{bmatrix} R_1(\bar{x}_{11}(t),t) + H_1(\bar{x}_{11}(t),t) \\ \vdots \\ R_1(\bar{x}_{1M}(t),t) + H_1(\bar{x}_{1M}(t),t) \\ R_2(\bar{x}_{21}(t),t) + H_2(\bar{x}_{21}(t),t) \\ \vdots \\ R_N(\bar{x}_{N1}(t),t) + H_N(\bar{x}_{N1}(t),t) \\ \vdots \\ R_N(\bar{x}_{NM}(t),t) + H_N(\bar{x}_{NM}(t),t) \end{bmatrix}$$

and

$$\underset{\sim}{e}^{(j)} = \begin{bmatrix} 0 \\ \vdots \\ 0 \\ 1 \\ \vdots \\ 1 \\ 0 \\ \vdots \\ 0 \end{bmatrix} \begin{matrix} \} \ (j-1)\times M \text{ terms} \\ \} \ M \text{ terms} \\ \} \ NM-jM \text{ terms} \end{matrix} \tag{4.4.13}$$

The solution $\underset{\sim}{\gamma}(t)$ is obtained by using standard matrix inversion techniques with the $N + 1$ right-hand-sides $\underset{\sim}{g}(t)$, $\underset{\sim}{e}^{(\ell)}$, $\ell = 1,\ldots,N$ and can be written as

$$\underset{\sim}{\gamma}(t) = \underset{\sim}{\gamma}^{(0)}(t) + \sum_{\ell=1}^{N} C_\ell(t)\, \underset{\sim}{\gamma}^{(\ell)}(t) \tag{4.4.14}$$

where

$$\underset{\sim}{\gamma}^{(0)}(t) = A^{-1}(t)\underset{\sim}{g}(t) \tag{4.4.15}$$

and

$$\underset{\sim}{\gamma}^{(\ell)}(t) = A^{-1}(t)\underset{\sim}{e}^{(\ell)}, \quad \ell = 1,\ldots,N. \tag{4.4.16}$$

Thus by examination of the components of the vectors in (4.4.14), the vorticity at $\bar{x}_{j\,k}(t)$ (i.e. "mid-point" of k^{th} interval on body j) is

$$\gamma_{j\,k}(t) = \gamma_{j\,k}^{(0)}(t) + \sum_{\ell=1}^{N} C_\ell(t)\gamma_{j\,k}^{(\ell)}(t) \quad . \tag{4.4.17}$$

This is a numerical approximation to a corresponding representation of the actual vortex strength $\gamma_j(x,t)$, namely

$$\gamma_j(x,t) = \gamma_j^{(0)}(x,t) + \sum_{\ell=1}^{N} C_\ell(t)\gamma_j^{(\ell)}(x,t), \quad j = 1,\ldots,N. \tag{4.4.18}$$

The preceding numerical technique allows a numerical approximation to the general solution of the N singular integral equations to be calculated, with $C_\ell(t)$, $\ell = 1,\ldots,N$ as arbitrary "constants", which are determined at each time step by imposing a Kutta condition on the trailing edge of each body which is moving relative to the fluid, or a zero circulation condition on a stationary body.

For unsteady interaction manoeuvres the appropriate conditions to determine $C_\ell(t)$, $\ell = 1,\ldots,N$ are given by equation (4.2.27) for a moving body and (4.2.26) for a stationary body. Thus for equation (4.2.26) it is necessary to obtain an estimate of the vorticity at the trailing edge of a moving body as the vorticity is only calculated at approximately the centre of each interval on the body. A satisfactory method is to use one of the expected properties of the solution to the singular integral equations as $x \to b_j(t)$ on body j. Namely, any solution of equation (4.4.1) must have the property that as $x \to b_j(t)$ on body j

$$\gamma_j(x,t) \to \frac{D_j(t)}{\sqrt{b_j(t)-x}} + E_j(t) + O(\sqrt{b_j(t)-x}) \qquad (4.4.19)$$

for some "constants" $D_j(t)$ and $E_j(t)$. In contrast to the steady case (see Chapters 2 and 3) the expression above contains a constant term. This is because a non-zero vortex strength is expected at the trailing edge whereas bodies in steady flow have zero vorticity at the trailing edge, as they cannot shed vortices into the flow.

By fitting this function to the vorticity on the last two intervals $\gamma_{j\,M}^{(\ell)}$ and $\gamma_{j\,(m-1)}^{(\ell)}$ on body j the "constants" $D = D_j^{\ell}(t)$ and $E = E_j^{\ell}(t)$ may be determined for each body j and each value of ℓ ($\ell = 0,1,\ldots,N$). The vorticity at the trailing edge must be finite, so the sum over ℓ of the inverse square-root terms must be zero, that is

$$D_j^{o}(t) + \sum_{\ell=1}^{N} C_\ell(t) D_j^{\ell}(t) = 0, \qquad (4.4.20)$$

for each moving body j. For a stationary body j equation (4.2.26) may be written as

$$\sum_{k=1}^{M} \gamma_{j\,k}(t)\,(x_{j\,k}(t)-x_{j\,k-1}(t)) = 0 \qquad (4.4.21)$$

which upon substitution of equation (4.4.17) becomes

$$\sum_{k=1}^{M} (\gamma_{j\,k}^{(0)}(t) + \sum_{\ell=1}^{N} C_\ell(t)\gamma_{j\,k}^{(\ell)}(t))(x_{j\,k}(t)-x_{j\,k-1}(t)) = 0. \qquad (4.4.22)$$

Equations (4.4.20) and (4.4.22) may now be combined as required by the type of interaction occurring to form a matrix equation which may be solved to determine $C_\ell(t)$, $\ell = 1,\ldots,N$.

Once the $C_\ell(t)$'s are known the vorticity on all intervals of each body at time t may be determined by using equation (4.4.17). This may then be used to determine the sway force and yaw moment on each body. To do this a finite difference scheme in time is used to approximate the

time derivative so that at time t_k from equation (4.3.4) the sway force is

$$Y_j(t_T) = -\frac{\rho}{t_T - t_{T-1}} \sum_{k=1}^{M} \left\{ \sum_{i=1}^{k} \gamma_{jk}(t_T)(x_{ji}(t_T) - x_{ji-1}(t_T)) \right.$$

$$\left. - \sum_{i=1}^{k} \gamma_{jk}(t_{T-1})(x_{ji}(t_{T-1}) - x_{ji-1}(t_{T-1})) \right\} . \qquad (4.4.23)$$

Similarly the yaw moment at time t_T is

$$N_j(t_T) = -\tfrac{1}{2}\rho \frac{1}{t_T - t_{T-1}} \sum_{k=1}^{M} (a_j(t_T) + b_j(t_T) - \bar{x}_{jk}(t_T))$$

$$\times (x_{jk}(t_T) - x_{jk-1}(t_T)) \left\{ \sum_{i=1}^{k} \gamma_{jk}(t_T)(x_{ji}(t_T) - x_{ji-1}(t_T)) \right.$$

$$\left. - \sum_{i=1}^{k} \gamma_{jk}(t_{T-1})(x_{ji}(t_{T-1}) - x_{ji-1}(t_{T-1})) \right\} . \qquad (4.4.24)$$

Thus the sway force and yaw moment may be calculated. As a result of the treatment of the wake and the time scheme used, the two formulae above actually calculate an approximation to the mean of the sway force and yaw moment for the time interval $[t_{T-1}, t_T]$. So, when graphing the force and moment it would be more accurate to plot the value at time $\frac{1}{2}(t_{T-1} + t_T)$ which was actually calculated at t_T.

4.5 RESULTS FOR UNBOUNDED TWO-DIMENSIONAL FLOW

The results which will be presented in this chapter are those for unbounded two-dimensional flow, although the numerical technique developed in the preceding discussion can be used for some restricted flows. For unbounded flow the kernel

$$K^{ij} = \frac{1}{2\pi} \log \sqrt{(y_i - y_j)^2 + (x - \xi)^2} \qquad (4.5.1)$$

and $L^{ij}(x)$ is given by (3.4.4).

Only results for the case $N = 2$ (that is, for interactions between two bodies) will be considered. Although the formulation was for N bodies, results for $N > 2$ would either be inaccurate, or involve the inversion of very large matrices with a consequent increase in the time and computer memory space required. The numerical method has been tested for convergence by varying both the number of mesh points on each body and the size of each time step, for interactions involving two bodies travelling in the same direction. The convergence was found to be satisfactory for the results presented in this thesis, if 30 mesh points were taken on each body, and if the time-steps were such that a change in the stagger of about one twentieth of the length of the larger body occurred in each time-step.

The numerical technique described in 4.4 was coded in FORTRAN and run on the University of Adelaide's C.D.C. 6400. A typical run of the program, allowing sufficient wake to build up before the ships came close together,had an execution time of 990 seconds. The execution time is large as at each time-step a new matrix had to be calculated and inverted.

An interaction situation for which some experimental results exist, and for which the above model is valid, is that for a moving body passing a stationary body. The non-dimensional sway force and yaw moment coefficients which will be used for this type of interaction are

$$C_{Y_j(t)} = \frac{Y_j(t)}{\rho U^2 \beta} \qquad (4.5.2)$$

and

$$C_{N_j(t)} = \frac{N_j(t)}{\rho U^2 \beta L/2}$$

respectively, where U is the velocity of the moving body, β is the half breadth and L is the length of the bodies. The sway force $Y_j(t)$ and yaw moment $N_j(t)$ are calculated by using (4.4.23) and (4.4.24).

Oltmann [18] has obtained experimental results for two elliptic-sectioned cylinders with beam/length = 0.125, with one body stationary and the other moving at constant speed. In Figures 4.2 and 4.3 the measurements of Oltmann's experiments are compared with values computed using the foregoing formulation of the net sway force for a separation η between the paths of the bodies of $0.625(\frac{1}{2}L)$. Oltmann's results are somewhat dependent on the velocity of the moving body, whereas, from the preceding formulation, it can be seen that the non-dimensional force and moment results are independent of Froude number, being the zero Froude number limits. Oltmann's experiments were conducted in the presence of a free surface, so the wave pattern of the moving body may have affected his results. In the "tiefgetaucht" case, the measurements were taken deeper in the fluid than in the "flachgetaucht", so the "tiefgetaucht" results would be expected to be less affected by free-surface effects.

The computed results in Figures 4.2 and 4.3 seem to give reasonable quantitative agreement with the experiments. There is good qualitative agreement with the peak attraction force in the "tiefgetaucht" case at Froude number $F_n = 0.144$ and 0.217. In Figure 4.2 the peak attraction force on the moving body is much larger than the peak repulsion force, so that for ships in passing manoeuvres the moving ship will tend to be attracted more than it is repelled, thus giving rise to the danger of a collision. In fact the moving body is experiencing a large attraction force for a range of stagger S of over half a body length.

In a previous study on this topic by Collatz [6], in which no circulation was allowed about the bodies, and no Kutta condition applied on the trailing edge, a force which is symmetric with respect to stagger was obtained. The results in Figure 4.2 of the present theory are quite different to those of Collatz and do not show particularly symmetric behaviour. In this respect the present theory is more satisfactory as it

could be expected that the wake would introduce some asymmetry. The steady results of Chapter 3 are also asymmetric, of course.

In Figure 4.3, for the stationary body, there is a close correspondence between Collatz's results and the present computed results, both giving good agreement with Oltmann's experiments. This is not too surprising, as Collatz's zero-circulation assumption is the condition applied to the stationary body (4.2.26).

Consider now the graphs of the yaw moment, Figures 4.4 and 4.5, and compare them with Oltmann's experimental results. It can be seen that the moments are of the correct magnitude, although the shapes of the curves are very different. Collatz's theory fails to give better agreement for the moving body, although it gives good results for the stationary body. The present computed results for the stationary body are of a similar shape to Collatz's, but are smaller in magnitude. The danger of a collision is highlighted by Figure 4.4, which shows the peak inward moment occurring at the same time as the peak attraction force, so the bodies are not only being sucked together but their bows are both turning inward, as well.

Figures 4.6 and 4.7 show the variation in the sway force as the length ratio (L_s/L_m) of the two bodies is varied, at a separation of 0.625 L_m, with the two bodies having the same breadth (breadth/L_m = 0.125). Figures 4.8 and 4.9 show the peak attraction and repulsion forces corresponding to the results in Figures 4.6 and 4.7.

For the moving body it can be seen that the effect of varying the length ratio gives two different kinds of responses, depending upon which body is the larger. When the stationary body is the larger (that is, $L_s/L_m > 1$), increasing the length ratio does not significantly change the value of the peak attraction and repulsion forces, but increases the length of stagger over which a large attraction force is acting on

the moving body. When the moving body is the longer and the length ratio decreases, the shape of the curve does not change greatly but the magnitude of the attractive force decreases rapidly. Figure 4.8 shows that the peak repulsion force varies slowly as the length ratio increases. It appears that there is a limiting value to the peak force. Thus, it may be worthwhile to investigate this further, as in situations when a ship passes a stationary ship, island or sandbank the force and moment on the moving vessel are of importance.

For the stationary body (Figures 4.7 and 4.8), increasing the length ratio leads to an increase in the peak values of both the attraction and repulsion sway force. The peak attraction occurs further away from zero stagger as the length ratio increases.

As the separation of the two bodies depends on the length of the moving body, for a larger moving body (that is, small length ratio) the separation is greater, so the force would be expected to decrease, and this can be seen in Figure 4.8. For the stationary body, Figure 4.9 shows that the peak sway force increases as the length ratio increases (that is, bodies closer together or stationary body larger), and there is no behaviour analogous to that seen for the moving body. In general it appears that for a body passing a smaller stationary body the force on the stationary body is greater than that on the moving body. This is important for berthed ships or ships moored to buoys as they will experience the greater force, not the ship moving past them.

The variation in peak force on two ellipses of equal size (one stationary, the other moving) for different values of the separation of the paths of the ellipses is shown in Figure 4.10. The force increases as the separation decreases, as would be expected.

Although these results are interesting and useful as a qualitative guideline, for practical applications with underkeel clearance, they

should be viewed with caution, since the clearance is important in altering the magnitude of forces and moments, as shown for steady interactions in Chapter 3.

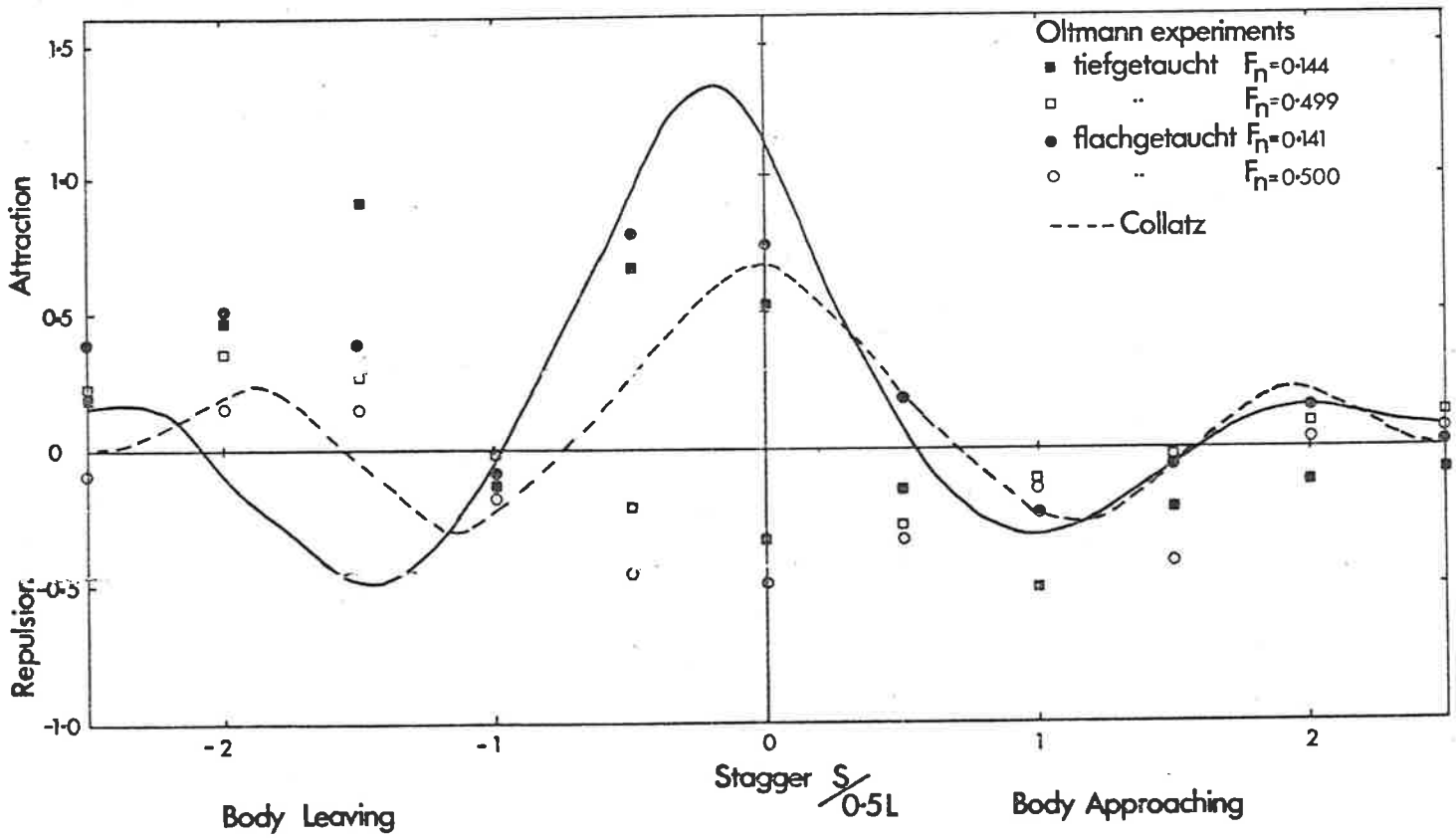

4.2 Coefficient of sway force C_y on moving body for two identical elliptic bodies with $\eta = 0.625(\frac{1}{2}L)$.

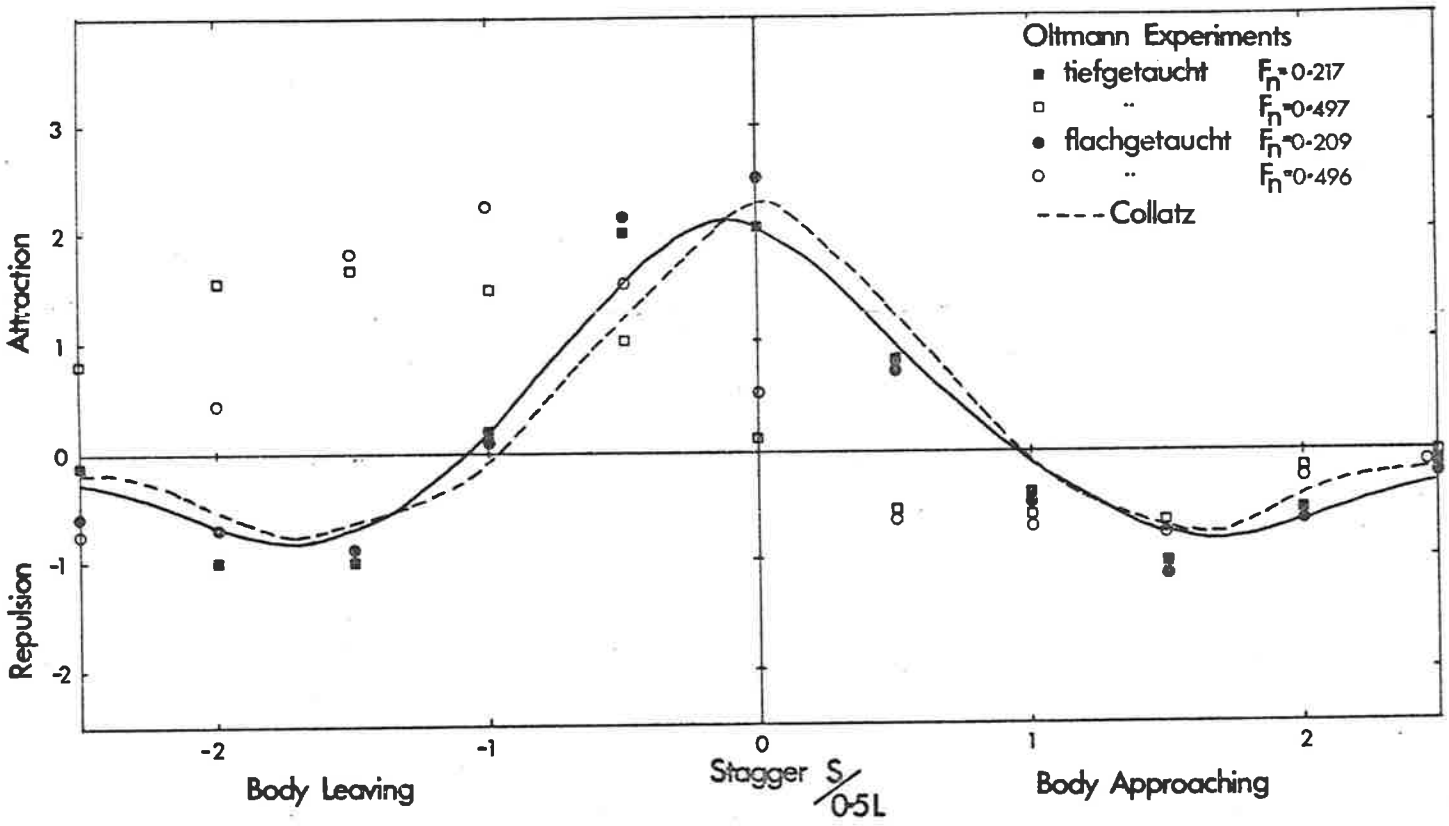

4.3 Coefficient of sway force C_y on stationary body for two identical elliptic bodies with $\eta = 0.625(\frac{1}{2}L)$.

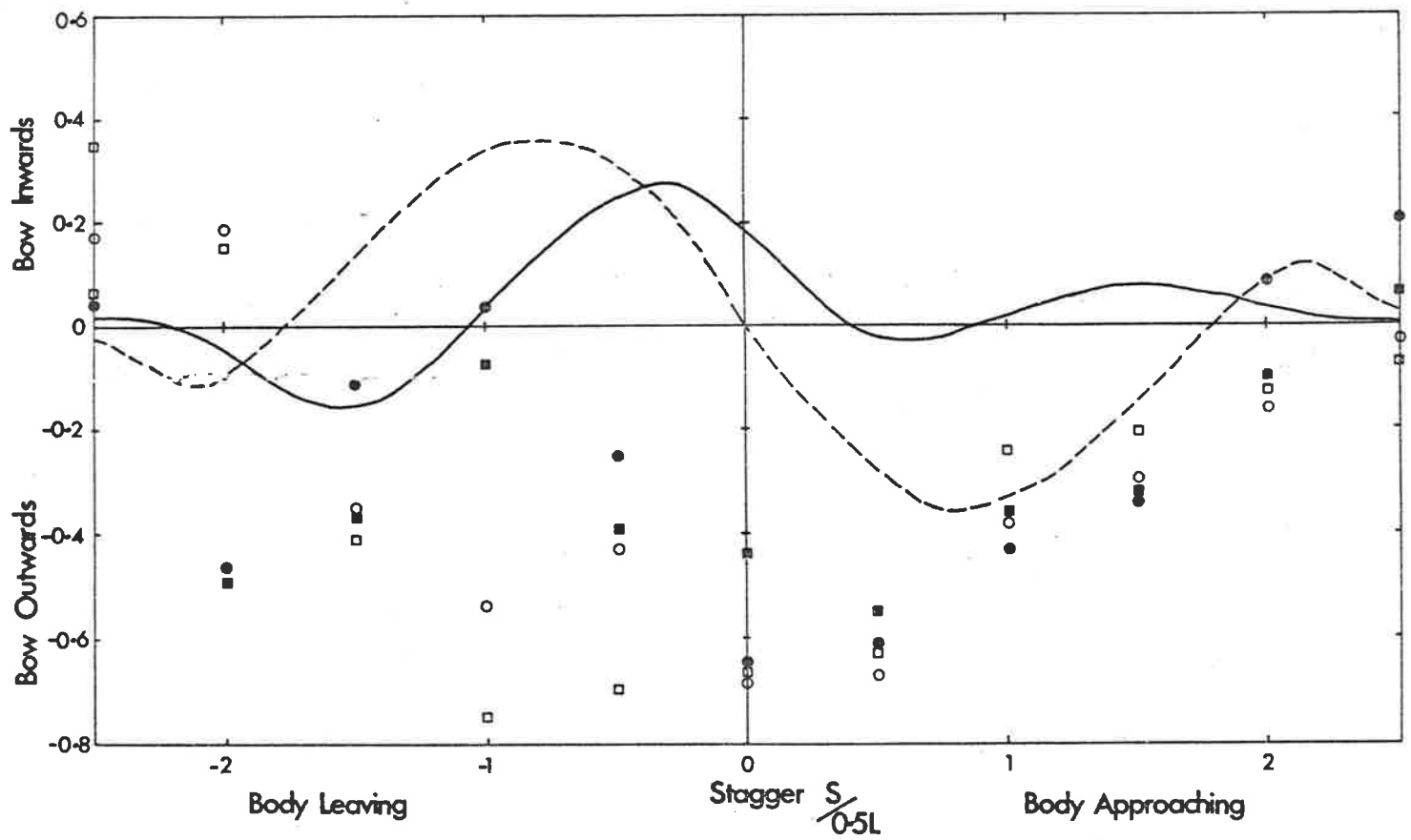

4.4 Coefficient of yaw moment C_N on moving body for two identical elliptic bodies with $\eta = 0.625(\frac{1}{2}L)$.

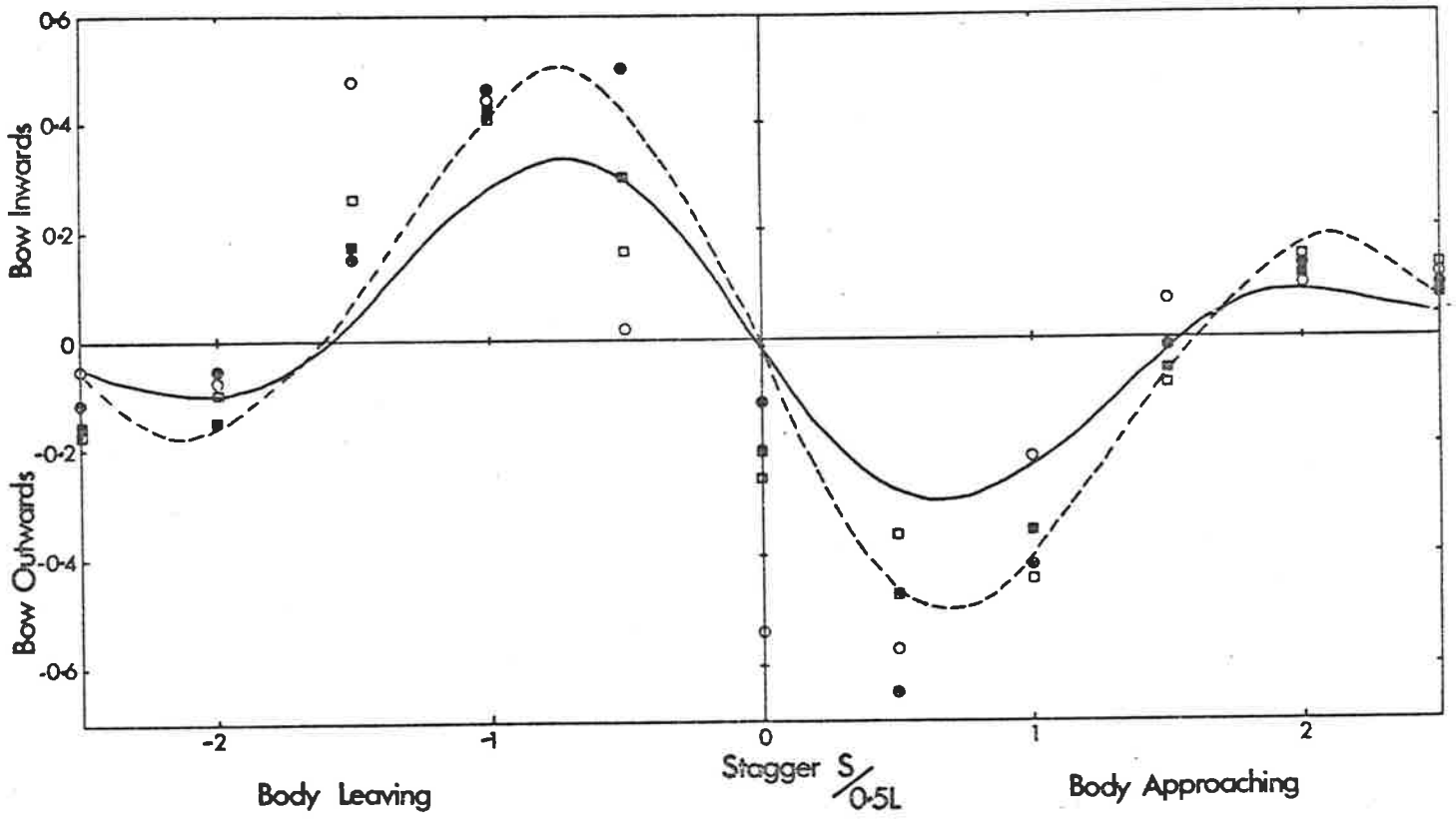

4.5 Coefficient of yaw moment C_N on stationary body for two identical elliptic bodies with $\eta = 0.625(\frac{1}{2}L)$.

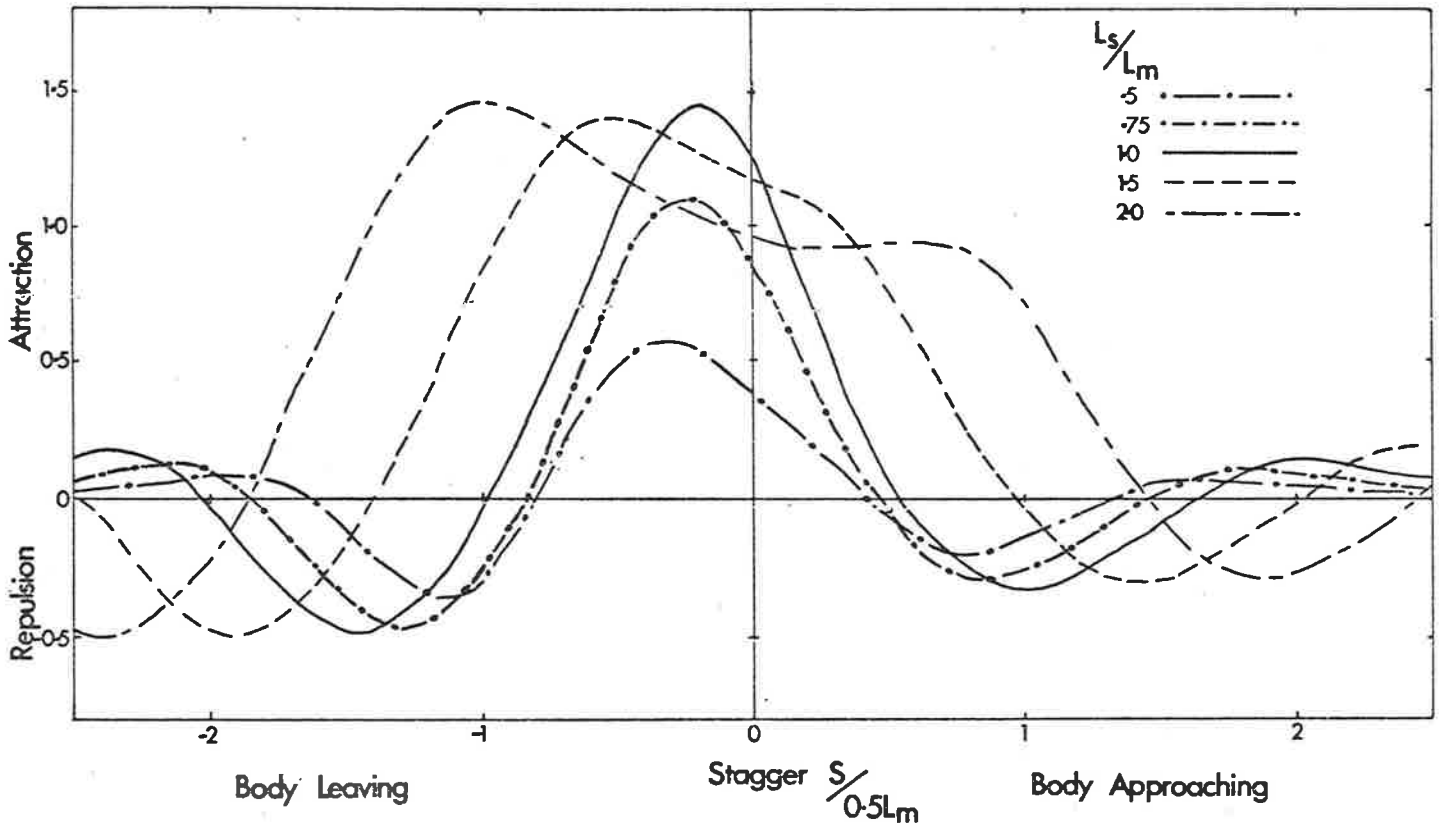

4.6 Coefficient of sway force C_y on moving body for $\eta = 0.625(\frac{1}{2}L_m)$.

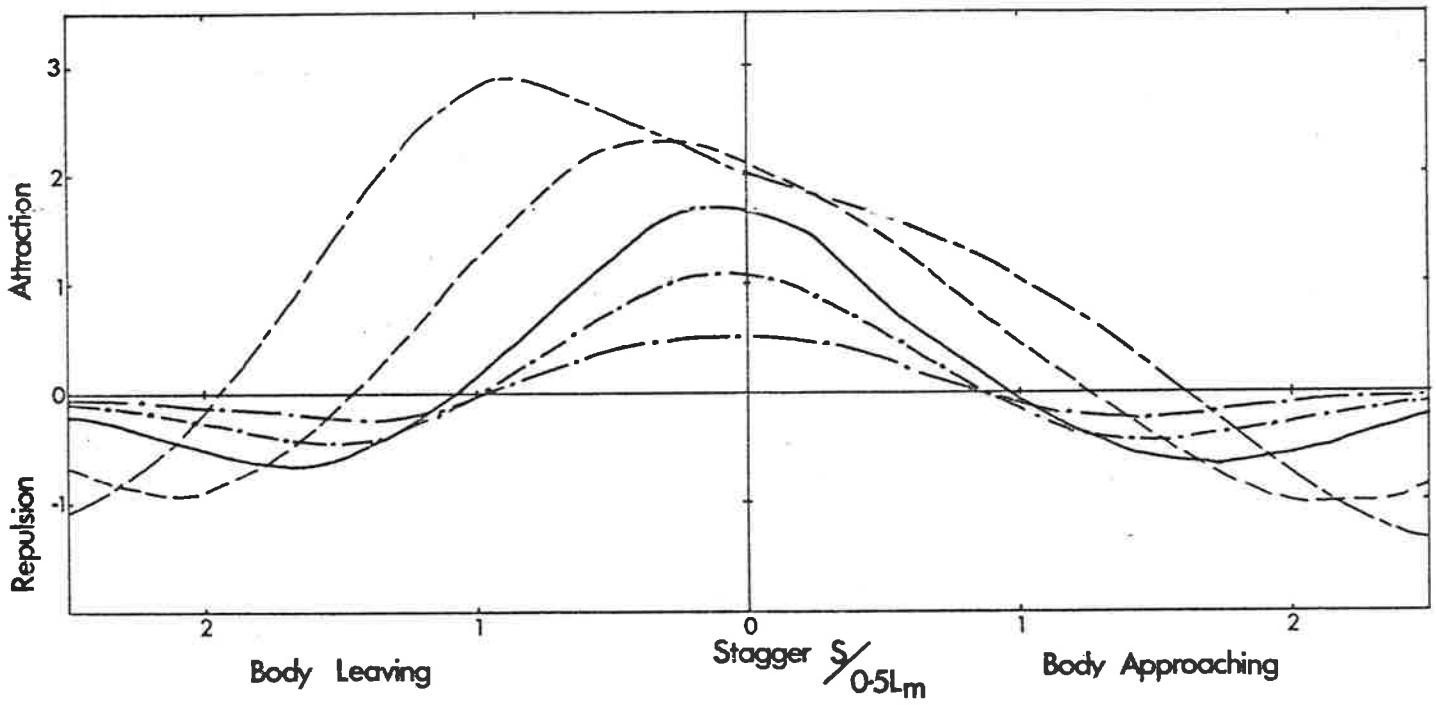

4.7 Coefficient of sway force C_y on stationary body for $\eta = 0.625(\frac{1}{2}L_m)$.

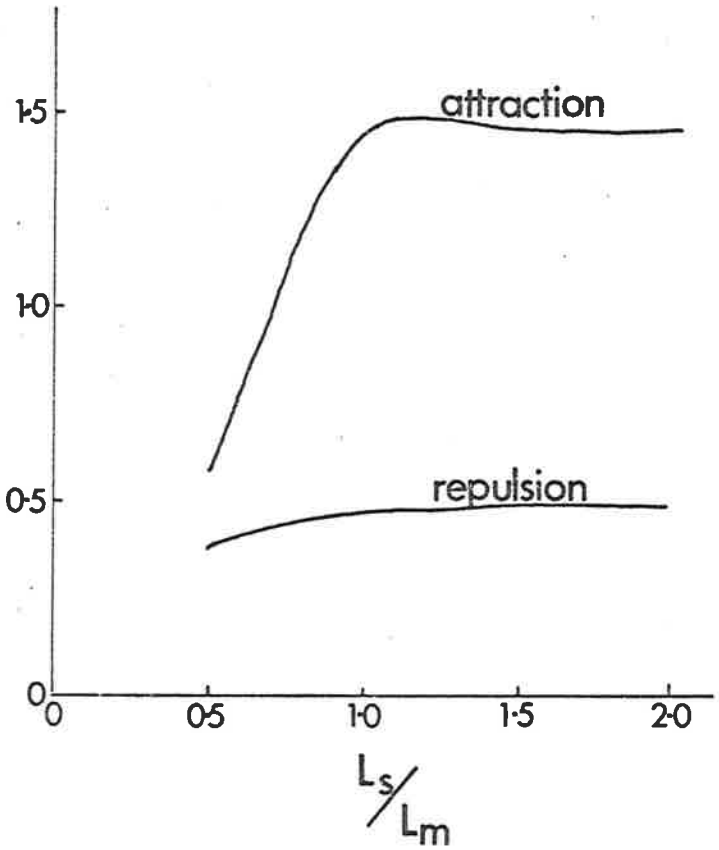

4.8 Variation of peak coefficient of sway force C_y on moving body for $\eta = 0.625(\frac{1}{2}L_m)$.

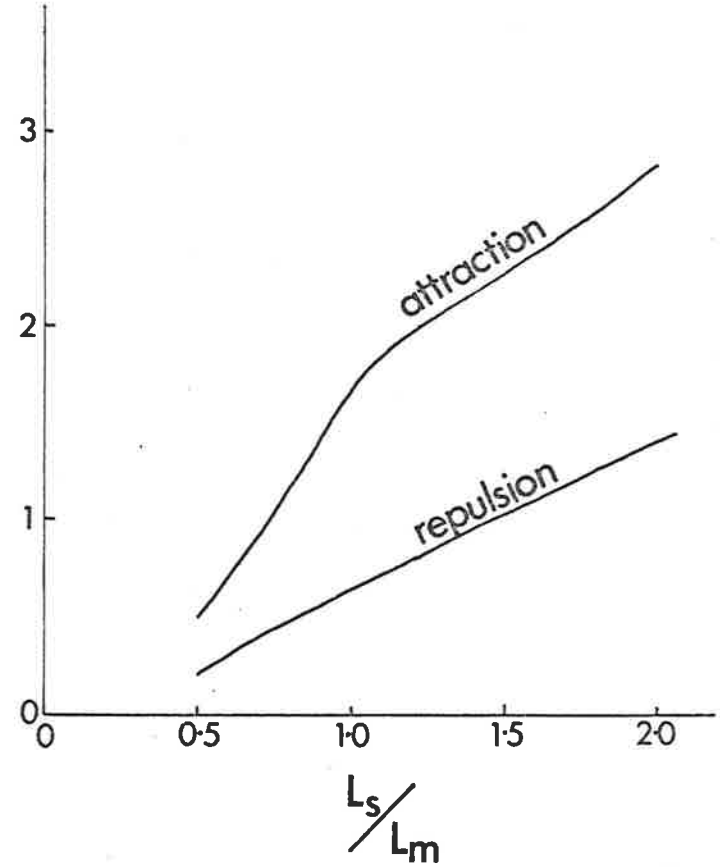

4.9 Variation of peak coefficient of sway force C_y on stationary body for $\eta = 0.625(\frac{1}{2}L_m)$.

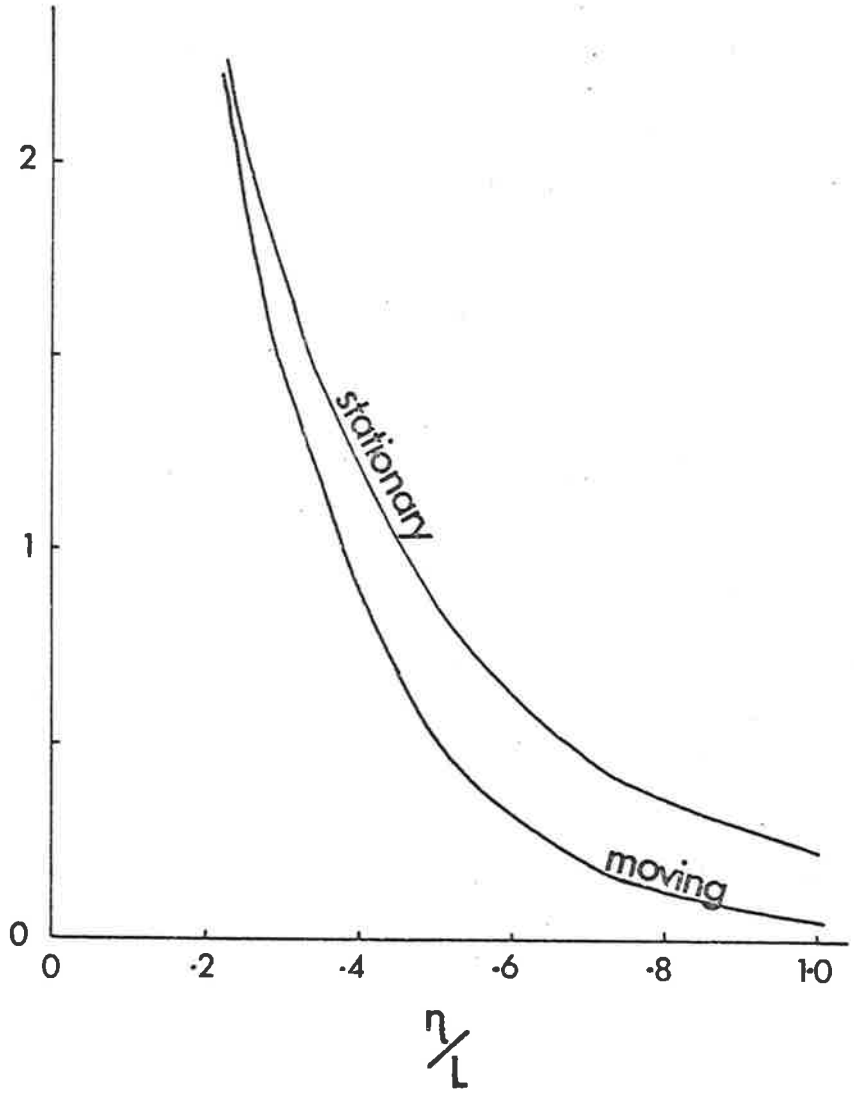

4.10 Variation of peak coefficient of sway force C_y on two identical bodies as the separation changes.

CHAPTER 5

UNSTEADY SHIP INTERACTIONS INCLUDING BOTTOM CLEARANCE EFFECTS

5.1 INTRODUCTION

The preceding chapters have shown the need for an unsteady shallow-water ship interaction theory which includes the effects of underkeel clearance. Yeung [29] has considered this problem and formulated it be using results from slender-body theory. He finds solutions to particular cases by using the Cauchy Inversion technique.

King [15] obtains the same governing system of integral equations as Yeung, by using the results of Tuck [23] used in earlier chapters. The system of integral equations is solved numerically by the technique described in 4.4, and the results compared with those of Yeung and the experiments of Remery [19]. The material contained in this chapter is a fuller version of that in King [15].

A theory for the unsteady problem of a ship approaching a wall at an angle in shallow water, which could be considered as an extension to the above theories, has been developed by Hess [11]. This has the added complexity that the kernels in the integral equation are dependent on the distance from the wall, which is now a time dependent quantity.

5.2 MATHEMATICAL FORMULATION

The geometry of the ships and wake used here is the same as that of Chapter 4, except that the ships are moving over a bottom of depth $h(y)$. The geometry of the j^{th} ship is given in Figure 5.1.

Using the notation of Chapter 3, from Tuck [23] for unsteady flow the thickness boundary condition on ship j is

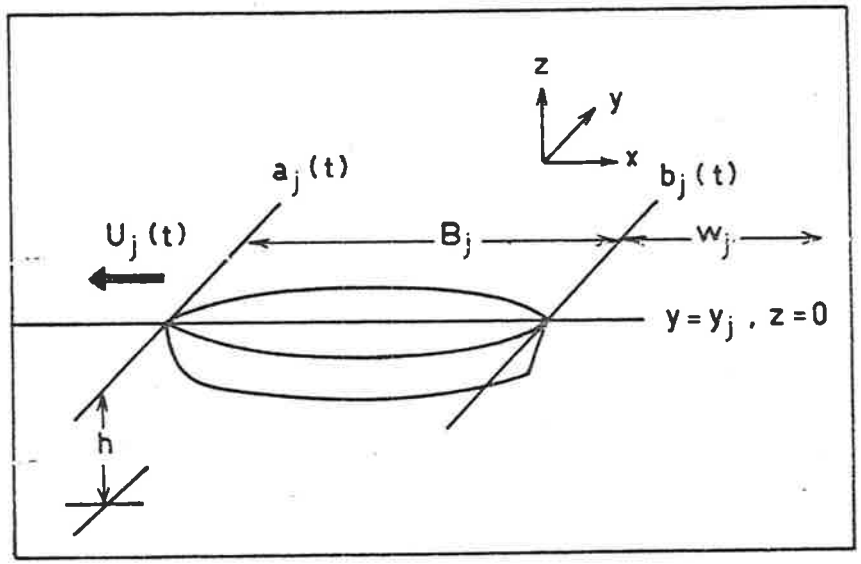

5.1 Geometry of j^{th} ship and its wake.

$$\Delta\phi_y = U_j(t)\Delta f_j'(x,t) \quad \text{at} \quad y = y_j \tag{5.2.1}$$

and the camber boundary condition on ship j is

$$\bar{\phi}_y - U\bar{f}_j'(x,t) = \frac{1}{2h_j C_j}\Delta\phi \text{ at } y = y_j \tag{5.2.2}$$

where

$$\Delta\phi_y = \phi_y(x,y_j+0,t) - \phi_y(x,y_j-0,t), \tag{5.2.3}$$

$$\Delta\phi = \phi(x,y_j+0,t) - \phi(x,y_j-0,t) \tag{5.2.4}$$

and $h_j = h(y_j)$. The wake condition (4.2.8) still applies, so the strength of the vortices in the wake does not vary with time.

The disturbance velocity potential due to N ships and their wakes, is given by (4.2.13) with the kernels H and G defined as in section 2.3. Substituting (4.2.13) into the thickness boundary condition (5.2.1) gives the source strength on ship j as

$$q_j(x,t) = U_j(t)\, S_j'(x)/h_j \ . \tag{5.2.5}$$

The camber boundary condition (5.2.2) yields a system of singular integral equations to determine the vortex strength, namely

$$\sum_{j=1}^{N}\int_{B_j+W_j}\gamma_j(\xi,t)H_y(x,y_i;\xi,y_j)d\xi + \frac{1}{2h_i C_i(x)}\int_{B_i}\gamma_i(x,t)u(x-\xi)d\xi$$

$$= U\bar{f}_i'(x) - \sum_{j=1}^{N}\int_{B_j} q_j(\xi,t)[\tfrac{1}{2}G_y(x,y_i+0;\xi,y_j)$$

$$+ \tfrac{1}{2}G_y(x,y_i-0;\xi,y_j)]d\xi \qquad i = 1,\ldots,N \tag{5.2.6}$$

where $u(x)$ is the Heariside step function. This system of integral equations can be written as

$$\sum_{j=1}^{N}\int_{B_j}\gamma_j(\xi,t)\left\{H_y(x,y_i;\xi,y_j) - \frac{\delta_{ij}\,u(x-\xi)}{h_j C_j(x)}\right\}d\xi$$

$$= F_i'(x,t) + G_i'(x,t) + H_i'(x,t) \quad i = 1,\ldots,N \tag{5.2.7}$$

where δ_{ij} is the Kronecker delta function and F, G and H are given by (4.2.22) to (4.2.24). It is still necessary to have a Kutta condition on the trailing edge of a moving ship (4.2.27) and a zero circulation condition on a stationary ship (4.2.26). The system of integral equations (5.2.7) is of the same form as (4.4.1) and can be solved numerically for the vorticity, by following the procedure described in section 4.4.

5.3 SWAY FORCE AND YAW MOMENT

To obtain a formula for the sway force and yaw moment on a given ship, the methods of section 2.8 and 4.3 are combined. The sway force on ship j at time t is given by

$$Y_j(t) = - \iint_{\substack{\text{surface} \\ \text{ship } j}} p \, dx \, dz$$

$$= - \rho \int_{B_j} dx \int_{C_j(x)} \phi_t \, dz \qquad (5.3.1)$$

using (4.2.6) and where $C_j(x)$ is the cross section curve of ship j at station x. Replacing ϕ_x by ϕ_t in (2.8.3) and using the path of integration shown in Figure 2.1 it can be shown that

$$\int_{C_j(x)} \phi_t \, dz = - \int_{S_{\pm\infty}} \phi_t \frac{\partial y}{\partial n} \, d\ell$$

$$= - h_j \frac{\partial \Delta\phi}{\partial t} \, . \qquad (5.3.2)$$

Substituting this into (5.3.1) gives

$$Y_j(t) = + \rho h_j \int_{B_j} \frac{\partial \Delta\phi}{\partial t} \, dx \qquad (5.3.3)$$

which by using (4.2.11) can be expressed as

$$Y_j(t) = \rho h_j \int_{B_j} \frac{\partial}{\partial t} \int_{a_j(t)}^{x} \gamma_j(\xi,t)\,d\xi\,dx \,. \qquad (5.3.4)$$

Similarly the yaw moment on ship j at time t can be found as

$$N_j(t) = \tfrac{1}{2}\rho h_j \int_{B_j} (a_j(t)+b_j(t)-2x) \frac{\partial}{\partial t} \int_{a_j(t)}^{x} \gamma_j(\xi,t)\,d\xi\,dx. \qquad (5.3.5)$$

5.4 RESULTS

To test the above formulation and suggested numerical technique, numerical results were obtained and compared with the experimental results of Remery [19]. The blockage coefficient is calculated using the formula derived by Taylor [21]. To simplify the calculation, the blockage coefficient is assumed to be constant along the whole ship. The term involving the blockage coefficient in (5.2.7) may then be evaluated analytically.

The experiments of Remery [19] which are used for comparison consist of a model of a moored 100 MDWT vessel being passed by a 30 MDWT vessel. The depth of water for all experiments was equivalent to a full scale depth of 18 metres over a flat bottom. So the appropriate form of the kernel K^{ij} in the numerical analysis of section 4.4 is given by (3.4.3).

Figures 5.2 and 5.3 show the results obtained for the passing manoeuvre with a separation of 61.4 metres between the parallel paths. The graphs show that satisfactory agreement is obtained with the experiments but that the magnitude of both the sway force and yaw moment on the stationary ship are slightly underestimated. When compared with the far field results of Yeung [26] the graphs are also quite similar, showing that the far field results are a good approximation even for close

interactions. Although both theoretical computations underestimate the force and moment, Beck [4] found a similar phenomenon for a ship in a canal, and found that when the forces for the interactions between the source distributions were added, a correction was obtained which gave better agreement.

Figures 5.4 and 5.5 show the results obtained when the separation is 96.4 metres, and again it can be seen that both the magnitude of the sway force and the yaw moment are underestimated. When comparing the two different experiments it is significant that the force and moment decrease quite rapidly as the separation increases.

The computer execution time for the computation necessary for Figures 5.2 and 5.3 was 553 seconds on a C.D.C. CYBER 173. The decrease in time when compared with that used in Chapter 4 is a result of the greater speed of the CYBER 173 compared to the 6400.

For the limited number of available comparisons with experiments, it was found that the present formulation and numerical technique produce satisfactory results. As the qualitative agreement is good the approach described here should be useful for giving predictions for ship interactions which are difficult to model by experiment. Many different simulations can be carried out by this method, such as investigating the effect of varying the depth of the water, which can cause large changes in the force and moment.

	Symbol	Unit	Moored Vessel	Passing Vessel
Deadweight	MDWT	1000 ton	100	30
Length	L	m	257	183
Beam	B	m	36.8	26.1
Draught	d	m	15.7	10.5

TABLE 5.1 Relevant Dimensions of Ships

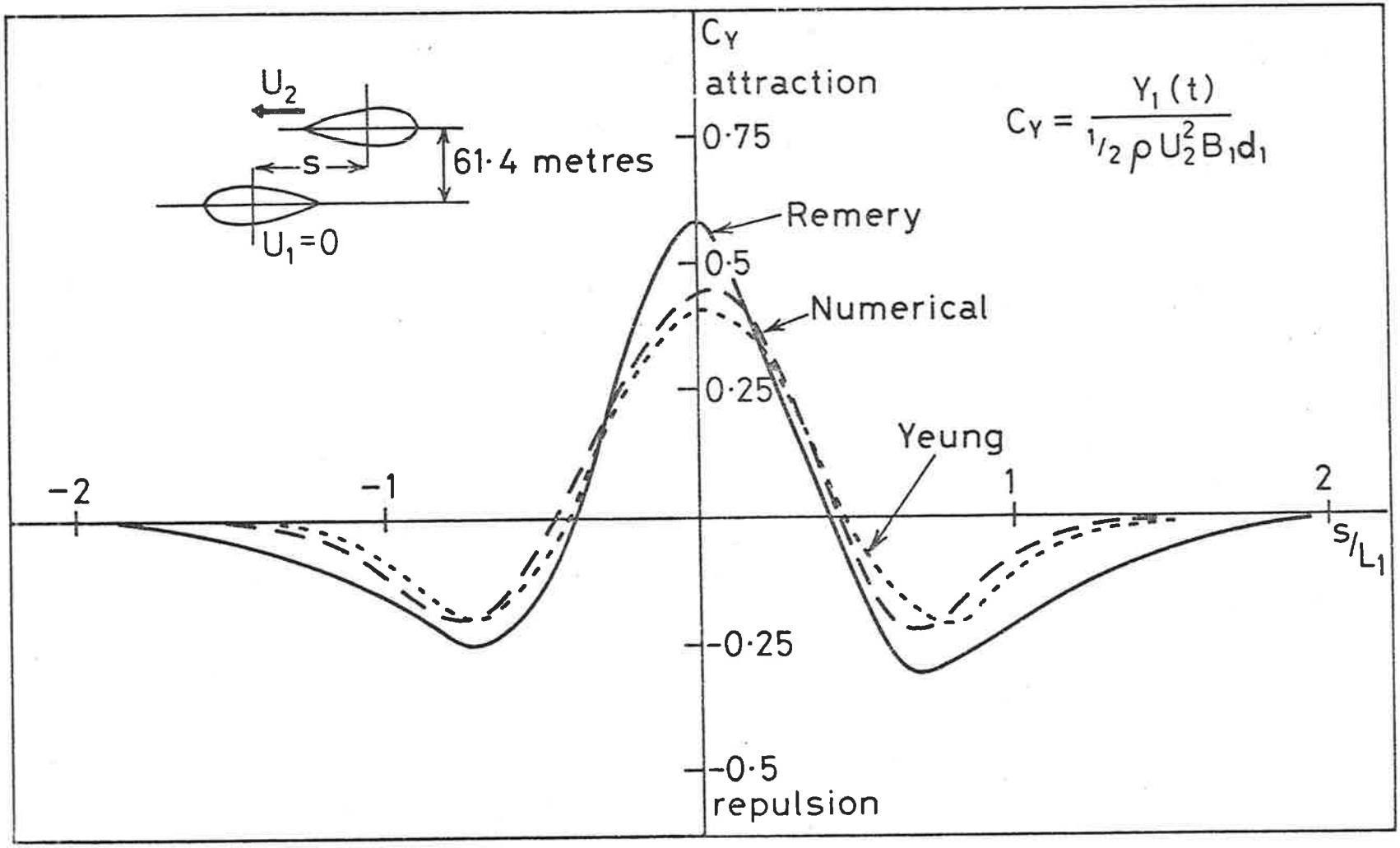

5.2 Sway force on the moored ship for a separation of 61.4 metres.

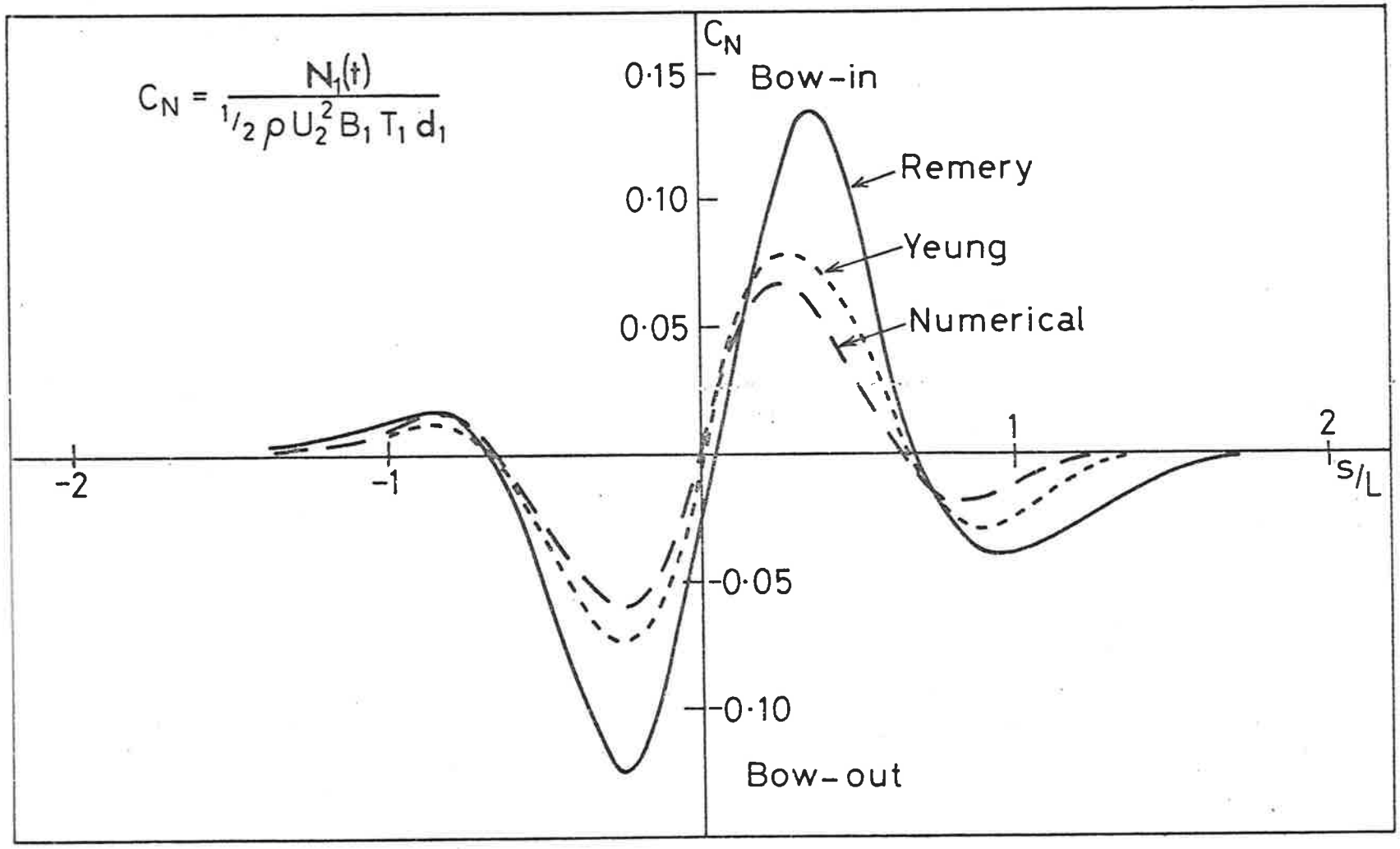

5.3 Yaw moment on the moored ship for a separation of 61.4 metres.

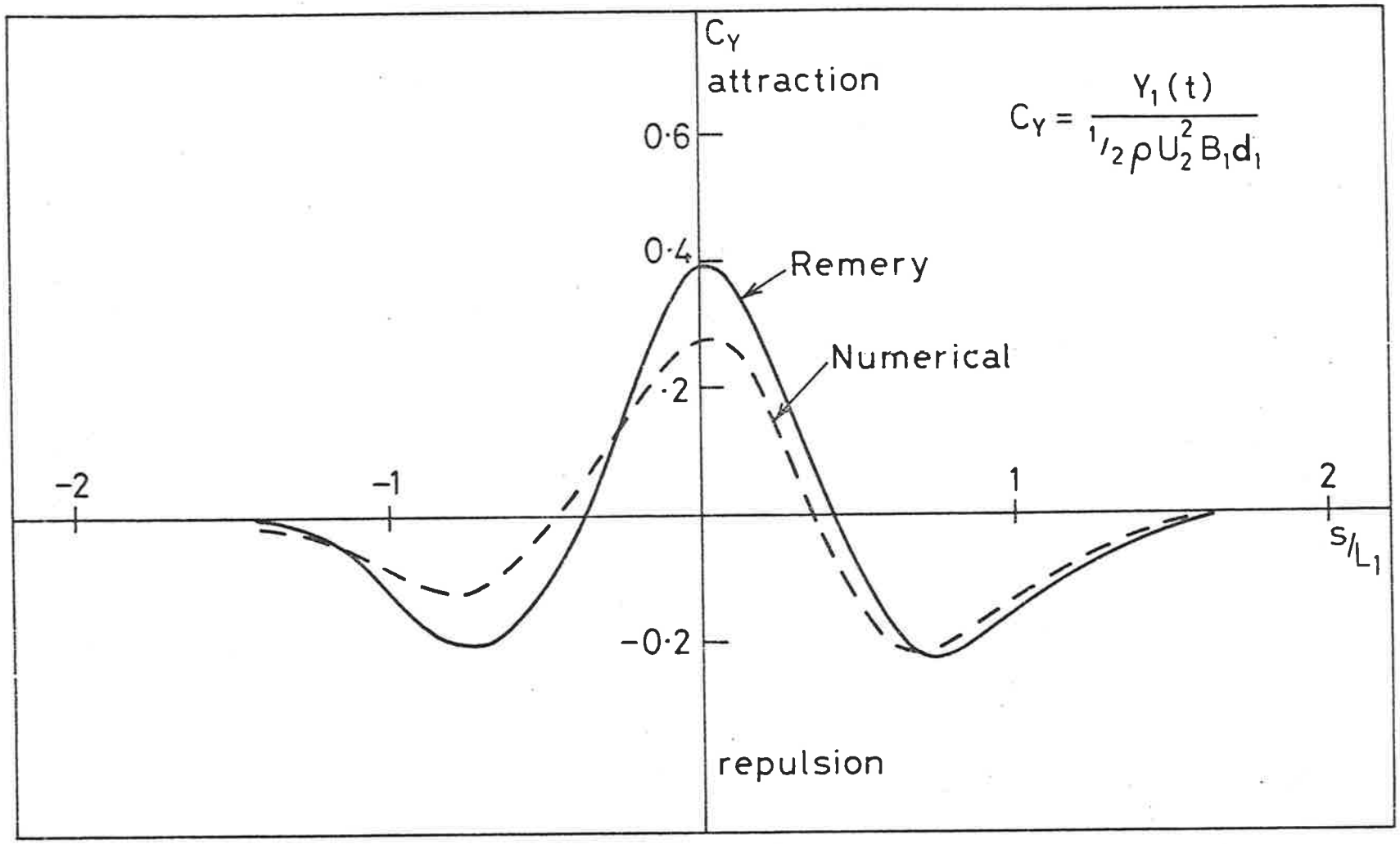

5.4 Sway force on the moored ship for a separation of 96.4 metres.

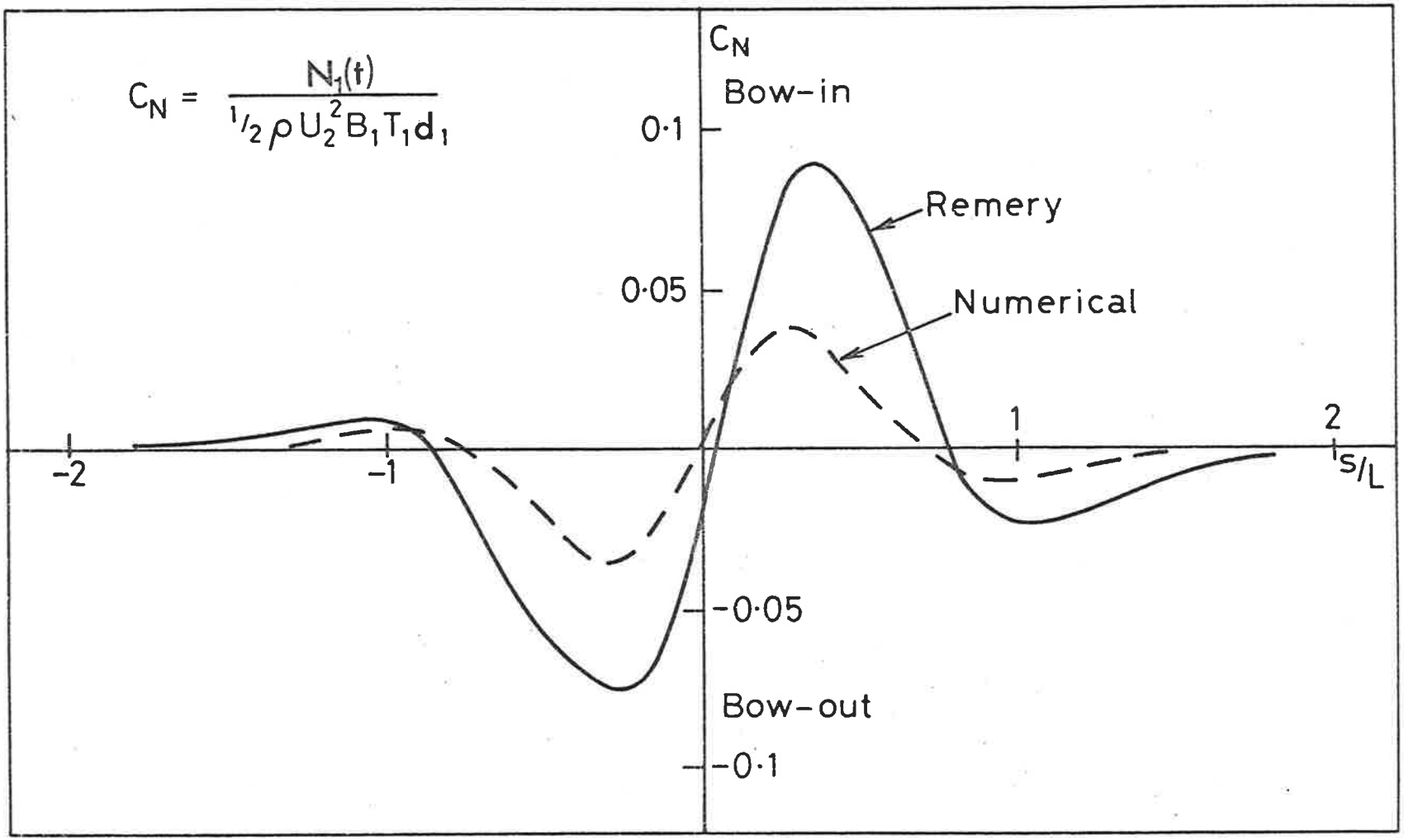

5.5 Yaw moment on the moored ship for a separation of 96.4 metres.

CHAPTER 6

CONCLUSION

This dissertation provides the formulation and a numerical solution technique for the computation of the lateral forces and moments occurring during ship interactions in shallow water. Although this is a valuable tool for studying hazardous ship manoeuvres, it is limited by the computer time required and the parallel path restriction. Also only the sway force and yaw moments are calculated, whereas the other forces and moments occurring, namely, squat, thrust, trim and pitch, can also be important. Squat is usually the most important of these for ships operating with a small underkeel clearance, as the increase in squat experienced by a ship, when another ship or obstacle is close by, may be sufficient to ground the ship.

A method for obtaining a power series approximation for the vorticity on a ship by extending the method described in Kida and Miyai [13] seems to hold some promise for steady two-dimensional interactions. Such a solution could be useful in decreasing the computational time of the problem. Unfortunately when both thickness and camber effects are included only the lower order coefficients of the series may be readily evaluated. An algorithm for finding coefficients of any order can be readily derived, but in practice a computer package capable of performing symbolic algebraic manipulation appears to be necessary.

REFERENCES

1. ABRAMOWITZ, M. & STEGUN, L.A., eds.
   Handbook of Mathematical Functions,
   National Bureau of Standards, Applied Mathematics Series No.55, (1964), Washington D.C., and Dover.

2. *Advances in Road Vehicle Aerodynamics*,
   N.S. Stephens, ed., B.H.R.A. Fluid Engineering, 1973.

3. ASHLEY, H. & LANDAHL, M.
   Aerodynamics of Wings and Bodies,
   1965, Addison-Wesley, Reading, Mass.

4. BECK, R.F.
   Forces and Moments on a Ship Moving in a Canal,
   J. of Ship Research, Vol. 21, No.2, June 1977, pp.107-119.

5. BROWN, G.J. & SEEMAN, G.R.
   An Experimental Investigation of the Unsteady Aerodynamics of Passing Highway Vehicles,
   Distributed by N.T.I.S., 1972.

6. COLLATZ, G.
   Experimentelle Untersuchung der Hydrodynamischen Wechselwinbung zweier Schiffskörper,
   Jahrbuch Schiffebautechnischer Gesellschaft, Vol. 57, 1963, pp.281-329.

7. DAND, I.W.
   Some Aspects of Manoeuvring in Collision Situations in Shallow Water,
   10th ONR Naval Hydrodynamics Symposium, M.I.T., June 1974.

8. DAND, I.W.
   Hydrodynamics Aspects of Shallow Water Collisions,
   The Naval Architect, Nov. 1976, pp.323-346.

9. GIESING, J.P.

Nonlinear Interaction of Two Lifting Bodies in Arbitrary Unsteady Motion,

Trans. ASME, Series D, Journal of Basic Engineering, Vol. 90, Sept. 1968, pp.387-394.

10. HESS, F.

Bank Suction Cancelled by Rudder Deflection: A Theoretical Model,

International Shipbuilding Progress, Vol. 25 (1978), No. 281, pp.7-13.

11. HESS, F.

Lateral Forces on a Ship Approaching a Vertical Wall: A Theoretical Model,

Journal of Ship Research (in press).

12. KARMAN, VON K. & BURGERS, J.M.

General Aerodynamic Theory - Perfect Fluids,

Vol. 2, Div. E of *Aerodynamic Theory*, Durand, W.F., ed.

Durand Reprinting Committee, 1943.

13. KIDA, T. & MIYAI, Y.

An Alternative Analytical Method for Ground-Effect Aerofoils,

Aero. Quarterly, Nov. 1976, pp.297-308.

14. KING, G.W.

Unsteady Hydrodynamic Interactions Between Ships,

J. of Ship Research, Vol. 21, No. 3, Sept. 1977, pp.157-164.

15. KING, G.W.

Unsteady Hydrodynamic Interactions Between Ships in Shallow Water,

6th Australasian Hydraulics and Fluid Mechanics Conference, Adelaide, Australia, Dec. 1977, pp.291-293.

16. KING, G.W. & TUCK, E.O.

Lateral Forces on Ships in Steady Motion Parallel to Banks or Beaches

Int. J. of Applied Ocean Research, 1979, in press.

17. NEWMAN, J.N.

Lateral Motion of a Slender Body Between Two Parallel Walls,

J. of Fluid Mechanics, 1969, Vol. 39, Part 1, pp.97-115.

18. OLTMANN, P.

Experimentelle Untersuchung der Hydrodynamischen Wechschwinkung Schiffsähnlicher Körper,

Schiff und Hafer, Vol. 22, 1970, pp.701-709.

19. REMERY, G.F.M.

Mooring Forces Induced by Passing Ships,

Proc. 6th Offshore Tech. Conf., Dallas, Texas, 1974, pp.349-363.

20. SEARS, W.R.,

Unsteady Motion of Airfoils with Boundary-Layer Separation,

A.I.A.A. Journal, Vol. 14, No. 2, 1976, pp.216-220.

21. TAYLOR, P.J.

The Blockage Coefficient for Flow about an Arbitrary Body Immersed in a Channel,

J. of Ship Research, Vol. 17, No. 2, pp.97-105.

22. TUCK, E.O.

Shallow Water Flows Past Slender Bodies,

J. of Fluid Mechanics, Vol. 26, 1966, pp.81-95.

23. TUCK, E.O.

Some Classical Water-Wave Problems in Varying Depth,

Proc. IUTAM Symp. on Waves on Water of Varying Depth, Aust. Acad. of Science, Canberra, pp.9-20, (Springer-Verlag).

24. TUCK, E.O.

Ship-Hydrodynamic Problems in Restricted Waters,

Annual Review of Fluid Mechanics, Vol. 10 (1978).

25. TUCK, E.O. & NEWMAN, J.N.

Hydrodynamic Interactions Between Ships,

Proc. 10th Symp. on Naval Hydrodynamics, 1974, pp.35-70.

26. YEUNG, R.W.

On the Interactions of Slender Ships in Shallow Water,

J. of Fluid Mechanics (1978), Vol. 85, Part 1, pp.143-159.

27. YEUNG, R.W. & HWANG, W.Y.

Nearfield Hydrodynamic Interactions of Ships in Shallow Water,

J. Hydronautics (1977), Vol. 11, pp.128-135.